

FORMATION AND PHYSICOCHEMICAL PROPERTIES
OF NON-IONIC OIL-IN-WATER NANOEMULSIONS
CONTAINING LIQUID AND SOLID TRIGLYCERIDES

Miss Prawarisa Wasutrasawat

A Dissertation Submitted in Partial Fulfillment of the Requirements
for the Degree of Doctor of Philosophy Program in Pharmaceutical Technology

Department of Pharmaceutics and Industrial Pharmacy

Faculty of Pharmaceutical Sciences

Chulalongkorn University

Academic Year 2012

Copyright of Chulalongkorn University

บทคัดย่อและแฟ้มข้อมูลฉบับเต็มของวิทยานิพนธ์ตั้งแต่ปีการศึกษา 2554 ที่ให้บริการในคลังปัญญาจุฬาฯ (CUIR)

เป็นแฟ้มข้อมูลของนิสิตเจ้าของวิทยานิพนธ์ที่ส่งผ่านทางบัณฑิตวิทยาลัย

The abstract and full text of theses from the academic year 2011 in Chulalongkorn University Intellectual Repository(CUIR)
are the thesis authors' files submitted through the Graduate School.

การเกิดและคุณสมบัติทางเคมีกายภาพของนาโนอิมัลชันไม่มีประจุชนิดน้ำมันในน้ำที่ประกอบด้วย

ไตรกลีเซอไรด์แบบของเหลวและของแข็ง

นางสาวปวีศา วสุธาสวัสดิ์

วิทยานิพนธ์นี้เป็นส่วนหนึ่งของการศึกษาตามหลักสูตรปริญญาวิทยาศาสตรดุษฎีบัณฑิต

สาขาวิชาเทคโนโลยีสารสนเทศ ภาควิชาวิทยาการเกษตรกรรมและเกษตรอุตสาหกรรม

คณะเกษตรศาสตร์ จุฬาลงกรณ์มหาวิทยาลัย

ปีการศึกษา 2555

ลิขสิทธิ์ของจุฬาลงกรณ์มหาวิทยาลัย

ปวริศา วสุธาสวัสดิ์: การเกิดและคุณสมบัติทางเคมีกายภาพของนาโนอิมัลชันไม่มีประจุชนิดน้ำมันในน้ำที่ประกอบด้วยไตรกลีเซอไรด์แบบของเหลวและของแข็ง. (FORMATION AND PHYSICO-CHEMICAL PROPERTIES OF NON-IONIC OIL-IN-WATER NANOEMULSIONS CONTAINING LIQUID AND SOLID TRIGLYCERIDES) อ.ที่ปรึกษาวิทยานิพนธ์หลัก: ศศ.ดร.วรางคณา วารีสน้อยเจริญ, อ.ที่ปรึกษาวิทยานิพนธ์ร่วม: PROF. JAYNE LAWRENCE, 172 หน้า.

เมื่อไม่นานมานี้การใช้นาโนอิมัลชันเพื่อการนำส่งยาได้รับความสนใจเพิ่มมากขึ้น ในงานวิจัยนี้ได้ศึกษาการเกิดและคุณสมบัติทางเคมีกายภาพของนาโนอิมัลชันชนิดน้ำมันในน้ำที่ถูกทำให้เสถียรโดยสารลดแรงตึงผิวชนิดไม่มีประจุ $C_{18:1}E_{10}$ และประกอบด้วยไตรกลีเซอไรด์แบบของเหลว (น้ำมันถั่วเหลือง, ไทรออกซ์ทาโนอิน) และของแข็ง (ไตรลอริน, ไทรพาลมิติน) ผลการศึกษาพบว่าการเกิดเป็นนาโนอิมัลชันได้รับอิทธิพลจากน้ำหนักโมเลกุลของไตรกลีเซอไรด์ ไตรกลีเซอไรด์ที่มีน้ำหนักของโมเลกุลขนาดกลาง (ไตรลอริน) ซึ่งมีน้ำหนักโมเลกุลใกล้เคียงกับสารลดแรงตึงผิว ทำให้เกิดระบบนาโนอิมัลชันได้มากที่สุด ตามด้วยไตรพาลมิตินและน้ำมันถั่วเหลืองซึ่งเป็นไตรกลีเซอไรด์ที่มีน้ำหนักของโมเลกุลขนาดใหญ่และไตรออกซ์ทาโนอินซึ่งเป็นไตรกลีเซอไรด์ที่มีน้ำหนักของโมเลกุลขนาดเล็ก นาโนอิมัลชันที่เกิดขึ้นถูกแบ่งออกเป็น 3 ส่วนตามลักษณะที่มองเห็น ได้แก่ ส่วน A (ใส) ส่วน B (โปร่งแสง) และ ส่วน C (ขุ่น) ทั้งนี้คุณสมบัติของนาโนอิมัลชันในส่วน A และ B เป็นไปในลักษณะเดียวกันและเป็นประโยชน์ในการเพิ่มการละลายยา เทสโทสเตอโรลโพรพิโอเนท (TP) ในขณะที่นาโนอิมัลชันในส่วน C มีคุณสมบัติที่แตกต่างและไม่มีผลเพิ่มการละลายของยา จากการศึกษาอุณหภูมิของการเปลี่ยนวัฏภาคและการกระเจิงในมุมเล็กของนิวตรอนพบว่าไตรกลีเซอไรด์จัดเรียงอยู่ในส่วนกลางของนาโนอิมัลชันที่ประกอบด้วยน้ำมันถั่วเหลือง, ไทรลอริน และ ไทรพาลมิติน แต่ไตรกลีเซอไรด์ในนาโนอิมัลชันที่ประกอบด้วยไตรออกซ์ทาโนอินจัดเรียงอยู่ทั้งในส่วนกลางและแทรกผ่านไปในส่วนหางของสารลดแรงตึงผิวด้วย นอกจากนี้ยังพบว่าการละลายของยาในนาโนอิมัลชันขึ้นอยู่กับคุณสมบัติทางกายภาพและจุดหลอมละลายของไตรกลีเซอไรด์ โดยยาจะละลายได้มากที่สุดในาโนอิมัลชันที่ประกอบด้วยไตรกลีเซอไรด์แบบของเหลว (น้ำมันถั่วเหลือง, ไทรออกซ์ทาโนอิน) และไตรกลีเซอไรด์แบบของแข็งที่มีจุดหลอมละลายต่ำกว่า (ไตรลอริน) ซึ่งจะอยู่ในนาโนอิมัลชันในสถานะเป็นของเหลว ในทางตรงกันข้ามการละลายของยาค่อนข้างจำกัดในนาโนอิมัลชันที่ประกอบด้วยไตรกลีเซอไรด์แบบของแข็งที่มีจุดหลอมละลายสูงกว่า (ไตรพาลมิติน) เนื่องจากไตรพาลมิตินอยู่ในสถานะของแข็งในนาโนอิมัลชัน ข้อมูลที่ได้รับจากการวิจัยนี้เป็นประโยชน์ในการออกแบบระบบนาโนอิมัลชันเพื่อการนำส่งยา ตลอดจนช่วยเพิ่มความเข้าใจเกี่ยวกับผลของไตรกลีเซอไรด์ต่อคุณสมบัติของของนาโนอิมัลชันและต่อการละลายของยาในนาโนอิมัลชัน

ภาควิชา วิทยาการเกษตรกรรมและเกษตรอุตสาหกรรมลายมือชื่อนิสิต.....
 สาขาวิชา เทคโนโลยีเกษตรกรรมลายมือชื่อ อ.ที่ปรึกษาวิทยานิพนธ์หลัก.....
 ปีการศึกษา 2555ลายมือชื่อ อ.ที่ปรึกษาวิทยานิพนธ์ร่วม.....

5177103233 : MAJOR PHARMACEUTICAL TECHNOLOGY

KEYWORDS : NANOEMULSIONS / TRIGLYCERIDE / POLYOXYETHYLENE-10-OLEYL ETHER / TESTOSTERONE PROPIONATE / SOLUBILISATION

PRAWARISA WASUTRASAWAT : FORMATION AND PHYSICOCHEMICAL PROPERTIES OF NON-IONIC OIL-IN-WATER NANOEMULSIONS CONTAINING LIQUID AND SOLID TRIGLYCERIDES. ADVISOR : ASST. PROF. WARANGKANA WARISNOICHAROEN, Ph.D., CO-ADVISOR : PROF. JAYNE LAWRENCE, Ph.D., 172 pp.

With the increasing attention in nanoemulsions (NE) formulation as drug delivery vehicles in recent years, in this study, the formation and physicochemical properties of the oil-in-water NE stabilized by the nonionic C_{18:1}E₁₀ surfactant containing either liquid triglycerides (soybean oil and trioctanoin) or solid triglycerides (tripalmitin and trilaurin) were investigated. The extent of NE formation was influenced by triglyceride molecular weight in that the intermediate molecular weight triglyceride, trilaurin, which is approximate equal to molecular weight of surfactant formed NE over the greatest range of compositions followed by the higher molecular weight triglycerides, (tripalmitin, soybean oil) and a lower molecular weight triglyceride (trioctanoin), respectively. The NE existence was divided into Regions A, B and C based on their appearances which were clear, translucent and cloudy, respectively. The results showed that the properties of NE in Regions A and B were similar and had advantages on improved solubilisation of lipophilic drug, testosterone propionate (TP), while NE in Region C had different properties and had no advantages on drug solubilisation. Phase inversion temperature and small angle neutron scattering studies suggested that soybean oil, tripalmitin and trilaurin formed a core in the NE droplets, while trioctanoin both formed a core in droplet and penetrated through the surfactant hydrophobic tail. The solubility of TP in NE was influenced by the nature and melting point of triglyceride. The drug would solubilise to the greater extent in NE containing either liquid triglycerides (soybean oil and trioctanoin) or a lower melting point solid triglyceride (trilaurin) which was in “liquid-like” state in NE. In contrast, solubilisation of TP was limited in NE containing higher melting point solid triglyceride, tripalmitin, owing to “solid-like” state of triglyceride inside NE. Conclusively, the information obtained from this study will help ultimately design NE as drug carrier as well as provide more understanding about the effect of the triglyceride nature on the properties and drug solubilisation capacity of NE.

Department :Pharmaceutics and Industrial Pharmacy..... Student's Signature.....

Field of Study :Pharmaceutical Technology..... Advisor's Signature.....

Academic Year : 2012..... Co-advisor's Signature.....

ACKNOWLEDGEMENTS

This dissertation could not have been completed without Assistant Professor Dr. Warangkana Warisnoichareon, who not only serves as my advisor but also gives me many invaluable advices, unfaltering support and noteworthy professionalism encouragement both in academic and all avenues of my life. I would like to express my sincere gratitude to my co-advisor, Professor Dr. Jayne Lawrence, for giving me an opportunity and leading me working on diverse exciting projects at King's College London. Her support, concern and kind guidance have fulfilled my Ph.D. study and research. I appreciate all her contributions of time, and ideas to make my Ph.D. experience productive and stimulating. I am also thankful for the excellent guidance she has provided as a successful professor.

I would like to acknowledge to Associated Professor Dr. Ubonthip Nimmannit who had introduced me to this program and given me the opportunity to join this course. I wish to express my warm and sincere thanks to Dr. Richard Heenan and Dr. Ann Terry, ISIS Facility, Science & Technology Facilities Council, Rutherford Appleton Lab, Harwell Science & Innovation Campus Oxford UK, for their welcomeness, kindness, helpful, and precious experiences. Besides my advisor, I would like to thank the rest of my thesis committee for their encouragement, insightful comments, and invaluable discusses over my dissertation. I am especially grateful to all my lab members and colleagues at King's College London; Jamie, Hisham, Lucy, Louis, Fab, Alexandra and Yulin for making a convivial place to work through our interactions and discussions during the long hours in the lab.

I wish to extend my warmest thanks to all those who have helped me with my work in Faculty of Pharmaceutical Sciences, Chulalongkorn University; Thermal Analysis group, School of Pharmacy; and Biophysical Pharmaceutics group, King's College London. My deepest gratitude goes to my family for their unflinching love and support throughout my life. Without their encouragement and understanding it would have been impossible for me to finish this work.

CONTENTS

	Page
ABSTRACT IN THAI.....	iv
ABSTRACT IN ENGLISH.....	v
ACKNOWLEDGEMENTS.....	vi
CONTENTS.....	vii
LIST OF TABLES.....	ix
LIST OF FIGURES.....	xii
LIST OF ABBREVIATIONS.....	xviii
CHAPTER I INTRODUCTION.....	1
CHAPTER II LITERATURE REVIEW.....	5
1. Nanotechnology and nanoparticles.....	5
1.1 Definition.....	5
1.2 Classification of nanoparticles.....	5
2. Micelles and nanoemulsions.....	7
2.1 Definition.....	7
2.2 Choices of composition.....	8
3. Formation of micelles and nanoemulsions.....	12
3.1 Formation of micelles.....	12
3.2 Formation of nanoemulsions.....	15
4. Structure of nanoemulsions.....	17
5. Pharmaceutical application of nanoemulsions.....	18

	Page
6. Physicochemical characterization of micelles and nanoemulsions.....	20
6.1 Phase behaviour.....	20
6.2 Phase inversion temperature.....	21
6.3 Dynamic light scattering.....	23
6.4 Small angle neutron scattering.....	24
6.5 Differential scanning calorimetry.....	30
CHAPTER III MATERIALS AND METHODS.....	32
CHAPTER IV RESULTS AND DISCUSSION.....	53
CHAPTER V CONCLUSION.....	128
REFERENCES.....	131
APPENDIX.....	157
VITA.....	172

LIST OF TABLES

Table	Page
1	Commercial nanoemulsions formulation..... 19
2	Molecular weight and molecular volume of the triglycerides..... 34
3	Physicochemical parameters of the chemicals for SANS..... 44
4	Composition of hydrogenated and deuterated chemicals for contrast matching 45
5	Composition of stock nanoemulsion formulation..... 46
6	Scattering length densities and related physicochemical parameters of the compounds used for SANS measurements..... 51
7	Sample list for SANS contrast matching experiments..... 52
8	Upper limit of amount of triglyceride incorporated into nanoemulsions denoted in Regions A, B and C at 10 and 20 wt% C _{18:1} E ₁₀ 60
9	The melting and recrystallisation temperature of the bulk triglyceride 87
10	Summary of the individual fitting parameters for micellar solutions containing different C _{18:1} E ₁₀ concentrations using a core-shell ellipsoid model and a hard sphere structure factor 112
11	Parameters obtained by simultaneously fitting the SANS data from the three contrasts examined for nanoemulsions prepared using 2.4% w/v C _{18:1} E ₁₀ and containing varying amounts of TON at 25°C using the core-shell ellipsoidal model together with a hard-sphere structure factor. 119
12	Parameters obtained by simultaneously fitting the SANS data from the three contrasts examined for nanoemulsions prepared using 2.4% w/v C _{18:1} E ₁₀ and containing varying amounts of TPN at 25°C using the core-shell ellipsoidal model together with a hard-sphere structure factor..... 125

Table	Page
13 The comparison of hydrodynamic droplet sizes of the NE containing SBO prepared by PIT method and sonication method.....	158
14 The comparison of hydrodynamic droplet sizes of the NE containing TPN prepared by PIT method and sonication method.....	159
15 The comparison of hydrodynamic droplet sizes of the NE containing TLN prepared by PIT method and sonication method.....	160
16 The comparison of hydrodynamic droplet sizes of the NE containing TON prepared by PIT method and sonication method.....	161
17 The variation in the mean hydrodynamic droplet size (mean±S.D., n=3) of the NE containing TON at different weight ratios of C _{18:1} E ₁₀ to triglycerides.....	161
18 The variation in the mean hydrodynamic droplet sizes (mean±S.D., n=3) of the NE containing SBO at different weight ratios (R) of C _{18:1} E ₁₀ to triglycerides.....	162
19 The variation in the mean hydrodynamic droplet sizes (mean±S.D., n=3) of the NE containing TPN at different weight ratios (R) of C _{18:1} E ₁₀ to triglycerides.....	163
20 The variation in the mean hydrodynamic droplet sizes (mean±S.D., n=3) of the NE containing TLN at different weight ratios (R) of C _{18:1} E ₁₀ to triglycerides.....	164
21 Variation in phase inversion temperature (mean±S.D., n=3) of systems prepared using either 10, 15, 20 or 25 wt% C _{18:1} E ₁₀ and containing either varying amounts of SBO or TPN.....	165
22 Variation in phase inversion temperature (mean±S.D., n=3) of systems prepared using either 10, 15, 20 or 25 wt% C _{18:1} E ₁₀ and containing either varying amounts of TLN or TON.....	166

Table	Page
23 Solubilization of testosterone propionate in micelles and NE stabilised using 10 wt% C _{18:1} E ₁₀ and containing either varying amounts of SBO, TPN, TLN or TON at 22 ± 2°C (mean ± S.D., n=4).....	167
24 Solubilization of testosterone propionate in micelles and NE stabilised using 20 wt% C _{18:1} E ₁₀ and containing either varying amounts of SBO, TPN, TLN or TON at 20 ± 2°C (mean ± S.D., n=4).....	168
25 The comparison of the mean hydrodynamic size (mean ± S.D., n=3) at 22 ± 2°C of the NE with and without saturated amount of testosterone propionate prepared using SBO, TPN, TLN and TON and stabilised by 10 wt% C _{18:1} E ₁₀	169
26 The comparison of the mean hydrodynamic size (mean ± S.D., n=3) at 22 ± 2°C of the NE with and without saturated amount of testosterone propionate prepared using SBO, TPN, TLN and TON and stabilised by 20 wt% C _{18:1} E ₁₀	170
27 The phase inversion temperatures (mean ± S.D., n=3) of the NE prepared using either 10 or 20 wt% C _{18:1} E ₁₀ and containing either varying amounts of SBO, TPN, TLN or TON with the presence of a saturated amount of testosterone propionate at 22 ± 2°C.....	171

LIST OF FIGURES

Figure		Page
1	The main types of nanotechnology used for drug delivery system.....	6
2	The formation and structure of triglyceride.....	11
3	A schematic diagram of a spherical micelle of surfactant molecules in aqueous solution.....	14
4	Packing properties of surfactants aggregate and the critical packing parameter	15
5	Schematic representation of the most commonly encountered nanoemulsion structures.....	18
6	Schematic diagram illustrating the phase behaviour of oil/water/surfactant systems.....	21
7	Protons accelerated into the Giga electronvolt regime can split heavy nuclei with a large neutron surplus, creating free neutrons as a part of the reaction products.....	25
8	Neutrons are scattered from the nuclei whereas X-rays are scattered from electrons. Negative neutron scattering lengths are represented by a black circle	27
9	Schematic representation of a SANS experiment of an oil-in-water nanoemulsion exploiting contrast matching.....	29
10	Schematic representation of drop, shell and core part of oil-in-water nanoemulsion.....	29
11	The chemical structures of a) tripalmitin (TPN), b) trilaurin (TLN) and c) trioctanoin (TON).....	33
12	The chemical structure of polyoxyethylene 10-oleyl ether (C _{18:1} E ₁₀) surfactant.....	33

Figure	Page
13 Preparation of oil-in-water (o/w) nanoemulsions stabilised by the nonionic surfactant polyoxyethylene 10-oleyl ether, C _{18:1} E ₁₀ , and containing a triglyceride.....	35
14 Tertiary phase diagram (a) and partially tertiary phase diagram (b) representing Regions A (clear), B (bluish or translucent) and C (cloudy or milky) of NE.....	37
15 Schematic representation of a small angle neutron scattering experiment.....	43
16 Schematic of form factors for SANS data fitting.....	47
17 Triangular phase diagrams for o/w nanoemulsions formed with C _{18:1} E ₁₀ , either a liquid triglyceride oil (a) soybean oil or (b) trioctanoin or solid triglycerides (c) tripalmitin or (d) trilaurin and water after 24 hours and one month storage at 22 ± 2°C. On the abscissa, surfactant concentration (in wt%) is increasing from Left to right while on the ordinate, oil concentration (in wt%) is increasing from bottom to top.....	54
18 Appearance of nanoemulsions within Regions A (clear), B (bluish or translucent) and C (cloudy or milky).....	57
19 Variation in the mean hydrodynamic droplet sizes of the nanoemulsions containing soybean oil over a period of a month stabilized by C _{18:1} E ₁₀ at different concentrations (mean ± S.D., n=3).....	64
20 Variation in the mean hydrodynamic droplet sizes of the nanoemulsions containing tripalmitin over a period of a month stabilized by C _{18:1} E ₁₀ at different concentrations (mean ± S.D., n=3).....	65
21 Variation in the mean hydrodynamic droplet sizes of the nanoemulsions containing trilaurin over a period of a month stabilized at by C _{18:1} E ₁₀ at different concentrations (mean ± S.D., n=3).....	66

Figure	Page	
22	Variation in the mean hydrodynamic droplet sizes of the nanoemulsions containing trioctanoin over a period of a month stabilized by C _{18:1} E ₁₀ at different concentrations (mean ± S.D., n=3).....	67
23	Variation in the mean hydrodynamic droplet sizes of the nanoemulsions containing SBO, TPN, TLN or TON at different weight ratios (0.2-1, shown as legend) of C _{18:1} E ₁₀ to triglycerides (mean ± S.D., n=3)...	70
24	Variation in phase inversion temperature of nanoemulsions prepared using either 10, 15, 20 or 25 wt% C _{18:1} E ₁₀ and containing either varying amounts of SBO, TPN, TLN or TON (mean ± S.D., n=3).....	73
25	Comparison in phase inversion temperature of nanoemulsions prepared using either 10, 15, 20 or 25 wt% C _{18:1} E ₁₀ and containing either varying amounts of SBO, TPN, TLN or TON (mean ± S.D., n=3).....	78
26	Solubilization of testosterone propionate in micelles and nanoemulsions stabilised using either a) 10 and b) 20 wt% C _{18:1} E ₁₀ and containing either varying amounts of SBO, TPN, TLN or TON at 22 ± 2°C (mean ± S.D., n=4).....	80
27	DSC thermogram of water heated at 1°C min ⁻¹	84
28	DSC thermogram of C _{18:1} E ₁₀ heated at 1°C min ⁻¹	84
29	DSC thermograms of bulk triglycerides (SBO, TPN, TLN and TON) heated at 1°C min ⁻¹	85
30	DSC thermograms of 10 or 20 wt% C _{18:1} E ₁₀ micellar solutions heated at 1°C min ⁻¹	86
31	DSC thermograms of TON-NE stabilised by 10 wt% or 20 wt% C _{18:1} E ₁₀ heated at 1°C min ⁻¹	88
32	DSC thermograms of SBO-NE containing varying amounts of SBO stabilised by a) 10 and b) 20 wt% C _{18:1} E ₁₀ and heated at 1°C min ⁻¹	89

Figure	Page
33 DSC thermograms of TLN-NE containing varying amounts of TLN stabilised by a) 10 and b) 20 wt% C _{18:1} E ₁₀ and heated at 1°C min ⁻¹	90
34 DSC thermograms of TPN-NE stabilised by a) 10 wt% C _{18:1} E ₁₀ and b) 20 wt% C _{18:1} E ₁₀ (1-8 wt% TPN) and c) 20 wt% C _{18:1} E ₁₀ (10-18 wt% TPN). The samples were heated at 1°C min ⁻¹	92
35 The comparison of the mean hydrodynamic sizes at 22 ± 2°C of the nanoemulsions with and without saturated amount of testosterone propionate prepared using a) SBO b) TPN c) TLN and d) TON and stabilised by 10 wt% C _{18:1} E ₁₀ (mean ± S.D., n=3).....	99
36 The comparison of the mean hydrodynamic sizes at 22 ± 2°C of nanoemulsions with and without saturated amount of testosterone propionate prepared using a) SBO b) TPN c) TLN and d) TON and stabilised by 20 wt% C _{18:1} E ₁₀ (mean ± S.D., n=3).....	100
37 The comparison of the phase inversion temperatures of the nanoemulsions prepared using either 10 or 20 wt% C _{18:1} E ₁₀ and containing either varying amounts of a) SBO, b) TPN, c) TLN or d) TON with and without the presence of a saturated amount of testosterone propionate at 22 ± 2°C (mean ± S.D., n=3).....	103
38 DSC heating curves (1°C min ⁻¹) of a) 10 or 20 wt% C _{18:1} E ₁₀ micellar solutions containing drug, and drug-loaded nanoemulsions stabilized using either 10 or 20 wt% C _{18:1} E ₁₀ and containing varying amounts of b) SBO and c) TON.....	104
39 DSC heating curves (1°C min ⁻¹) of nanoemulsions containing a saturated amount of testosterone propionate and various amounts of TLN stabilized using either a) 10 or b) 20 wt% C _{18:1} E ₁₀	106

Figure	Page	
40	DSC heating curves ($1^{\circ}\text{C min}^{-1}$) of nanoemulsions containing a saturated amount of testosterone propionate and various amounts of TPN stabilized using either a) 10 or b) 20 wt% $\text{C}_{18:1}\text{E}_{10}$	107
41	Three contrasts (core, drop and shell) of SANS data for 1.2% w/v, 2.4% w/v and 4.8% w/v $\text{C}_{18:1}\text{E}_{10}$ micelles (from top to bottom) at 25°C simultaneously fitted to the core-shell ellipsoid model with a hard sphere.....	109
42	Three contrasts of SANS data for 12% w/v (top) and 24% w/v (bottom) of $\text{C}_{18:1}\text{E}_{10}$ micelles at 25°C simultaneously fitted to the core-shell ellipsoid model with a hard sphere.....	110
43	Schematic representation of the shape and molecular architecture of 2.4% w/v $\text{C}_{18:1}\text{E}_{10}$ micellar droplet.....	112
44	SANS data of TON-1.0 nanoemulsions with three contrasts (core, drop, shell) at 25°C , simultaneously fitted to the core-shell ellipsoid model with a hard sphere.....	114
45	SANS data of TON-2.1 nanoemulsions with three contrasts (core, drop, shell) at 25°C , simultaneously fitted to the core-shell ellipsoid model with a hard sphere.....	115
46	SANS data of TON-2.4 nanoemulsions with three contrasts (core, drop, shell) at 25°C , simultaneously fitted to the core-shell ellipsoid model with a hard sphere.....	115
47	SANS data of TON-3.0 nanoemulsions with three contrasts (core, drop, shell) at 25°C , simultaneously fitted to the core-shell ellipsoid model with a hard sphere.....	116
48	SANS data of TON-3.6 nanoemulsions with three contrasts (core, drop, shell) at 25°C , simultaneously fitted to the core-shell ellipsoid model with a hard sphere.....	116

Figure	Page
49 SANS data of TON-5.0 nanoemulsions with three contrasts (core, drop, shell) at 25°C, simultaneously fitted to the core-shell ellipsoid model with a hard sphere.....	117
50 SANS data of TPN-1.0 nanoemulsions with three contrasts (core, drop, shell) at 25°C, simultaneously fitted to the core-shell ellipsoid model with a hard sphere.....	122
51 SANS data of TPN-2.4 nanoemulsions with three contrasts (core, drop, shell) at 25°C, simultaneously fitted to the core-shell ellipsoid model with a hard sphere.....	122
52 SANS data of TPN-3.2 nanoemulsions with three contrasts (core, drop, shell) at 25°C, simultaneously fitted to the core-shell ellipsoid model with a hard sphere.....	123
53 SANS data of TPN-4.0 nanoemulsions with three contrasts (core, drop, shell) at 25°C, simultaneously fitted to the core-shell ellipsoid model with a hard sphere.....	123
54 SANS data of TPN-5.5 nanoemulsions with three contrasts (core, drop, shell) at 25°C, simultaneously fitted to the core-shell ellipsoid model with a hard sphere.....	124
55 SANS data of TPN-7.0 nanoemulsions with three contrasts (core, drop, shell) at 25°C, simultaneously fitted to the core-shell ellipsoid model with a hard sphere.....	124
56 A schematic representation of the molecular architecture of a) TON-2.4 or b) TPN-2.4 nanoemulsion droplets	127

ABBREVIATIONS

a	Minor axis
Å	Angstrom
a_o	The area per molecule
b	Major axis
CMC	Critical micelle concentration
CMT	Critical micelle temperature
C_mE_n	Polyoxyethylene alkyl ether surfactant (m = number of ethylene oxide units in the head group and n = number of carbon atoms in the alkylchain)
CP	Cloud point
CPP	Critical packing parameter
<i>d</i>	Deuterated
<i>D</i>	Particle diameter
D_0	Free particle diffusion coefficient
D ₂ O	Deuterated water
DDAPS	3- <i>N,N</i> -dimethyldodecylammoniopropanesulfonate
DSC	Differential scanning calorimetry
$\text{dry}V_{\text{shell}}/V_{\text{core}}$	Ratio of volume fraction of the dry head group and core
EB	Deuterated Ethyl butyrate
EC	Deuterated Ethyl caprylate
$F(Q)$	Single particle form factor
<i>h</i>	Hydrogenated
HLB	Hydrophilic-lipophilic balance

H_2O	Water
ILL	Institute Laue Langevin
$I(Q)$	Intensity of the scattered radiation
K_B	Boltzmann constant
ME	Microemulsion
M_w	Molecular weight
n	Refractive index
η	Viscosity of the medium
N_A	Avogadro's number
N_{agg}	Aggregation number
NE	Nanoemulsion
NIST	National institute of Standards and Technology
O/W	Oil in water
PCS	Photon correlation spectroscopy
PIT	Phase inversion temperature
$P(Q)$	Form factor
Q	Scattering vector
RAL	Rutherford Appleton laboratory
R	Radius
R_{core}	Core radius
R_h	Hydrodynamic radius
R_{shell}	Shell thickness
$S(Q)$	Interparticle structure factor
SANS	Small angle neutron scattering

SAXS	Small angle X-ray scattering
SLD	Scattering length densities
SBO	Soya bean oil
SPH	Hard sphere
T	Temperature in kelvin
TEM	Transmission electron microscopy
TLN	Trilaurin
TON	Trioctanoin
TPN	Tripalmitin
TP	Testosterone propionate
UV	Ultraviolet-visible spectroscopy
V	Volume
W/O	Water in oil
X	Axial ratio
%	Percentage
ρ	Scattering length densities
λ	Wavelength
γ	Interfacial tension of the oil-water interface
δ	Shell thickness
ΔA	Change in interfacial area on emulsification
ΔS	Change in dispersion entropy
ΔG_f	Free energy of microemulsion formation
$\phi_{\text{oil in shell}}$	Volume fraction of the oil in the shell

CHAPTER I

INTRODUCTION

Nanoemulsions (NE) are defined as the emulsion systems consisting of oil and water stabilised by surfactant with or without cosurfactant with the size ranging from 2 to 200 nm (Fryd and Mason, 2012; Solans and Solé, 2012). NE are considered to be different from microemulsions (ME) in that, for ME, they are spontaneously formed, thermodynamically stable and transparent. For NE, they require energy for emulsification, are kinetically stable and are not necessary to be transparent. In the present study, the clear NE will be defined instead of ME when the emulsions formed using some amounts of energy were previously defined as ME (Anton and Vandamme, 2011). Oil-in-water NE have attracted considerable attention as drug delivery vehicles for poorly-water soluble drugs (Date and Nagarsenker, 2007; Shah *et al.*, 2010, Ghai and Sinha, 2012). The oil phase of the emulsion system can act as solubilizer for the lipophilic compound (Narang *et al.*, 2007; Teo *et al.*, 2010).

Even though NE are acknowledged to have considerable potential as drug delivery vehicles, they are surprisingly yet to be widely commercially exploited. This lack of commercial use is largely due to the complexity in formulating NE, in particular the difficulty in finding pharmaceutically acceptable materials for their preparation and also by the need for cosurfactant that can lead to the destruction of the NE upon dilution due to the partitioning of the cosurfactant out of the interfacial region into the continuous phase (Tadros, 1984). The choices of surfactant selection

for NE formation based on critical packing parameter (CPP) and hydrophilic lipophilic balance (HLB) are limited, since the parameters do not take into account; for the CPP, the addition of oil and environment of surfactant at the interface (Solans *et al.*, 2002) and for the HLB, the surfactant concentration and the oil to water ratio (Attwood, 1994, Lijuan *et al.*, 2009). Therefore, the experimental work is needed in order to formulate NE (Wang *et al.*, 2009; Maali and Hamed, 2012).

Recently, the non-ionic polyoxyethylene ether (POE) surfactants have been reported as a choice for formulating NE for pharmaceutical use due to their biocompatibility, rather low toxicity and ability to produce NE without the need for any cosurfactants (Matsuyama *et al.*, 2006; Jiao, 2008; Feng *et al.*, 2009). Moreover, NE containing POE surfactant can be prepared by low energy emulsification such as the phase inversion temperature method (Izquierdo *et al.*, 2004, Anton and Vandamme, 2009). For the pharmaceutical choices of oils, triglycerides are considered to be acceptable since they are from natural sources. Triglyceride-contained NE are of great interest within the last years for solubilization of lipophilic compounds (Kunieda *et al.*, 2001; Engelskirchen *et al.*, 2007).

In general, the small molecular volume oils can be more solubilized by the surfactant than the larger molecular volume oils (Warisnoicharoen *et al.*, 2000a; Djekic and Primorac, 2008). It seemed to be true for oil solubilization by most of the POE surfactants. Surprisingly, however, for the polyoxyethylene-10-oleyl ether (POE-10 or C_{18:1}E₁₀) surfactant, the reverse trend was found in that the larger molecular volume oils especially triglyceride oils were able to be solubilised to the greater extent and provided the larger area of NE existence compared to those of smaller oil (Malcolmson *et al.*, 1998). From the previous study, POE-10-stabilized

NE can solubilise the larger molecular volume oil; for triglycerides, such as soybean oil to much greater extent than Miglyol and tributyrin; and for ethyl ester oils, such as ethyl oleate to much greater extent than ethyl caprylate and ethyl butyrate (Warisnoicharoen *et al.*, 2000a). For the solubilization of lipophilic drug, POE-10-stabilized NE exhibited a significant increase in solubilization of testosterone propionate over the corresponding micellar solution (Malcolmson *et al.*, 1998).

In the present study, the oil-in-water NE stabilized by the nonionic POE-10 surfactant containing either liquid triglycerides, consisting of C8 acyl chain length (trioctanoin or TON) and mostly C18 acyl chain length (soybean oil or SBO), or solid triglycerides, consisting of C12 acyl chain length (trilaurin or TLN) and C16 acyl chain length (tripalmitin or TPN) were studied. The difference in the nature of triglycerides in term of phase behaviour was determined since there were no reports on the comparison the area of NE existence between those using solid and liquid triglycerides. Although, the solid triglycerides have been used for the formulation of solid-lipid nanoparticles (SLN) (Windbergs *et al.*, 2009); however, there were several studies reported that some triglycerides in the nanoparticles can exist in a supercooled state at room temperature and the triglycerides could remain liquid for long time. Hence, in this case, the SLN containing solid triglycerides can be considered as o/w emulsions instead of the SLN (Bunjes and Westesen, 2001; Bunjes and Unruh, 2007).

The NE containing solid and liquid triglycerides were investigated for the amount of drug solubilization using the testosterone propionate as the model drug. The characterization of the NE was required since the understanding of physico-chemical properties of NE is important in order to see whether there is any correlation between molecular structure and drug solubilisation capacity. The NE were characterized for

phase inversion temperature and the size determination using dynamic light scattering. The differential scanning calorimetry (DSC) analysis was used to study the state of triglycerides in the NE. Moreover, the details of some NE structure would be supported using small angle neutron scattering (SANS) in combination with contrast variation. The information obtained from this study would help ultimately design NE as a drug carrier as well as provide the more understanding on the effect of the triglyceride nature on the properties and drug solubilisation capacity of the NE.

CHAPTER II

LITERATURE REVIEW

1. Nanotechnology and nanoparticles

1.1 Definition

Nanotechnology is the engineering and manufacturing of materials by controlling the shape and size at nanometer scale. Nanotechnology for medical use generally involves the use of nanomaterials, which for this purpose is described as materials with one or more components, which have at least one dimension in the range 1-100 nm. For the drug delivery system, nanoparticles come onto the scene as a type of drug delivery vector. Nanoparticles are a sub-set of nanomaterials and are generally defined as single particles with a diameter less than 100 nm, although sometimes particles of dimensions less than 1000 nm are also classified as nanoparticles (Farokhzad and Langer, 2009).

1.2 Classification of nanoparticles

The pharmaceuticals developed on the basis of nanotechnology are termed as “nanopharmaceuticals”. When considering their application as drug delivery vehicles, commonly defined nanoparticle vectors include liposomes, micelles, solid lipid

nanoparticles, polymeric micelles, microemulsions and nanoemulsions (Liggins and Burt, 2002; Gabizon, 2003; Paciotti *et al.*, 2006; Klumpp *et al.*, 2006; Dong *et al.*, 2009). **Figure 1** shows a range of the different types of nanoparticulate-based systems that have been explored as drug delivery systems along with their particle size range. The main components used to formulate these systems are polymers and lipids. Each of these carriers has its own individual physicochemical characteristics and differs in their stability, drug loading capacity, drug release rate and targeting ability.

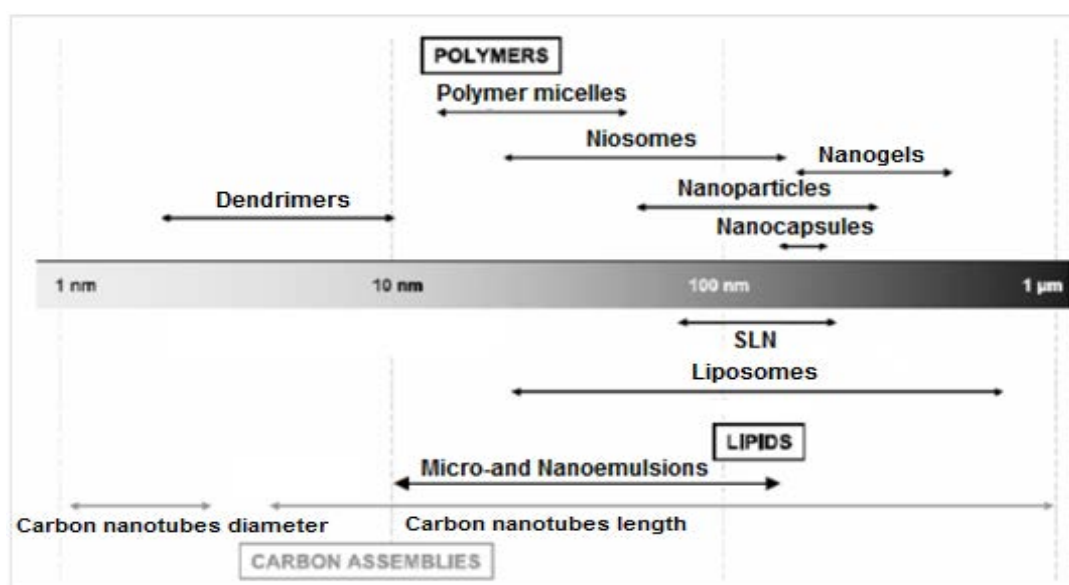


Figure 1 The main types of nanotechnology used for drug delivery system. The major components are either lipids or polymers. (Modified from Couvreur and Vauthier, 2006).

2. Micelles and nanoemulsions

2.1 Definition

Micelles are defined as an aggregation of amphiphilic surfactant molecules, which occurs in solution at a well-defined concentration called the critical micelle concentration (cmc). In polar media such as water, the hydrophobic part of the amphiphiles forming the micelle tends to locate away from the polar phase while the polar parts of the molecule (head groups) tend to be in contact with surrounding polar solvent, sequestering the hydrophobic tail regions in the micelle center. Inverse micelles by contrast have their surfactant molecules orientated such that their head groups are at the micelle center and their hydrophobic chains are on the exterior of the aggregates. Inverse micelles are formed in non polar media such as organic solvent (Husseini and Pitt, 2008). Micelles, particularly normal micelles are used in pharmaceutical because of their ability to increase the apparent aqueous solubility of poorly water soluble substances. Micelles have the potential to play a vital role in the pharmaceutical industry as drug delivery vehicles. However this role is presently limited, as many of the commercially available surfactants do not possess sufficient drug solubilising capacity to be practically useful (Croy and Kwon, 2005).

Nanoemulsions (NE) are emulsions with an extremely small droplet size which sometimes the definition can overlap with microemulsions (ME) (Gutierrez *et al.*, 2008; McClements, 2012). Although there are many similarities between ME and NE, namely they both are comprised of oil, water and surfactant and sometimes a co-surfactant and contain small (~ 5-100 nm for ME, and 20-200 nm for NE) surfactant-

stabilized droplets of narrow size distribution. There is one major difference between ME and NE in that ME are thermodynamically stable while NE are only kinetically stable (Anton and Vandamme, 2011). As a consequence, while ME are spontaneously formed by simply admixing the required ingredients, high-energy emulsification procedures, such as high-pressure homogenizers (Schultz *et al.*, 2004), sonicators and ultrasound generators (Kentish *et al.*, 2008; Gaikwad and Pandit, 2008) are generally needed to produce NE. In addition, low energy-emulsification procedures (e.g. phase inversion temperature, phase inversion composition and self-emulsifying methods (Izquierdo *et al.*, 2004; Maestro *et al.*, 2008) are also used to produce NE. As stated above that ME are clear in their appearance, however, NE can be clear, translucent and cloudy. The potential ability of NE to increase drug solubilising capacity, along with their stability, have been amongst some of the reasons why NE are a particularly attractive drug delivery system (Brime *et al.*, 2002; Shafiq *et al.*, 2007; Date and Nagarsenker, 2007). The ability of NE to increase drug solubilisation is considered over that of corresponding micelles due to the oil core inside the NE, supposing that the drug is soluble in the oil.

2.2 Choices of composition

Non-ionic surfactants are used in variety of pharmaceutical formulations including micelles, ME and NE (Matsuyama *et al.*, 2006; Feng *et al.*, 2009; Maali and Hamed Mosavian, 2012) since their advantages with respect to compatibility, stability, and toxicity are quite significant compared to cationic, anionic, or amphoteric counterparts. The nonionic molecules are comprised of both polar and

non-polar segments acquiring a wide range of interfacial activity and versatile functions as emulsifiers. Due to the uncharged nature of the head group, these surfactants are less sensitive than charged surfactants to salt, changes in pH and ionic strength of the aqueous phase. However, they are quite sensitive to temperature changes (Li *et al.*, 2009). The non-ionic are generally better tolerated than their anionic and cationic counterparts; the cmc of non-ionic surfactants is generally much lower than the cmc in the corresponding hydrocarbon chain length charged surfactants (Tan *et al.*, 2010; Inoue and Yamakana, 2011). The interfacial tension that polyethoxylated nonionic surfactants produce at the concentration they form aggregates is usually higher compared to that of ionic surfactants, making the nonionic surfactants less destructive on cell membranes and thus less irritating. The nonionics are usually more bulky in size, less polar and less preferentially adsorbed at the surface, therefore, having a tendency to associate together at much lower concentration to reduce the surface free energy (Jiao, 2008). In addition, they are less likely to undergo destruction upon introduction into the body and remain in their micellar form, even after administration into the blood stream where a large dilution occurs.

Polyoxyethylated nonionic surfactants are widely employed in various pharmaceutical applications among the nonionics and had shown the promising results, polysorbates, polyoxyethylene sorbitan, Tyloxapol, and Poloxamers are well known examples (Anton *et al.*, 2007; Date *et al.*, 2010; Djekic *et al.*, 2012). These surfactants contain a common hydrophilic moiety of the molecules, polyethylene oxide which has a repeated $(\text{CH}_2\text{CH}_2\text{O})_n$ ether structure with n generally in a range of 10 to 100 units. Even though, it is commonly accepted that the polyoxyethylene head

group serves as the hydrophilic region while the rest of the molecules serves as the lipophilic one. The hydrophilic polar head or the lipophilic alkyl tail may not be completely elucidated from the molecular structure owing to the amphiphilic nature of these nonionics which part of the molecule exhibiting dual nature with both hydrophilicity and lipophilicity (Jiao, 2008). The aqueous solubility of these nonionics depends both on the alkyl chain length and the number of ethylene oxide units in the molecule. According to the HLB system, the higher the polyethylene oxide in the molecule, the higher HLB value of surfactant and as consequence more soluble in aqueous solution (Tadros, 2005). The non-ionic surfactant used in this context contains an ethylene oxide alkyl ether type, C_mE_n , where m is the chain length of the hydrocarbon, and n is the number of ethylene oxide units that make up the hydrophilic head group (Morales *et al.*, 2006, Engelskirchen *et al.*, 2007). The use of a non-ionic surfactant polyoxyethylene 10-oleyl ether ($C_{18:1}E_{10}$) to stabilize the NE is attractive as it is possible to produce NE without the need for a cosurfactant and is favorable for the emulsification with various oils (Malcolmson *et al.*, 1997; Ko *et al.*, 2003; Morales *et al.*, 2006).

In formulation of NE which will be used as drug delivery, it is very important to determine which oils would form NE at a given surfactant. The choice of the oil phase is sometimes difficult because it is important for both the area of existence of NE and the solubilisation capacity (Djekic and Primorac, 2008). The amphiphilic oils such as medium- or long-chain triglycerides and fatty acid ester are regularly used in the pharmaceutical formulation because they are compatible with biological systems and environmental friendly compared with ordinary hydrocarbon oils. These oils

influence the surfactant layer curvature in aggregates or self organized structures when solubilised (Kunieda *et al.*, 2001).

Medium-chain and long-chain triglycerides from vegetable oil are commonly selected in commercial application because these oils could provide desirable physical and drug absorption properties (Haus, 2007). Lymphatic transport could be promoted by long chain triglyceride which delivers drug into lymph before entering the systemic circulation while avoiding hepatic first-pass metabolism (Khoo *et al.*, 2003). Triglyceride is made up of three fatty acids and glycerol backbone (**Figure 2**). The three fatty acids can be all the different, all the same or only two the same. Fatty acids vary in the length of their carbon atom chain and the number of double bonds they contain. Medium chain triglycerides are shown to be solubilised with lower concentration of PEG-8 caprylic/capric glycerides surfactant than long chain triglycerides (Djekic and Primorac, 2008). In contrast to the previous study which had shown that the POE-10 can solubilise long chain triglycerides to a greater extent than its medium or short chain (Warisnoicharoen *et al.*, 2000a). Hence, the formation of NE depends on both the structure of oils and surfactants.

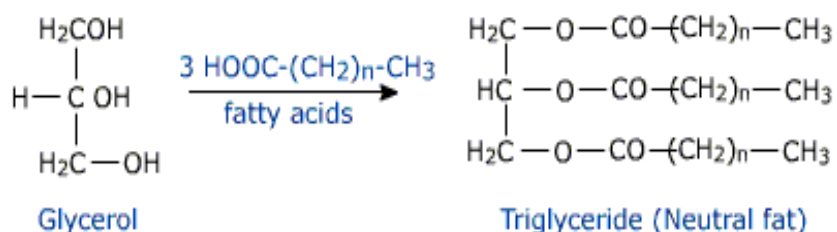


Figure 2 The formation and structure of triglyceride.

3. Formation of micelles and nanoemulsions

3.1 Formation of micelles

The process of micelle formation is known as micellisation which can form a variety of aggregates, dependent upon surfactant molecular structure and concentration. The concentration at which aggregation occurs is traditionally known as the „cmc“, irrespective of the type of aggregate formed. During the micellisation process, the hydrophobic part of a surfactant associates to form the core region and the hydrophilic part is facing outwards into the external aqueous medium assemble between the core and aqueous phase (**Figure 3**) (Pasquali, 2010). Below the cmc, the number of individual surfactant molecules adsorbing at the air-water interface increase with increasing concentration of surfactants. The spontaneous aggregation of micelles can be understood by considering the thermodynamics of the system; micelles can form spontaneously because of a balance between the entropy and enthalpy of the system. In water, the hydrophobic effect is the driving force for micelle formation, despite the fact that assembling of the surfactant molecules together reduces their individual entropy (Chevalier and Zemb, 1990). Micelles only form when the concentrations of surfactant reach the „cmc“ of the surfactant, driven entropically via the expulsion of ordered water molecules into bulk aqueous phase. The change in free energy is expressed by (Attwood *et al.*, 1974):

$$\Delta G = RT \ln(\text{CMC}) \quad (1)$$

where;

ΔG = free energy (J mol^{-1})

R = the gas constant ($8.314 \text{ J K}^{-1} \text{ mol}^{-1}$)

T= the temperature of the system (K)

In general, the cmc value of polyoxyethylated nonionic surfactants is about two folds lower than the corresponding anionics surfactant with the same alkyl chain length. The assembly of the surfactants into micelles can be largely explained by the relative interactions between the hydrophilic and hydrophobic segments with one another and the surrounding medium (Adams *et al.*, 2003). The enthalpy such as the electrostatic interactions that occur between the charges of surfactants head groups (ionic surfactant) and hydration forces (non-ionic surfactant) are important to take in considerations (Chen, 1986; Zdziennicka *et al.*, 2012).

The shape of the micelle formed is influenced to a large extent by the geometry of the surfactant molecule based on packing considerations of surfactants which is called the critical packing parameter (CPP) and is defined as

$$\text{CPP} = \frac{v}{a_0 l_c} \quad (2)$$

where;

v= the volume of the hydrocarbon chain (nm^3)

a_0 = the cross-sectional area of the surfactant head group (nm^2)

l_c = extended length of the surfactant alkyl chain (nm)

This parameter provides a simple geometric characterization of the surfactant molecule which is useful when considered the structure of aggregate forming in solution which can be used to indicate the structure of the surfactant system as illustrated in **Figure 4**. Consideration of the packing of molecules into spheres shows that when $CPP < 1/3$, which is the case for surfactants having a single hydrophobic chain and a simple ionic or large nonionic head group, a spherical micelle will be formed. Most surfactants of pharmaceutical interest fall into this category. It is easily seen that if increasing the hydrophobic volume of surfactant tail then the value of CPP will exceed $1/3$ and nonspherical structures such as bilayers ($CPP \approx 1$) will form (Stuart and Boekema, 2007). One important factor not considered in this simple geometrical model is the interaction between the head groups in the aggregate.

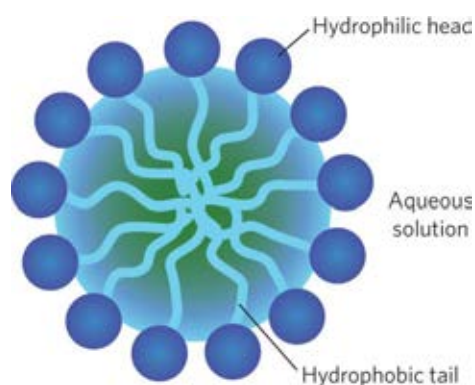


Figure 3 A schematic diagram of a spherical micelle of surfactant molecules in aqueous solution (Pasquali, 2010).

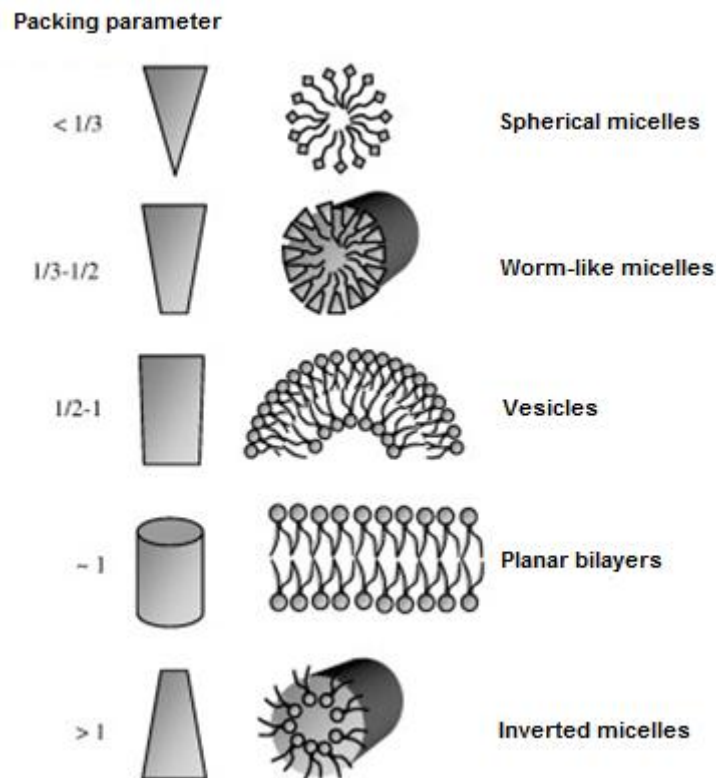


Figure 4 Packing properties of surfactant aggregate and the critical packing parameter (Stuart and Boekema, 2007).

3.2 Formation of nanoemulsions

The formation of NE can be easily explained using a simplified thermodynamic rationalization. The free energy of NE formation is considered to depend upon both the extent to which the surfactant lowers the interfacial tension at the oil-water interface and the change in entropy of the system upon NE formation such that (Tadros *et al.*, 2004):

$$\Delta G_f = \gamma \Delta A - T \Delta S \quad (3)$$

where;

ΔG_f = the free energy of nanoemulsion formation (J mol^{-1})

γ = the interfacial tension of the oil-water interface (mN m^{-1})

ΔA = the change in interfacial area on emulsification (m^2)

ΔS = the change in dispersion entropy ($\text{J K}^{-1} \text{mol}^{-1}$)

T = temperature (K)

An extreme lowering of interfacial tension is a key factor in the formation and stability of NE systems. The interfacial tension between the oil and aqueous phases must be small enough to compensate for the increase in entropy resulting from the dispersion of one phase in another (Bellare *et al.*, 1999). For a spontaneous process to occur ΔG_f must be negative. In order to achieve a negative value of ΔG_f , γ should usually be extremely low (10^{-2} - 10^{-5} mN m^{-1}) (Kunieda and Friberg, 1981). From a stand point of entropy a large number of small droplets are favoured over a small number of large ones. When NE is formed there is a large, unfavourable change in ΔA due to the large number of small droplets formed, at least in part, counterbalanced by the ultra low interfacial tension present in NE (Ruckenstein and Krishnan, 1980). There are also favourable, entropic contributions arising from the processes of dispersing the oil in water and other processes such as surfactant diffusion in the interfacial layer and monomer-micelle surfactant exchange (Solans *et al.*, 2002). Overall, if a negative free energy of formation is achieved when large reduction in interfacial tension is accompanied by a significant favourable entropic change, ME is formed spontaneously and the resulting dispersion is thermodynamically stable. For NE, as there is more oil incorporating in the droplet resulting in the less negative free

energy and leading to the kinetically stable system. The advantage of ME over NE is the thermodynamic stable; however, the NE which exhibit sufficiently high kinetic stability can be exploited as a delivery vehicle in pharmaceutical use (Girard *et al.*, 1997; Tadros *et al.*, 2004).

4. Structure of nanoemulsions

Nanoemulsions are classified into oil-in-water (o/w), water-in-oil (w/o) and bicontinuous types (**Figure 5**). Evidence appears to suggest that when a small amount of oil is present, o/w nanoemulsion droplets are likely, and when only a small amount of water is present, w/o droplets occur. If there are comparable amount of oil and water, bicontinuous systems are most possible (Hall, 1987). In addition, the type of NE stabilized by nonionic surfactants is highly dependent on temperature. If the temperature is below the phase inversion temperature (PIT) the surfactant is preferentially soluble in the water and the o/w type is formed. In contrast, at the temperatures above the PIT, the surfactant prefers to reside in the oils favoured the formation of w/o droplets (Izquierdo *et al.*, 2004; Morales *et al.*, 2006).

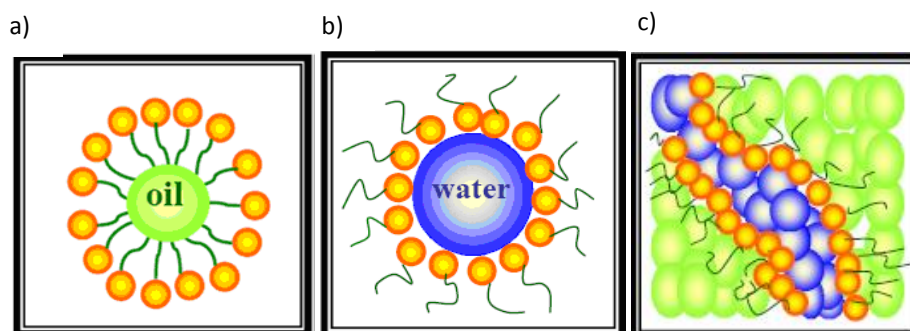


Figure 5 Schematic representation of the most commonly encountered nanoemulsion structures: (a) oil-in-water and (b) water-in-oil (c) bicontinuous types.

5. Pharmaceutical application of nanoemulsions

The interest in nanoemulsions in terms of their drug delivery potential has experienced a continuous increase in the last years, as evidenced by the numerous publications on the subject (Gutiérrez *et al.*, 2008; Date *et al.*, 2010). The attraction of nanoemulsions for pharmaceutical applications is a consequence of: (i) their very small droplet size and high surface area which are suitable for efficient delivery of active ingredients through the membrane, (ii) their high kinetic stability offering a number of advantages over traditional, unstable dispersions, (iii) high solubilizing capacity for a wide range of drug molecules and (iv) ease of preparation and sterilization by filtration (Kentish *et al.*, 2008; Maestro *et al.*, 2008; Shah *et al.*, 2010).

Oil-in-water NE have been widely employed for the solubilisation and increased bioavailability of hydrophobic molecules. NE have been shown to enhance the oral bioavailability of a range of drugs (Shafiq *et al.*, 2007; Singh and Vingkar,

2008). NE also provide protection to the drug against oxidation and enzymatic hydrolysis (Solans and Kuneida, 1997). There were a number of reports on the use of NE as drug carriers for a whole range of administration routes including transdermal (Dixit *et al.*, 2008), pulmonary (Bivas-Benita *et al.*, 2004) and intravenous (Ahmed *et al.*, 2008). The phenomenon of drug solubilization in NE has been investigated (Tiwari and Amiji, 2006; Talegaonkar *et al.*, 2008). In o/w NE, hydrophobic molecules are solubilised within the oil core; while hydrophilic molecules are located at a position between the hydrophobic chains of the surfactant and the surfactant head group dependent upon its hydrophilicity (Torchilin, 2001). The primary locus of drug solubilisation depends on drug hydrophobicity and its interaction with the oil, surfactant and/or cosurfactant. The examples of commercial NE formulations as drug delivery are shown in **Table 1**.

Table 1 Commercial nanoemulsions formulation (Tiwari and Amiji, 2006).

Drug therapeutic	Brand	Manufacturer	Indication
Propofol	Diprivan®	Astra Zeneca	Anesthetic
Dexamethasone	Limethason®	Mitsubishi Pharmaceutical, Japan	Steroid
Palmitate Alprostadil	Liple®	Mitsubishi Pharmaceutical, Japan	Vasodilator platelet inhibitor
Flurbiprofen axetil	Ropion®	Kaken Pharmaceuticals, Japan	Nonsteroidal analgesic
Vitamin A,D,E,K	Vitalipid®	Fresenius Kabi, Europe	Parenteral nutrition

6. Physicochemical characterization of micelles and nanoemulsions

As NE have attracted attention as potential drug delivery systems, the relationship between their solubilisation capability and physico-chemical properties are still needed to be fully elucidated. There are a wide range of different techniques that can be used to characterize NE. A number of researchers have characterised NE with respect to the effect of the composition, for examples, the phase behavior, the size and shape of the NE droplets (Rube *et al.*, 2005; Yuan *et al.*, 2008; Kuntsche *et al.*, 2011, Sharma and Warr, 2012). A full understanding of the influence of the physico-chemical properties of the internal microemulsion droplets is required. It is generally recognized that at least two complementary methods are required to fully characterize NE.

6.1 Phase behaviour

The study of phase behaviour is used to determine the types of NE formed and their stability which is related to the composition of the three main components; oil, surfactant (or surfactants) and water. Phase diagrams are simple to be prepared and can convey a large amount of information on the phase behaviour of a system. Each apex of the triangle represents 100% of that particular component (Kumar and Mittal, 1999). **Figure 6** illustrates some of the possible structures that are commonly formed by a ternary mixture of oil, surfactant and water (Talegaonkar *et al.*, 2008). It appears clearly that micelles and bilayers are the building blocks of the self-assembled structures commonly formed. In relevance to the present study is the fact that the area

in phase diagram between microemulsion and coarse emulsion are of interest. The formations of this area are referred as nanoemulsion in which the formation and stability will be observed.

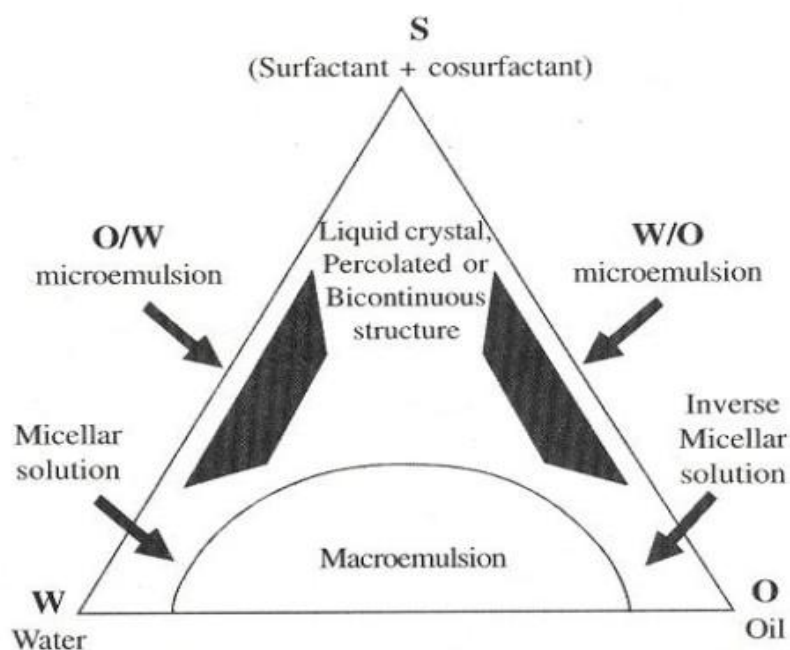


Figure 6 Schematic diagram illustrating the phase behaviour of oil/water/surfactant systems. (modified from Talegaonkar *et al.*, 2008).

6.2 Phase inversion temperature

The transition from an o/w to w/o NE may occur with certain non-ionic surfactants upon altering either phase volume and/or temperature. It is well known that most of non-ionic surfactants, especially the polyoxyethylene types, form aqueous micellar solutions which exhibit a phase inversion temperature (PIT) upon

heating (Corti *et al.*, 2002). Once the system reaches the PIT, the solution turns from clear to cloudy and *vice versa*, as the solution temperature is increased and decreased. However, it is not possible to observe the PIT of the cloudy NE as the temperature where the solution turns cloudy cannot be determined with cloudy solutions. The interactions between the surfactant monomers in the aggregate change from repulsive to attractive forces at higher temperature. For instant, increasing the temperature of aqueous polyoxyethylene ether surfactants causes the ethylene oxide units to become dehydrated leading to a decrease in the effective surfactant head group area and, then, the changes of aggregate shape to be more elongated or even bicontinuous in nature and finally inverted to form water in oil structure (Tadros, 2005). The information obtained from the PIT experiment indicates the arrangement of the oil in the surfactant aggregate. The observed changes in PIT are typically explained in terms of the way in which oils of different molecular volume/weight are solubilized into the droplets (Schuber and Kaler, 1996). When there is a drop in PIT from their corresponding micelle, it means that the micellar aggregates are originally slightly asymmetric. In contrast, PIT increases when the oil concentration increases indicating that the oil forms a core in the centre of the NE droplet (Aveyard and Lawless, 1986; Malcolmson *et al.*, 1998). If there is no increase in the PIT once oil concentration increases; this will suggest that the oil chains intimately mix with the surfactant chains rather than forming a substantial core in the centre of the NE droplet.

6.3 Dynamic light scattering

In dynamic light scattering (DLS) or photon correlation spectroscopy (PCS) study, time-dependent fluctuations of the light intensity from NE droplets are measured. These fluctuations, due to Brownian motion of the aggregates in solution, can be analyzed in terms of the scattered intensity which contains information about the dynamics of the scattering particles. Large particles will move more slowly and hence result in lower intensity fluctuations. Analysis of the autocorrelation function is obtained over a period of time and with sufficient data points the diffusion coefficient of the particles can be determined. The information about the diffusion coefficient (D_0) can then be used to calculate size, hydrodynamic radius (R_h) using the Stokes-Einstein equation (Miller, 1924):

$$R_h = \frac{k_B T}{6\pi\eta D_0} \quad (4)$$

where;

R_h = hydrodynamic radius (nm)

k_B = Boltzmann constant (1.38065×10^{-23} J K⁻¹)

T= absolute temperature (K)

D_0 = diffusion coefficient (nm²s⁻¹)

η = viscosity of the medium (Nm⁻²s)

The DLS or PCS has been widely used to determine the size distribution profile of small particles in solution (Anton *et al.*, 2007; Nobbmann and Morfesis,

2009) as well as to assess the stability profile of systems by measuring droplet diameters as a function of time. For example, Izquierdo *et al.* (2005) used this method to investigate the stability of o/w NE containing water/mixed nonionic surfactants/isohehexadecane. The results showed that the mechanism that led to instability of the NE were Ostwald ripening. Moreover, the droplet size determination can determine the effect of the components in the systems. For example, Sadurni *et al.* (2005) reported that the droplet size increased from 14 to 39 nm when the oil/surfactant ratios were varied from 10/90 and 40/60 respectively. Some limitation in light scattering studies of NE is that in many cases the systems need to be diluted before testing which is likely to modify the structure and composition of the different domains and possibly result in the disappearance of NE droplets (Tadros, 1984).

6.4 Small angle neutron scattering

Neutron scattering is one of the most powerful and versatile experimental methods to study the structure and dynamics of materials on the nanometer scale. Small angle neutron scattering (SANS) is a diffraction technique which exploits the wave particle duality of a neutron and its unique nuclear properties to provide information about the size and shape of molecules and their assemblies (Chen, 1986; Bergstrom and Pedersen, 1999). Although SANS is a great technique, it is also slow and expensive; the experiment takes several days and is performed at large international facilities. Here, the running costs correspond to thousands of Euros per instrument day. Hence, neutron scattering should be used only where other methods are inadequate.

There are two common ways of producing neutrons; one is by the fission of a heavy atom such as uranium-235 in a nuclear reactor which is known as a continuous source (Lindner and Zemb, 1991). The neutron source at the Institute Laue Langevin (ILL), Grenoble, France and at the National Institute of Standards and Technology (NIST), Gaithersburg, USA are examples of reactor sources. The other way to produce neutrons is by using a spallation source where the neutrons are produced by bombarding a target of heavy elements with high-energy particles resulting in the production of protons, muons, and neutrons as illustrated in **Figure 7** (King, 2004). The Rutherford-Appleton Laboratory (RAL), Didcot, UK is an example of a spallation source. The neutron source at RAL is used exclusively in the present study.

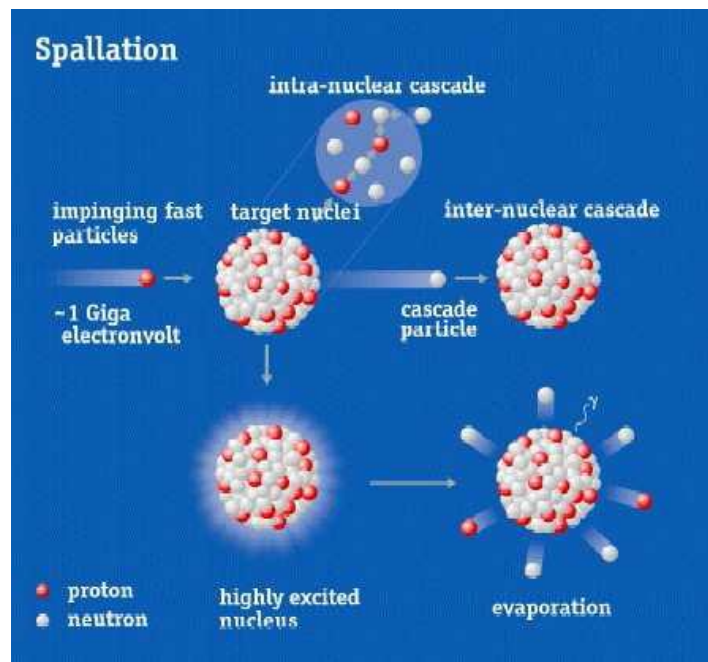


Figure 7 Protons accelerated into the Giga electronvolt regime can split heavy nuclei with a large neutron surplus, creating free neutrons as a part of the reaction products (King, 2004).

Neutrons are being moderated to thermal velocities close to the source and then transported to the neutron scattering instruments in neutron guide systems. When neutrons pass through a sample, they collide with nuclei and are scattered. The results of the SANS studies provide complimentary and more detailed information about NE than the light scattering studies. The neutron scattering differs from the light scattering and X-ray scattering in which the light scattering and X-ray are both scattered by electrons whereas neutrons are scattered by the nucleus. The interaction of a neutron with the nucleus of an atom is weak, although not negligible, making them a highly penetrating probe and allowing the study of solutions (Hayter and Penfold, 1983). As neutrons scatter from materials by interacting with the nucleus of an atom rather than the electron cloud, this means that the scattering power of an atom is not strongly related to its atomic number. In fact, hydrogen and deuterium which have different and opposite scattering length densities are an essential property in a neutron scattering experiment (**Figure 8**). Owing to this difference of scattering length, part of the structure of interest can be highlighted by selective deuteration or conversely can be rendered invisible to neutrons by contrast-matching which makes it possible to highlight or hide different parts of the systems (Rübe *et al.*, 2005). The hydrogenated and deuterated chemicals used are selected to highlight specific components (surfactants, oils and water) in the nanoemulsion droplets. Typically, both deuterated (D) and protonated (H) oils and water are used with the normal protonated version of the surfactant, as D/H/H, D/H/D and H/H/D combinations of water/surfactant/oils for the drop, shell and core contrast respectively (**Figure 9**). The drop, shell and core parts represent the whole NE droplet, the surfactant part and the triglyceride that is incorporated in the centre of the NE droplet, respectively (**Figure 10**).

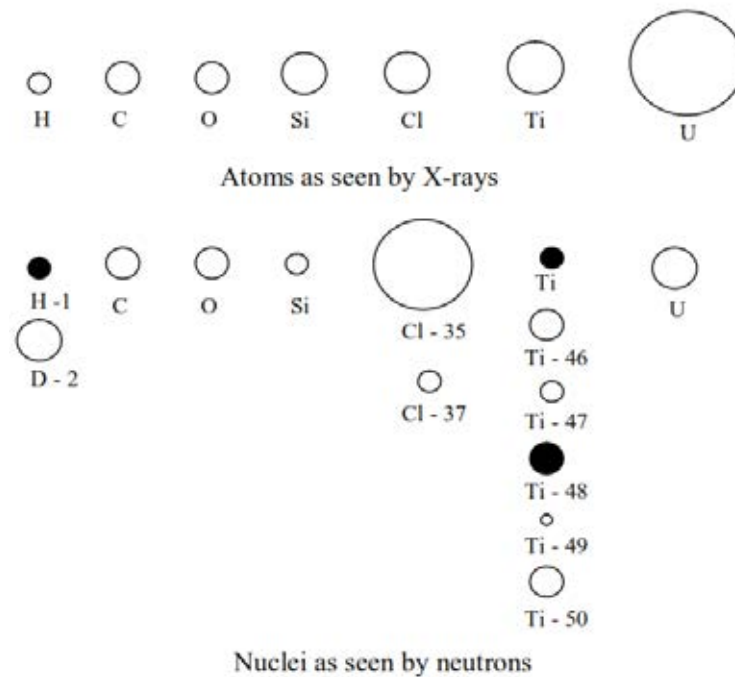


Figure 8 Neutrons are scattered from the nuclei whereas X-rays are scattered from electrons. Negative neutron scattering lengths are represented by a black circle (Hsieh, 2010).

By combining all three contrasts that are studied for NE composition study and simultaneously analyzing the data, it is possible to obtain structural information about NE droplets with a high degree of confidence. The time-of-flight technique is used to obtain the energy and wavelength of each neutron allowing fixed scattering geometries to be used. Briefly the initial position and velocity of a pulse of neutrons are fixed, and their final position and the time after the pulse that the neutrons detected are measured (Summers *et al.*, 2001).

The SANS studies allow a better understanding of the relationship between the microstructure of the NE droplets and the amount of oil solubilised. In comparison to

PCS, SANS covers length scales which are associated with the internal structure of NE droplets. The advantages of using neutrons as the scattering source include their ability to interact through short-range nuclear interactions due to the fact that they do not possess a charge and are very penetrating which in turn do not destroy the sample. Also, they interact differently with hydrogen and deuterium, making it possible to highlight parts of system under study. In most cases, neutron scattering is performed in combination with other experimental techniques.

Recently, Hsieh (2010) studied the NE systems containing ethyl butyrate (EB) and ethyl caprylate (EC) formed by 3-N, N-dimethyl dodecyl ammonio propane-sulfonate (DDAPS). The results showed the advantage of SANS over DLS in that SANS can be used to obtain detailed structural information on the droplets by selective deuteration of various components. For example, the DLS result only indicated an increase in droplet size when the EC content increased where the size of droplet containing EB content did not increase but similar to the corresponding DDAPS micelles. The SANS results further explained that at least 90% of EB resided in the surfactant shell of the ME whereas only 50% of EC resided in the surfactant shell in DDAPS-stabilised ME. It is clear from the results that the smaller molecular volume oil, EB, does not form a core in the centre of the NE droplet but rather is dispersed throughout the NE. In contrast, the larger molecular volume oil, EC, forms at least in part a distinct core, which provides an extra locus for drug solubilisation (Hsieh, 2010).

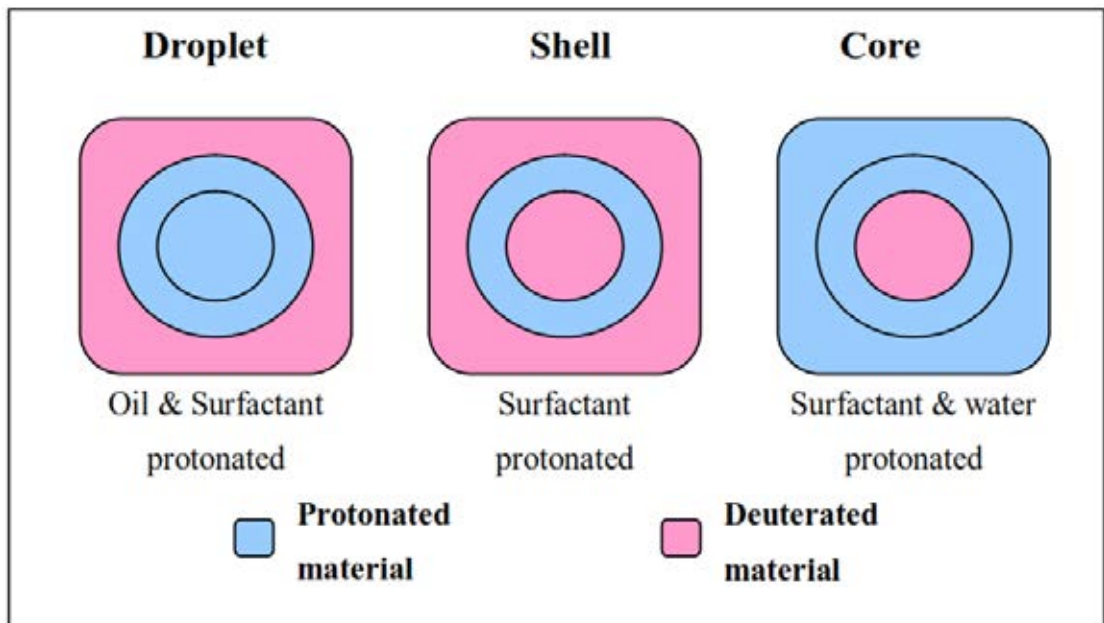


Figure 9 Schematic representation of a SANS experiment of an oil-in-water nanoemulsion exploiting contrast matching.

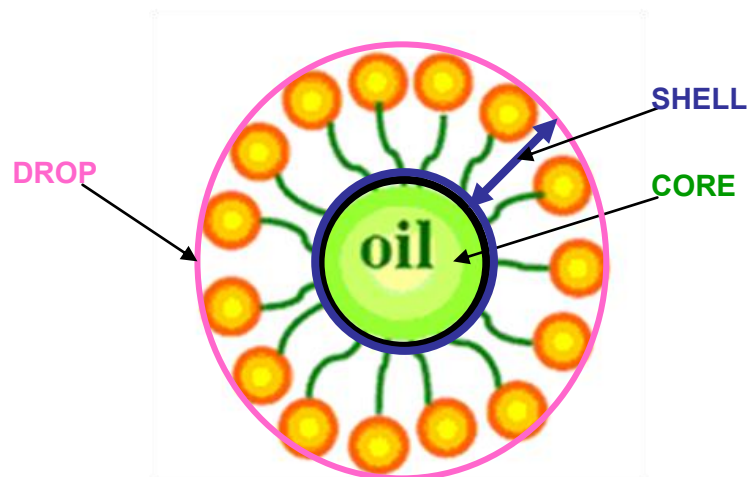


Figure 10 Schematic representation of drop, shell and core part of oil-in-water nanoemulsion.

6.5 Differential scanning calorimetry

The differential scanning calorimetry (DSC) is one of the most commonly used technique of thermal characterization of physico-chemical transformations of substances. It is an analytical instrument designed to monitoring the heat exchanges between the sample and a reference either *versus* time at constant temperature or *versus* temperature during a heating or cooling program. The heat capacity and changes in heat capacity as a function of temperature are measured. Chemical processes such as crystal structure transitions, phase changes (e.g. melting), and biopolymer denaturation can be initiated by elevating the temperature of the sample (Clause, 1998; Dalmazzone *et al.*, 2009).

For the study of the emulsion, DSC is permitted to study various phenomena that are accompanied by either a release or an adsorption of energy, the obvious one is freezing and melting of the dispersed phase (Clause, 2010). The multi-cell DSC can measure the apparent change in heat capacity involved in the solidification and melting properties of these complex fluids. The surfactant molecules are capable of partitioning between continuous aqueous phase or interior of dispersed oil droplets or interface and they have effects not only on the initial temperature of crystallization but also on the rise of solid fat content (Hindle *et al.*, 2000, Relkin and Sourdet, 2005). The energy released during the droplets melting is evidenced on the obtained thermogram as an endothermic peak and the energy released during the droplets solidifying is evidenced on the obtained thermogram as an exothermic peak (Coupland, 2002). The emulsification procedure and ingredients complexity have a dominate role in characteristics of oil droplets, such as particle size diameters and size

distributions, compositions and physical properties of surrounding surface layers and also crystallization of oil content and polymorphism (Arima *et al.*, 2007). The DSC technique has been proposed for following the evolution of emulsion, for example, the previous research reported the differences in freezing curve of water in oil emulsions from -39°C to -12°C obtained at different times showing that the emulsion is separated into two distinct phases (Clausse *et al.*, 2008). In addition, several studies indicated that the addition of vitamin E was shown to protect oil-in-water NE against storage degradation and the effects of vitamin E addition depended on the lipid composition (Relkin *et al.*, 2008, Relkin *et al.*, 2009). Moreover, studies performed on fat thermal transitions showed that crystallization temperature of dispersed fat droplets in nanoparticles was lowered, compared to bulk fat, and the degree of supercooling temperature was different depending on triglyceride composition, mean droplet size and lipophilic or hydrophilic nature of emulsifiers (Westesen and Bunjes, 1995; Bunjes, 2011).

Oil in water NE is useful for enhancing the hydrophobic molecules in which depending on the NE compositions, for example, type of oils incorporated in NE. Therefore, in the present study, oil-in-water NE stabilised by the nonionic polyoxyethylene 10-oleyl ether containing series of triglyceride either liquid triglycerides, soybean oil (SBO) and trioctanoin (TON) or solid triglycerides, tripalmitin (TPN) and trilaurin (TLN) are investigated. The effect of triglyceride on NE formation is examined. The physico-chemical properties of oil-in-water NE are observed by various characterization techniques which will all be described in next chapters.

CHAPTER III

MATERIALS AND METHODS

1. Materials

Testosterone propionate (TP), polyoxyethylene-10-oleyl ether ($C_{18:1}E_{10}$, Brij 96, PEO-10) are all purchased from Sigma Chemicals Ltd. (Dorset, UK). Trilaurin (TLN, purity >90%), C_{12} triglyceride, and soybean oil (SBO), a mixture of predominately (i.e. > 75%) $C_{18:1}$ and $C_{18:2}$ triglycerides, were from ACROS Organic (New Jersey, USA). Tripalmitin (TPN, purity >85%), C_{16} triglyceride in both protonated (*h*-) and deuterated (*d*-) forms was purchased from Sigma Chemicals Ltd. (Dorset, UK). Trioctanoin (TON, purity >90%), *h*- C_8 and *d*- C_8 triglycerides, trioctanoin (TON, purity >90%) was purchased from Fluka Chemicals (St. Gallen, Switzerland). Isopropanol was purchased from Fisher Scientific (Leicestershire, UK). D_2O (99.9 atom% D) was obtained from Aldrich Chemical Company (Dorset, UK). All chemicals were used as received. Double distilled, spectroscopically pure water, obtained from a well-seasoned glass apparatus was used throughout the experiments. **Figure 11 and Table 2** show the chemical structures of TON, TPN and TLN and the molecular weight and molecular volume of SBO, TON, TPN and TLN. It is noted that the chemical structure of SBO is varied due to the natural sources of the raw material. The chemical structure of $C_{18:1}E_{10}$ is illustrated in **Figure 12**.

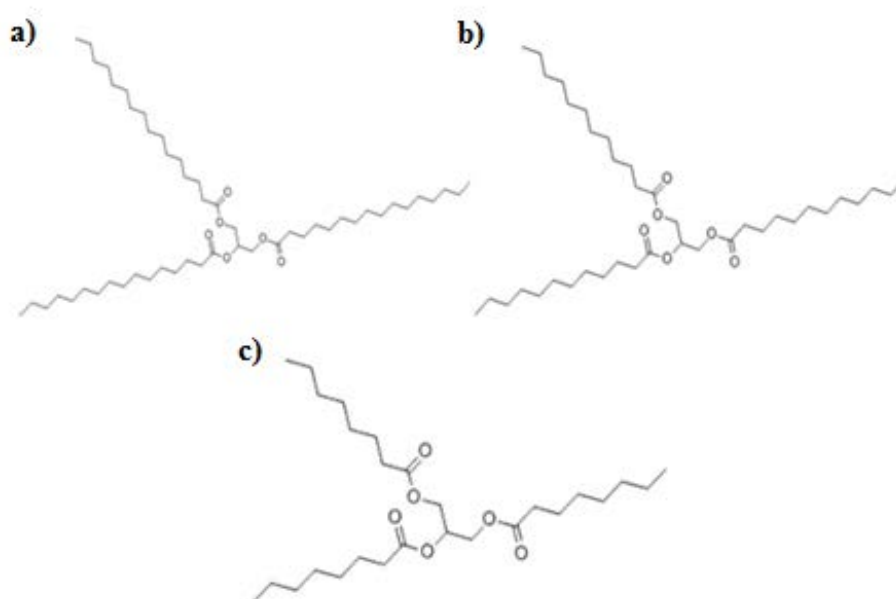


Figure 11 The chemical structures of a) tripalmitin (TPN), b) trilaurin (TLN) and c) trioctanoin (TON).

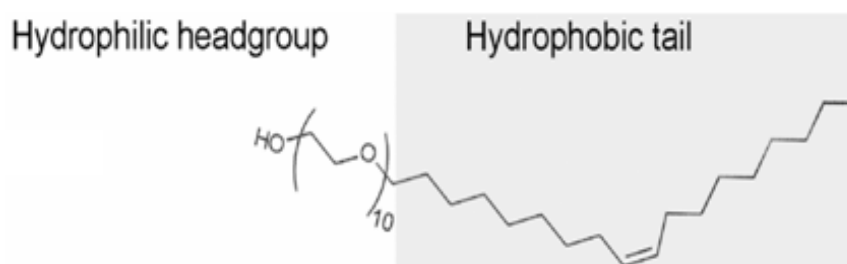


Figure 12 The chemical structure of polyoxyethylene 10-oleyl ether (C_{18:1}E₁₀) surfactant.

Table 2 Molecular weight and molecular volume of the triglycerides

Triglyceride	Molecular weight (g/mole)	Molecular volume (Å³)
Soybean oil	885.5	1563
Tripalmitin	807.3	1492
Trilaurin	639.0	1168
Trioctanoin	470.7	844

2. Preparation of nanoemulsions and determination of phase diagrams

2.1 Preliminary study of preparation method

2.1.1 Phase inversion temperature method

A number of individual samples are prepared based on the phase inversion temperature (PIT) or heating and cooling method (Brooks *et al.*, 1998, Anton *et al.*, 2007). Briefly, nanoemulsions (NE) were individually prepared by weighing the required amount of triglyceride, surfactant (C_{18:1}E₁₀) and water at room temperature. For each sample a total of 5 g was prepared. A small magnetic stirrer was placed into the sample vial and the samples were heated to 70-75°C for ten minutes and cooling to 22 ± 2°C with vigorous stirring throughout. After preparation the samples were placed in tightly sealed containers and stored at room temperature (22 ± 2°C). The overall procedure was depicted in **Figure 13**.

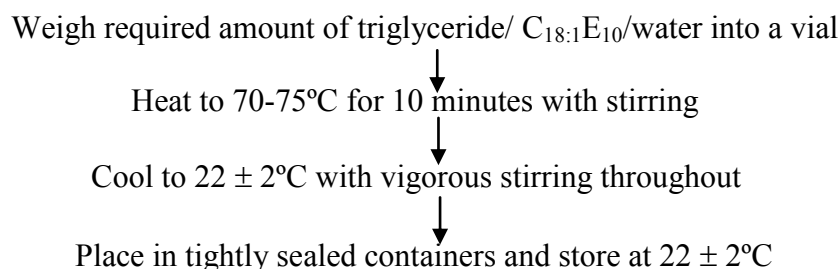


Figure 13 Preparation of oil-in-water (o/w) nanoemulsions stabilised by the nonionic surfactant polyoxyethylene 10-oleyl ether, C_{18:1}E₁₀, and containing a triglyceride.

2.1.2 Sonication method

Samples were individually prepared by weighing the required amount of triglyceride, surfactant (C_{18:1}E₁₀) and water at room temperature. For each sample a total of 5 g is prepared. Samples were subjected to emulsify by ultrasonication using 20 kHz ultrasonicator equipped with an ultrasonic probe with a 3-mm diameter, in which case the required amount of triglyceride, C_{18:1}E₁₀ and water were mixed and the resulting mixture was sonicated until the solution homogeneously mixed (Kentish *et al.*, 2008, Cucheval and Chow, 2008). After the sonication the mixtures were stirred at room temperature. The samples were placed in tightly sealed containers and stored at room temperature (22 ± 2°C) after preparation.

From the results, it was found that both methods produced the NE (see **Appendix**). However, the phase inversion temperature method was preferred over the sonication method due to ease of preparation, less time consuming compared to the

sonication method, economic reason and the avoidance of contamination of the metal precipitation that may occur during sonication.

2.2 Determination of phase diagrams

As mentioned earlier, the phase inversion temperature method was used to prepare the NE and subsequently determined for area of NE formation. After preparation, the samples were routinely examined visually immediately for stability after preparation, 24 hours, one week, two weeks and one month. A range of compositions were visually examined for any physical change i.e. the change from clear to cloudy or phase separation. NE were said to have been formed when samples were one-phase fluid, non-birefringent and stable for at least one month. Non-birefringent systems that did not change their meniscus after tilting to an angle of 90° were classified as NE gels and would not be further studied. Stable formulations were plotted on a triangular phase diagram in 3-component systems (triglyceride/surfactant (SAA)/water) where each apex of the triangular plot represents 100% of one of the three ingredients (**Figure 14a**). Each point within the triangle represents different combinations of the three components. Determination of the area of NE existence was performed at least in duplicate to ensure an accuracy of better than ± 1 wt% triglyceride. Clear NE would be plotted in the triangular phase diagram and described as Region A, bluish or translucent NE was denoted as Region B and cloudy or milky NE as Region C. The partial triangular diagram in **Figure 14b** represents an example of the Regions A, B and C of NE.

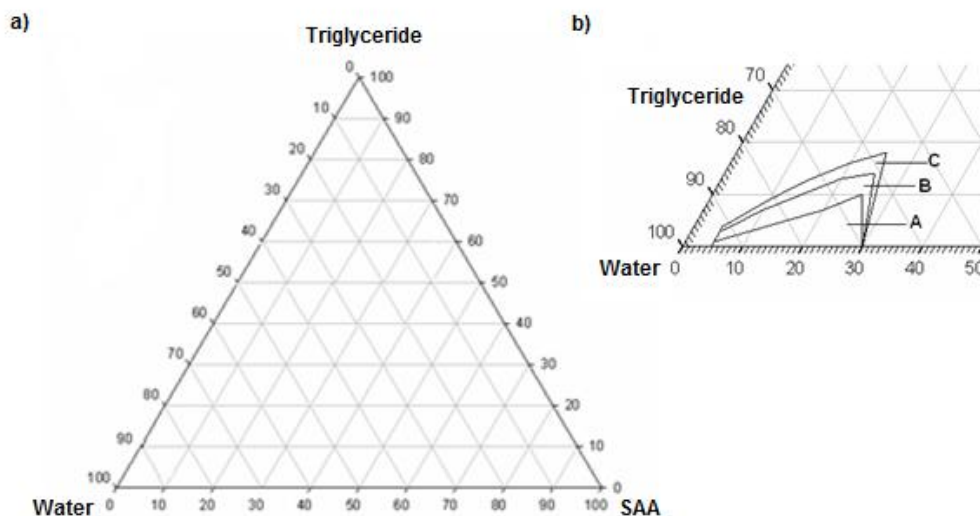


Figure 14 Tertiary phase diagram (a) and partially tertiary phase diagram (b) representing Regions A (clear), B (bluish or translucent) and C (cloudy or milky) of NE.

3. Characterization of nanoemulsions

3.1 Analysis of hydrodynamic droplet size

Photon correlation spectroscopy (PCS) was employed to investigate the size distribution of o/w NE samples when the concentrations of oil phase were varied. PCS measurement was made on dilute samples using a Brookhaven light scatterer (Brookhaven Instruments Corporation, Holtsville, USA) at a scattering angle of 90° and temperature of $22 \pm 2^\circ\text{C}$. The samples were clarified by ultra-filtration through a $0.45 \mu\text{m}$ cellulose acetate filter (Millipore, Goettingen, Germany) immediately prior to examination by PCS. The average diameter and polydispersity of each sample were determined assuming that the hydrodynamic size of NE was the size of the equivalent

spherical particle (Malcolmson *et al.*, 2002). All samples were stored in the concentrated form and diluted to 1 wt% of surfactant before PCS measurement in order to avoid the effects of multiple scattering. To observe their stability profile within 1 month, samples were measured after equilibrated for 24 hours, 1 and 2 weeks and 1 month at $22 \pm 2^\circ\text{C}$ and were reported as the average of three measurements. The relationship between the visual appearance and the light scattering study was observed. The changes in hydrodynamic size with different triglyceride and $\text{C}_{18:1}\text{E}_{10}$ contents and different weight ratios of $\text{C}_{18:1}\text{E}_{10}$ to triglycerides and the size changes in different NE Regions were determined.

3.2 Phase inversion temperature determination

The phase inversion temperatures (PIT) of the clear NE, i.e. compositions within Region A, and the corresponding micellar solution were determined by repeatedly heating the samples until the temperature at which they become cloudy and cooling the samples to ambient, at a rate of $\sim 1^\circ\text{C min}^{-1}$ with stirring throughout. The temperatures at the onset of turbidity (upon heating) and the appearance of clarity (when cooling) were noted. The recorded PIT quoted were the mean of 3 separate determinations of the clouding temperature.

3.3 Differential scanning calorimetry study

A multi-cell differential scanning calorimeter (MC-DSC, TA Instruments, Lindon, USA) and thermal analysis system, equipped with NanoAnalyze software

(TA Instruments, Lindon, USA), were used to determine the state of the triglyceride incorporated into the NE. Pure triglyceride systems (SBO, TPN, TLN and TON), water, C_{18:1}E₁₀ and 10 and 20 wt% micellar solution were first determined to observe the melting point of the solid triglycerides and any thermal event, if any, occurred in water, C_{18:1}E₁₀ and the micellar solution. Then, the thermal behaviours of NE in regions A, B, C formulated with 10 and 20 wt% C_{18:1}E₁₀ were observed. The DSC measurements were carried out as follows: 0.4 mg of sample was weighed, using a microbalance (OHAUS, Nanikon, Switzerland), into a standard 1-mL MC-DSC stainless steel cell which was immediately closed with a lid. A cell containing 0.4 mg distilled water was used as a reference. All DSC measurements were performed in the temperature scanning mode. NE were routinely cooled to 0°C and left for 30 minutes at this temperature before heating to 80°C at a constant scanning rate of 1°C min⁻¹. Notably, the NE were cooled to 0°C to avoid any phase transition being masked due to thermal lag. NE were examined at 24 hours and 1 month after preparation and at least two fresh samples of each composition were tested. Moreover, the effect of different rates of heating, 0.25°C min⁻¹ and 1°C min⁻¹ was also investigated. A number of samples were heated from 20 to 80°C to ensure that cooling the samples to 0°C would not alter the results of the DSC experiment.

4. The incorporation of testosterone propionate in nanoemulsions

4.1 Testosterone propionate solubilisation

The amount of testosterone propionate (TP) incorporated in 10% and 20% micellar solution and NE formulated with 10 and 20 wt% C_{18:1}E₁₀ and triglycerides concentration in Regions A, B, C was determined by adding an aliquot (approximately 50 mg) of TP to 4 microcentrifuge tube, each containing 1 mL of the micellar solution or NE (Regions A, B, C). The microcentrifuge tubes were tightly closed and covered in foil to prevent the possibility of any photosensitive reaction (Porkka-Heiskanen *et al.*, 1992). The samples were equilibrated at room temperature on a circular rotating wheel for 4 or 7 days to ensure that TP have reached the maximum solubility potential. The excess drug (TP) was removed by centrifugation (16,000 g Biofuge pico, Heraeus, Osterode, Germany) for 10 minutes. A blank sample (i.e. the corresponding micellar/ NE without drug) was treated in the same way. A calibration curve for TP was obtained by dissolving an accurately known quantity of TP (approximately 40 mg) in 20 mL isopropanol. This stock solution was then serially diluted by taking 50, 100, 150, 200, 250 and 300 µl aliquots and making up to 25 mL with isopropanol. The UV spectra of the TP containing standard solutions in 1-cm path length cuvette was then determined with the absorbance reading at 240 nm (UV/Vis Spectrophotometer LAMBDA 35, Perkin-Elmer, USA). The concentration of TP in the NE samples was assessed from calibration curve after correction with the absorbance of the blank. The levels of TP incorporation into the corresponding

micellar solution, o/w NE formed in Regions A, B and C were compared. The experiment was done in four measurements.

4.2 Characterization of drug-loaded nanoemulsions

The effects of the incorporation of maximum saturated drug in each NE system on the size and stability of the NE droplets formulated with 10 and 20 wt% C_{18:1}E₁₀ were examined by visual observation and light scattering (PCS) as previously described. In addition, the effects of drug on the NE droplet were examined by DSC (as mentioned in 3.3) to observe any changes in the thermal behaviour.

5. Statistical analysis

The data were expressed as means \pm S.D. from at least three independent sets of experiments, unless otherwise indicated. Data shown in the Figures were from the representative set of experiments. Differences between groups were statistically analyzed using the one-way analysis of variance (ANOVA) with the posthoc test for repeated measures and the p-value of ≤ 0.05 are acceptable to be statistically significant.

6. Small-angle neutron scattering

6.1 Experimental set up

Small angle neutron scattering (SANS) studies were performed on the LOQ beam line at the ISIS pulsed neutron source (ISIS, Rutherford-Appleton Laboratory, STFC, Didcot, Oxford). The LOQ instrument gives a scattering vector, $Q = (4\pi/\lambda) \sin(\theta/2)$, range of 0.008 to 0.22 \AA^{-1} . Due to the limited beam time allowance, only some compositions in Region A of the liquid triglyceride (TON) and the solid triglyceride (TPN) were chosen for SANS experiment. All the samples are measured in disc-shape quartz cuvettes of 1 mm path length. SANS measurements were made at 25°C using a 12-nm diameter neutron beam. The pattern of scattering of neutrons after passage through the sample were recorded on $^3\text{He-CF}_4$ filled ORDELA 64 cm^2 , two-dimensional detector of resolution of 5 mm, positioned at 4.1 m from the sample. Wavelength dependent corrections were made to allow for the incident spectrum, detector efficiencies and measured sample transmissions in order to create a composite SANS pattern. The transmission and scattering runs of pure H_2O or D_2O were measured for the same length of time as the samples and were subtracted from all the corresponding sample runs in order to obtain the scattering from the surfactant aggregates. A schematic of the basic set up of SANS measurements is shown in

Figure 15.

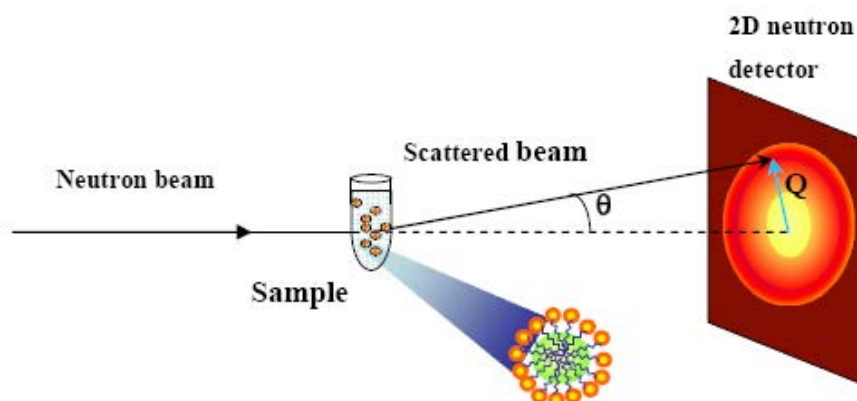


Figure 15 Schematic representation of a small angle neutron scattering experiment.

Scattering data were corrected for wavelength-dependent transmission factors, as well as cell, background, and any incoherent scattering. The overall NE droplet contrast was generated with triglyceride-h/ C_{18:1}E₁₀-h/ D₂O, and the external surfactant shell and core contrast were highlighted with triglyceride-d/C_{18:1}E₁₀-h/D₂O and triglyceride-d/ C_{18:1}E₁₀-h/H₂O, respectively. The program FISH is used to analyze the data (Heenan, 1989) which will be interpreted the location of triglyceride solubilization in the NE droplet.

6.2 SANS sample preparation




Nanoemulsions were individually prepared by weighing the required amount of h- or d-triglyceride, surfactant and either doubled distilled water (H₂O) or deuterated water (D₂O) at 22 ± 2°C. For each sample, a total of 1 g was prepared. A small magnetic stirrer was placed into the sample vial and the samples were heated to 70-75°C for ten minutes and cooling to 22 ± 2°C with vigorous stirring throughout. In

all experiments using deuterated material, the weight of the deuterated material added was corrected for the difference in density to ensure that the same volume of each component was present in the final samples. **Table 3** shows the density differences between the hydrogenated and deuterated forms of the compounds studied. The terminology used in the present study to describe the contrasts was explained further. Typically, both deuterated and hydrogenated triglycerides and water were used with the normal hydrogenated version of the surfactant, as D/H/H, D/H/D and H/H/D combinations of triglyceride/surfactant/water for the core, shell and drop contrast, respectively (**Table 4**). The hydrogenated and deuterated chemicals used were selected to highlight specific components in the NE droplets.

Table 3 Physicochemical parameters of the chemicals for SANS.

Chemicals	Molecular weight (g/mol)	Density (g/cm³)
<u>Hydrogenated</u>		
h-Brij 96	708.94	1.03
h-TON	470.65	0.90
h-TPN	807.29	0.92
H ₂ O	18.01	1.00
<u>Deuterated</u>		
d-TON	521.05	0.99
d-TPN	906.07	1.03
D ₂ O	20.03	1.11

Table 4 Composition of hydrogenated and deuterated chemicals for contrast matching.

Compositions	Core	Shell	Droplet
<div style="display: flex; align-items: center;"> <div style="width: 15px; height: 15px; background-color: blue; margin-right: 5px;"></div> Hydrogenated <div style="width: 15px; height: 15px; background-color: pink; margin-right: 5px; margin-left: 10px;"></div> Deuterated </div>			
Solvent	H ₂ O	D ₂ O	D ₂ O
Surfactant	h-Brij96	h-Brij96	h-Brij96
Triglyceride	d-TG	d-TG	h-TG

When preparing NE for neutron scattering study, a stock solution was freshly prepared and then diluted immediately prior to use to the required final surfactant concentration. It was necessary to produce a stock solution as it was often not possible to prepare the required (low surfactant) NE compositions directly. **Table 5a-b** lists the stock NE compositions used in the study and indicates the codes by which these stock solutions are referred to in the results. Samples for SANS measurements were individually ten-fold diluted from a stock solution. Hence, Concentrations of TON were from 0.1% up to 0.5% w/v and those of TPN were from 0.1% up to 0.7% w/v, stabilized by 2.4% w/v of surfactant concentration.

Table 5 Composition of stock nanoemulsion formulation**a) Tripalmitin**

Nanoemulsion composition (%w/w)	TPN-1	TPN-2.4	TPN-3.2	TPN-4	TPN-5.5	TPN-7
<u>Surfactant</u>						
POE (C _{18:1} E ₁₀)	24	24	24	24	24	24
<u>Triglyceride</u>						
Tripalmitin (TPN)	1.0	2.4	3.2	4.0	5.5	7.0
<u>Aqueous phase</u>	75.0	73.6	72.8	72.0	70.5	69.0
Ratio of C_{18:1}E₁₀/TPN	24	10	7.5	6	4.4	3.4

b) Trioctanoin

Nanoemulsion composition (%w/w)	TON-1	TON-2.1	TON-2.4	TON-3.0	TON-3.6	TON-5
<u>Surfactant</u>						
POE (C _{18:1} E ₁₀)	24	24	24	24	24	24
<u>Triglyceride</u>						
Trioctanoin (TON)	1.0	2.1	2.4	3.0	3.6	5.0
<u>Aqueous phase</u>	75.0	73.9	73.6	73.0	72.4	71.0
Ratio of C_{18:1}E₁₀/TON	24	11.4	10	8.0	6.7	4.8

6.3 Analysis of SANS data

The SANS data were analysed using solid-body models of the scattering species. This method allows for the construction of many kinds of geometrical models (e.g. spherical particles, ellipsoid and rod-shape structures etc.). The program FISH

was used for this purpose (Heenan, 1989). The structures of the micelles and microemulsions were established by analyzing the scattering data using a standard and well-established model for the interparticle structure factor $S(Q)$, the hard sphere model (Percus and Yevick, 1958). **Figure 16** shows schematics of the form factors used in this study.

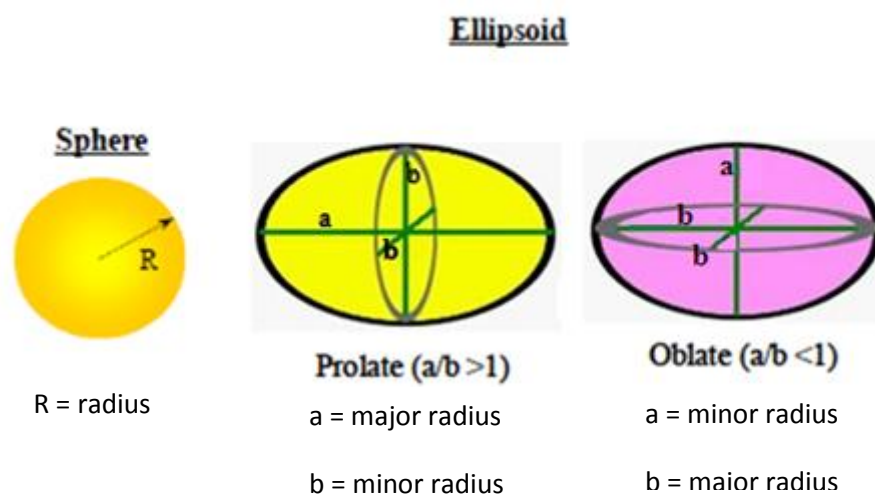


Figure 16 Schematic of form factors for SANS data fitting.

6.3.1 Description of SANS model

The absolute SANS intensity of scattering, $\frac{\partial \Sigma}{\partial \Omega}(Q)$, for N discrete particles per unit volume, in solution is given by (Heenan, 1989):

$$\frac{\partial \Sigma}{\partial \Omega}(Q) = N \cdot P(Q) \cdot S(Q) \quad (5)$$

where the form factor $P(Q) = [|F(Q)|^2]$ is a function that describes how $\partial \Sigma / \partial \Omega$ is modulated by interference effects between radiations scattered by different parts of

the same scattering body. It describes the scattering observable from an isolated body in the absence of interference effects and depends on the particle size and shape. $S(Q)$ is the interparticle structure factor which represents the effect of interference due to neighbouring scatterers. For very dilute systems $S(Q)$ tends to unity, and is often ignored.

Micelles and nanoemulsions can be described by core/shell model where the micelle core consists of the tails of the surfactant and the shell consists of the surfactant head group. The NE core consists of the oil or with some of surfactant tails and the shell consist of the whole surfactant. The contribution to scattering intensity from the structure factor for the ellipsoidal core-shell particles was modeled assuming hard-sphere interactions. This approach was found to describe scattering of microemulsions quite well (Nagao *et al.*, 2005).

For the core/shell particles studied here $F(Q)$ is a sum of terms for a core (radius R_c), a shell (thickness δ) and a surfactant head group region, thickness h , as

$$F(Q) = [(\rho_c - \rho_s)V_c f(Q, R_c)] + [(\rho_s - \rho_h)(V_T - V_h) f(Q, R_c + \delta)] + [(\rho_h - \rho_w)V_T f(Q, R_T)] \quad (6)$$

where ρ_c , ρ_s , ρ_h , and ρ_w are the neutron scattering length densities of the particle core, shell, head group and solvent, respectively. V_T , V_h and V_c are the volumes of the whole particle, head group region and core, respectively and total radius of particle R_T is $R_c + \delta + h$.

For a spherical particle, the following expression can be used to calculate $F(Q, R)$, the form factor for a sphere of radius R :

$$F(Q, R) = \frac{3(\sin(QR) - QR \cos(QR))}{(QR)^3} \quad (7)$$

For an ellipsoid with axial ratio X (prolate if $X > 1$, oblate if $X < 1$), both $F(Q)$ and $F^2(Q)$ require numerical integration over angle γ between Q and the axis of the ellipsoid to include a random distribution of orientations. The particle form factor of a monodisperse ellipsoid is given by:

$$F^2(Q) = (\Delta\rho)^2 V^2 \int_0^{\pi/2} f^2(u) \sin(\gamma) d\gamma \quad (8)$$

where $f(u)$ is $F(Q, R=u)$ in equation (7), $u = QR(\sin^2 \gamma + X^2 \cos^2 \gamma)^{1/2}$ and

$$V = \frac{4\pi}{3} XR^3$$

6.3.2 Model fitting of the simultaneously fit SANS data

Before fitting the data, parameters such as the scattering length density (SLD) of the different components, volume of the core (V_{core}) and volume of the shell (V_{shell}) etc., were calculated. These parameters are listed in **Table 6**. According to the experiments performed in this study, the core-shell spherical and ellipsoidal shape models were fitted to the experimental scattering curves. The preliminary fits showed that the best model was the oblate ellipsoid form factor. The SANS data of the NE with three different contrasts were then fitted by the simultaneous model in order to evaluate the inner structure of the NE droplets simultaneously using a monodisperse, core-shell ellipsoid model together with a hard-sphere structure factor. Useful results have previously been obtained for oil/surfactant/water systems by simultaneous fit (Lugo *et al.*, 2010; Toth and Madarasz, 2006; Wang *et al.*, 2008).

For each NE composition studied in the SANS experiments, three separate SANS experiments were performed. In the first experiment, the NE was prepared using D₂O, *h*-oil, and *h*-surfactant (i.e. the drop contrast), in the second using D₂O, *d*-oil and *h*-surfactant (i.e. the shell contrast) and in the third using H₂O, *d*-oil and *h*-surfactant (i.e. the core contrast). The first experiment yields information primarily about the size and shape of the whole NE droplet, the second experiment about the surfactant shell, and the final experiment predominantly gives information about the location of oil in the nanoemulsion droplet. All three sets of scattering data obtained for each composition were simultaneously analysed to give a self-consistent model, thereby giving a high level of confidence in the final results. The sample codes used for the contrast matching samples for SANS measurements are shown in **Table 7a-b**.

Table 6 Scattering length densities and related physicochemical parameters of the compounds used for SANS measurements

Compositions		Mol wt ^a (g/mol)	Bulk density ^a (g/cm ⁻³)	Molar volume ^a (Å ³)	Neutron-scattering-length density (x10 ¹⁰ cm ⁻²)	
					Hydrogenous ^a	Deuterated ^b
Water	H ₂ O	18.01	1.00	29.99	-0.56	6.33
C _{18:1} E ₁₀ whole	C ₃₈ H ₇₆ O ₁₁	708.94	1.03	1143.34	0.28	n/a
C _{18:1} E ₁₀ tail	C ₁₈ H ₃₅	251.47	0.75	556.97	-0.20	n/a
C _{18:1} E ₁₀ head	C ₂₀ H ₄₁ O ₁₁	457.47	1.30	586.38	0.74	n/a
TON (trioctanoin)	C ₂₇ H ₅₀ O ₆	470.65	0.90	868.68	0.31	6.27
TPN (tripalmitin)	C ₅₁ H ₉₈ O ₆	807.29	0.92	1457.62	0.05	6.21

^a All parameters except those in the last column are for hydrogenous species. ^b Deuterated assumes 99% and 85% replacement of H for TON and TPN respectively, and the same molar volume as *h*-species.

n/a= not applicable

Table 7 Sample list of nomenclature for SANS contrast matching experiments.

(a) Tripalmitin

Contrast	TPN-1	TPN-2.4	TPN-3.2	TPN-4	TPN-5.5	TPN-7
Core	TPN-1c	TPN-2.4c	TPN-3.2c	TPN-4c	TPN-5.5c	TPN-7c
Shell	TPN-1s	TPN-2.4s	TPN-3.2s	TPN-4s	TPN-5.5s	TPN-7s
Droplet	TPN-1d	TPN-2.4d	TPN-3.2d	TPN-4d	TPN-5.5d	TPN-7d

(b) Trioctanoin

Contrast	TON-1	TON-2.1	TON-2.4	TON-3.0	TON-3.6	TON-5
Core	TON-1c	TON-2.1c	TON-2.4c	TON-3.0c	TON-3.6c	TON-5c
Shell	TON-1s	TON-2.1s	TON-2.4s	TON-3.0s	TON-3.6s	TON-5s
Droplet	TON-1d	TON-2.1d	TON-2.4d	TON-3.0d	TON-3.6d	TON-5d

CHAPTER IV

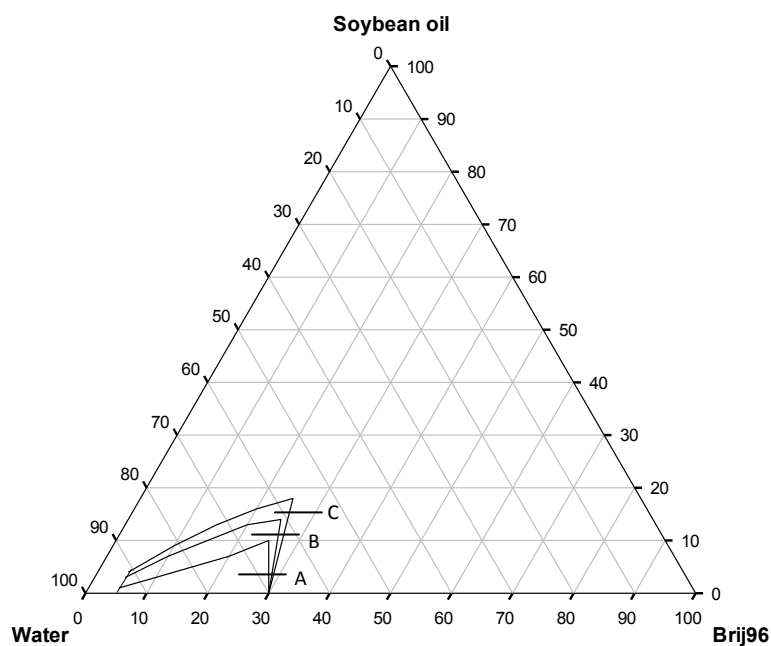
RESULTS AND DISCUSSION

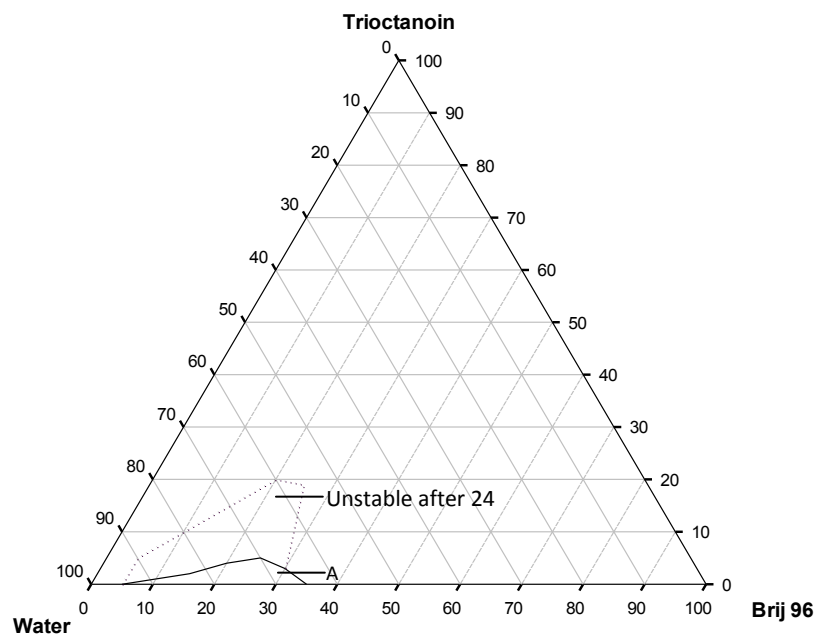
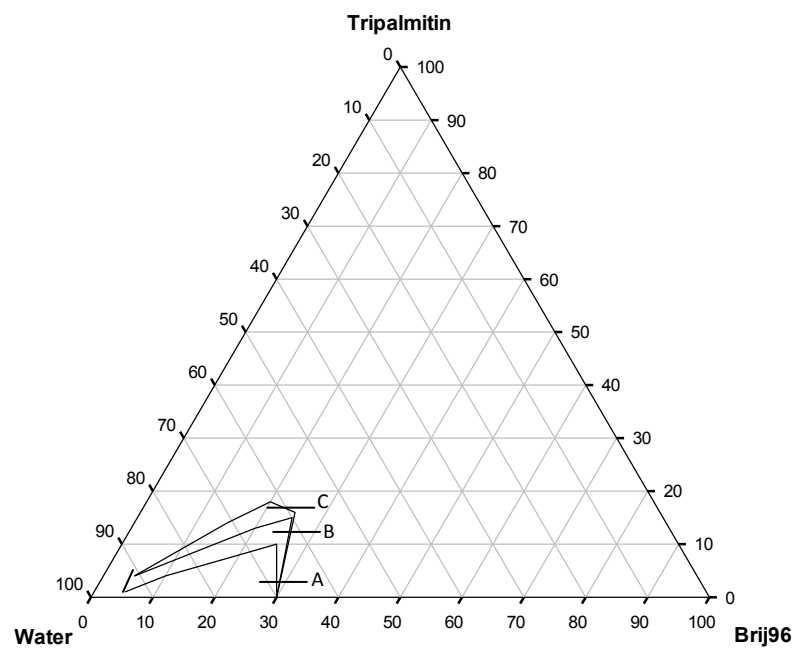
1. Sample appearance and phase behavior

In order to understand the phase behavior of the nanoemulsion formulations (NE), the area of NE existence was determined by varying the amount of each of the component and plotted on a weight basis on a ternary phase diagram. The phase diagram assemblies have been used regularly to observe the microemulsions formation (clear samples) (Prince, 1975; Spornath and Aserin, 2006; Djekic *et al.*, 2011; Lawrence and Rees., 2012). In this study, the samples that were stable for 1 month were plotted on phase diagram. **Figure 17a-d** shows the ternary phase diagram for systems composed of $C_{18:1}E_{10}$ (Brij 96), water and either liquid triglyceride, soybean oil (SBO) and trioctanoin (TON), or solid triglyceride tripalmitin (TPN) and trilaurin (TLN) after one month preparation. The appearances of 1 month stable samples prepared by heating and cooling method are shown in **Figure 18**. It can be seen that the sample appearances altered from optically transparent samples which were described as Region A, bluish/translucent samples denoted as Region B and cloudy/milky samples as Region C on ternary phase diagram. It was noted that their stability was also observed by their appearance together with their hydrodynamic droplet size as described in next session. Moreover, the NE appearances observed were found to be the same after storage for 24 hours, one week,

two weeks and one month with the exception of the NE containing TON. The appearance changed from clear to milky as the triglyceride concentrations increased at steady surfactant concentration. As can be seen from **Figure 17a-d**, samples prepared with SBO, TPN and TLN could form the NE in all Regions A, B and C with the biggest formation area at region A. Reassuringly, the extent of Region A established for SBO is similar to the Region of existence of one phase, clear microemulsions as previously reported (Warisnoicharoen *et al.*, 2000a; Flanagan *et al.*, 2006).

a) Soybean oil (SBO)



b) Trioctanoin (TON)**c) Tripalmitin (TPN)**

d) Trilaurin (TLN)

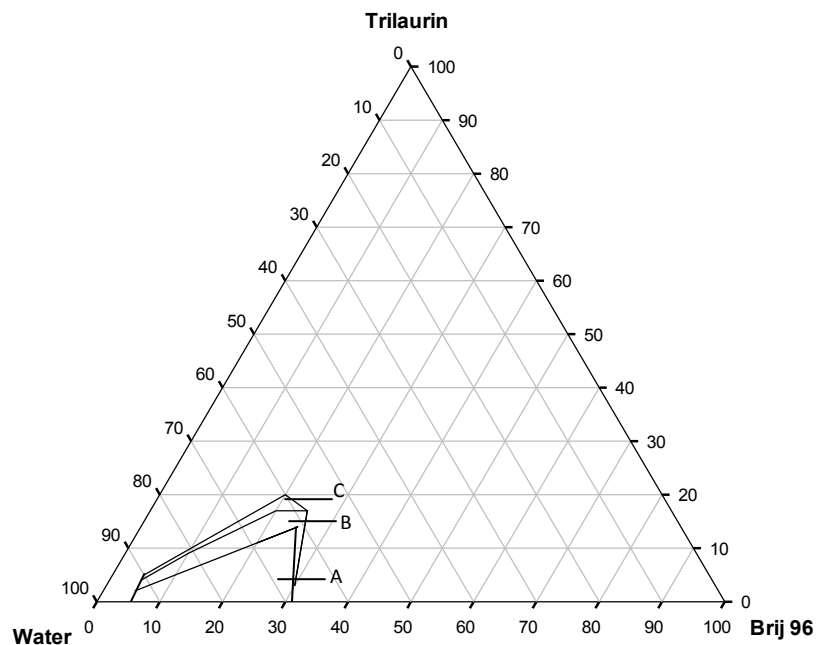


Figure 17 Triangular phase diagrams for o/w nanoemulsions formed with $C_{18:1}E_{10}$, either a liquid triglyceride oil (a) soybean oil or (b) trioctanoin or solid triglycerides (c) tripalmitin or (d) trilaurin and water after 24 hours and one month storage at $22 \pm 2^\circ\text{C}$. On the abscissa, surfactant concentration (in wt%) is increasing from left to right while on the ordinate, oil concentration (in wt%) is increasing from bottom to top.

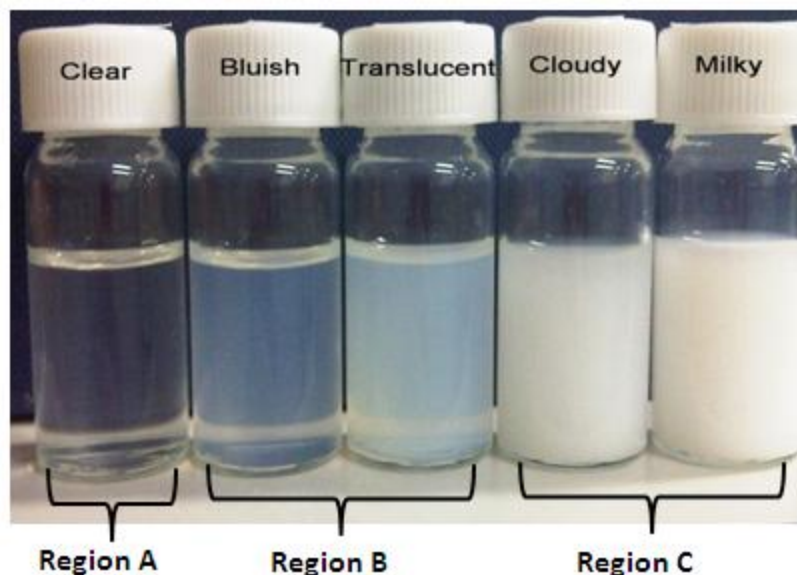


Figure 18 Appearance of nanoemulsions within Regions A (clear), B (bluish or translucent) and C (cloudy or milky).

The $C_{18:1}E_{10}$ concentration range over which micelle are formed maps on to the concentration range over which $C_{18:1}E_{10}$ forms NE. In all instances, NE were formed between minimum and maximum $C_{18:1}E_{10}$ concentration ranges of 5-10 and 25-30 wt%, respectively. In addition, regardless of the nature of the triglyceride added, the maximum level of triglyceride incorporation occurred at a $C_{18:1}E_{10}$ concentration was in between 20 and 25 wt%. While in Region A, the maximum oil solubilisation occurred at 25 wt% $C_{18:1}E_{10}$. Gel formation was frequently observed at $C_{18:1}E_{10}$ concentrations above 30 wt% and when high amounts of triglyceride (i.e. outside the NE area) were incorporated into systems containing 25 and 30 wt% of $C_{18:1}E_{10}$ similar to the results obtained by Flanagan *et al.* who reported the phase diagram of a similar microemulsion system comprising of water, polyoxyethylene oleyl ether, and soybean oil (Flanagan *et al.*, 2006). Samples

containing triglyceride levels greater than those recorded for Region C were either gels (at high surfactant concentrations) or exhibited two phases and were therefore not studied further.

Significantly, once the NE in all Regions had been formed it was possible to dilute the NE to very much lower $C_{18:1}E_{10}$ concentrations without any phase separation, this is an important result for the use of the NE as delivery vehicles. These observations are consistent with previous reports which suggest that the NE droplet structure is mainly controlled by the phase behavior of the initial concentrate. And it is largely independent of dilution when NE were formed with the oil completely dissolved in a single phase (Izquierdo *et al.*, 2004; Morales *et al.*, 2006; Wang *et al.*, 2008). The excess water is performed as dilution medium and not participating in NE droplet. As expected, the molecular weight and molecular volume of the triglycerides used influenced the amount of triglyceride incorporated. Thus samples containing the triglyceride of intermediate molecular weight, TLN, exhibited a larger total stable NE area (i.e. Regions A+ B+C). For example TLN-containing samples prepared with 20 wt% $C_{18:1}E_{10}$ could incorporate a maximum of 10 wt% oil in the clear, one phase Region A, whereas samples containing either SBO or TPN could only incorporate 8 wt% oil at the same surfactant concentration. For ease of comparison **Table 8** lists the upper limit of the amount of each triglyceride incorporated into each Region at 10 and 20 wt% $C_{18:1}E_{10}$. It is of note that there was little difference, over a period of 1 month at least, between the level of incorporation of the liquid triglyceride, SBO and the solid triglyceride of similar molecular weight, namely TPN. The smallest triglyceride, TON, exhibited the smallest

NE region with a very small Region A with a maximum level of TON incorporation of only 4 wt% at 20 wt% C_{18:1}E₁₀ and with no Regions B and C being observed. Interestingly, immediately after preparation, TON did produce the largest Region A in fact the largest total NE formation area with a maximum level of TON incorporation of up to 10 wt% and 20 wt% at 10 wt% C_{18:1}E₁₀ and 20 wt% C_{18:1}E₁₀ respectively as indicated by the dotted line in **Figure 17b**. However, after 24 hours these initially clear NE became cloudy, milky or phase separated into 2 phase system consisting of a lower clear and upper turbid phase, leaving the small Region A reported in Figure 1b and leading to the smallest NE region formed with C_{18:1}E₁₀. For the purposes of the present study, the very unstable nature of the majority of the TON-contained NE makes them of little interest for drug delivery purposes and therefore only NE that were stable for 1 month would be considered here. The extent of the area of NE existence obtained for TON was slightly larger than that of the small, C₄ liquid triglyceride, tributyrin, that was previously reported (Warisnoicharoen *et al.*, 2000a).

Table 8 Upper limit of amount of triglyceride incorporated into nanoemulsions denoted in Regions A, B and C at 10 and 20 wt% C_{18:1}E₁₀.

Triglyceride	10 wt% C _{18:1} E ₁₀			20 wt% C _{18:1} E ₁₀		
	Region A (wt%)	Region B (wt%)	Region C (wt%)	Region A (wt%)	Region B (wt%)	Region C (wt%)
Soybean oil	4	6	9	8	12	16
Tripalmitin	4	7	9	8	13	18
Trilaurin	5	8	10	10	15	20
Trioctanoin	1	N/A	N/A	4	N/A	N/A

Region A = optically transparent NE, Region B = bluish or opalescent NE, Region C = cloudy/milky NE. N/A = not applicable, TON did not exhibit Regions B or C

Many researchers have reported that the smaller the oil molecular volume in the ethyl esters and triglycerides group, the greater the level of incorporation into alkylamine-N-oxide surfactants, polyoxyethylene-10-dodecyl ether surfactant and PEG-8 caprylic/capric glycerides surfactant stabilized oil-in-water dispersion due to the greater interaction between the hydrophobic chains of the surfactant comprising the interfacial region and the disperse oil phase (Malcolmson and Lawrence, 1995; Djekic and Primorac, 2008). Similar findings suggested that if the alkane chain length of the oil is less than the surfactant chain length, the oil acts like surfactant penetrating the interfacial layer and thus increasing the effective chain volume of the surfactant which result in bigger ME formation (Chen *et al.*, 1986). In addition, the short chain oils increased the surfactant head group area to the greatest extent favoring an o/w droplet structure where the longer chain oils served to increase the effective volume of the core and decreased the

surfactant head group resulting in the increase in the droplets size and eventually could reduce the chances of o/w droplet formation (Tchakalova *et al.*, 2008; Hsieh, 2010). Conversely, it has been also previously reported that samples prepared using liquid triglycerides of varying molecular volume and stabilised by C_{18:1}E₁₀ tended to unusually exhibit the reverse trend, with the largest and smallest region being formed in systems containing large molecular volume triglycerides (SBO) and small molecular volume triglyceride (Miglyol 812 and tributyrin), respectively. (Malcolmson *et al.*, 1998; Warisnoicharoen *et al.*, 2000a). The reason for the reverse trend is possibly due to the long alkyl chain surfactant which may assist the incorporation of the longer chains oil; and the relative differences in length of the short chain oil and the long hydrophobic chains of a surfactant. The long hydrophobic chain of a surfactant might not be able to interact with short oil chain strongly, thus the way oil incorporated in surfactant did not favour NE formation. As agreed with previously reported, the result obtained in this study showed that the NE existing area was smallest in the smallest triglyceride studies here (TON). It is interesting that in the present study samples containing TLN exhibited the larger area of NE existence than the NE containing the higher molecular weight triglycerides, SBO and TPN. The reason for the differences may be a consequence of differences in triglycerides chain length study depending upon the molecular volume of the triglycerides which is clearly the important factor for NE formation (Kunieda *et al.*, 2001; Djekic and Primorac, 2008). It is noted that the molecular volume of TLN is 1168 Å³ which is slightly bigger than the molecular volume of C_{18:1}E₁₀ (1143 Å³) where the molecular volume of Miglyol 812 (C₁₀) is 1019 Å³ (Malcolmson *et al.*, 1998). According

to the molecular volume of TLN, Miglyol 812 and the length of the hydrocarbon chains that it contains, the TLN is expected to be surrounded by the oleyl hydrocarbons of $C_{18:1}E_{10}$ and by a mantle of EO chains and does not significantly penetrate into the hydrocarbon chains of the surfactants as anticipated for SBO and TPN while Miglyol 812 does. TLN represented the biggest NE existence was probably the consequences of the molecular volume of TLN were comparable to $C_{18:1}E_{10}$. Nevertheless beside the oil molecular volume, the NE formation as well depends to great extent on others factors such as chemical structure of oils, the hydrophilic-lipophilic balance of surfactants and oils used, the surfactant structure and the original shape of micellar solution.

2. Hydrodynamic droplet size determination

The variation in hydrodynamic droplet size (D_h) of the NE with increasing triglyceride concentrations was investigated for five concentrations of $C_{18:1}E_{10}$ (5, 10, 15, 20 and 25 wt%) at 25°C. Results are shown in **Figures 19-22**. For all four triglycerides, the D_h of the NE droplets increased as the amount of triglyceride increased, the addition of the triglycerides to the aqueous $C_{18:1}E_{10}$ solution resulted in an increase in the apparent hydrodynamic size of 11 ± 1.2 nm obtained for micellar solution. Significantly, once the NE had been formed it was possible to dilute the NE to very much lower $C_{18:1}E_{10}$ concentrations without any phase separation, or indeed any obvious increase in size of the NE droplets. It can be seen from **Figures 19-21** that for SBO-NE, TPN-NE and TLN-NE respectively, the variation in D_h with varied triglyceride concentrations tended to increase in an approximately linear fashion with no obvious break in size being observed for

samples in Regions A and B with the D_h between about 10-40 nm suggesting that the bigger triglyceride core formed with an increase in triglyceride concentration. Interestingly for NE in Region C, the D_h were sharply increased from about 40 nm to 130 nm. The dramatic change in size of the NE between Regions B and C is indicative of a change in the structure of the droplets found in Region A to upper limit of Region B. It is most probably a consequence of a large amount of triglyceride present, which resulted in the formation of a large triglyceride core in the centre of the NE droplet packed loosely with surfactant or the NE might totally form in different way. It might reasonably be expected that in the larger NE in which the interfacial surfactant region represents only a small proportion of the NE volume, the triglyceride will behave more-like the bulk triglyceride.

In agreement with visual observation, the dynamic light scattering measurements showed that with the exception of the TON-NE (**Figure 22**), the samples were generally stable for at least 1 month as the D_h did not produce any significant change over this time period (**Figures 19-21**). The D_h of TON-NE that were unchanged in 1 month were NE consisting of 10 wt% $C_{18:1}E_{10}$ and 1 wt% TON, 15 wt% $C_{18:1}E_{10}$ and up to 2 wt% TON, 20 wt% $C_{18:1}E_{10}$ and up to 4 wt% TON and 25 wt% $C_{18:1}E_{10}$ and 5 wt% TON, matching with the upper limit on the ternary phase diagram. The D_h of those samples that were not on phase diagram were significantly increased from 24 hr to 1 week after preparation and eventually were phase separated completely within 1 month.

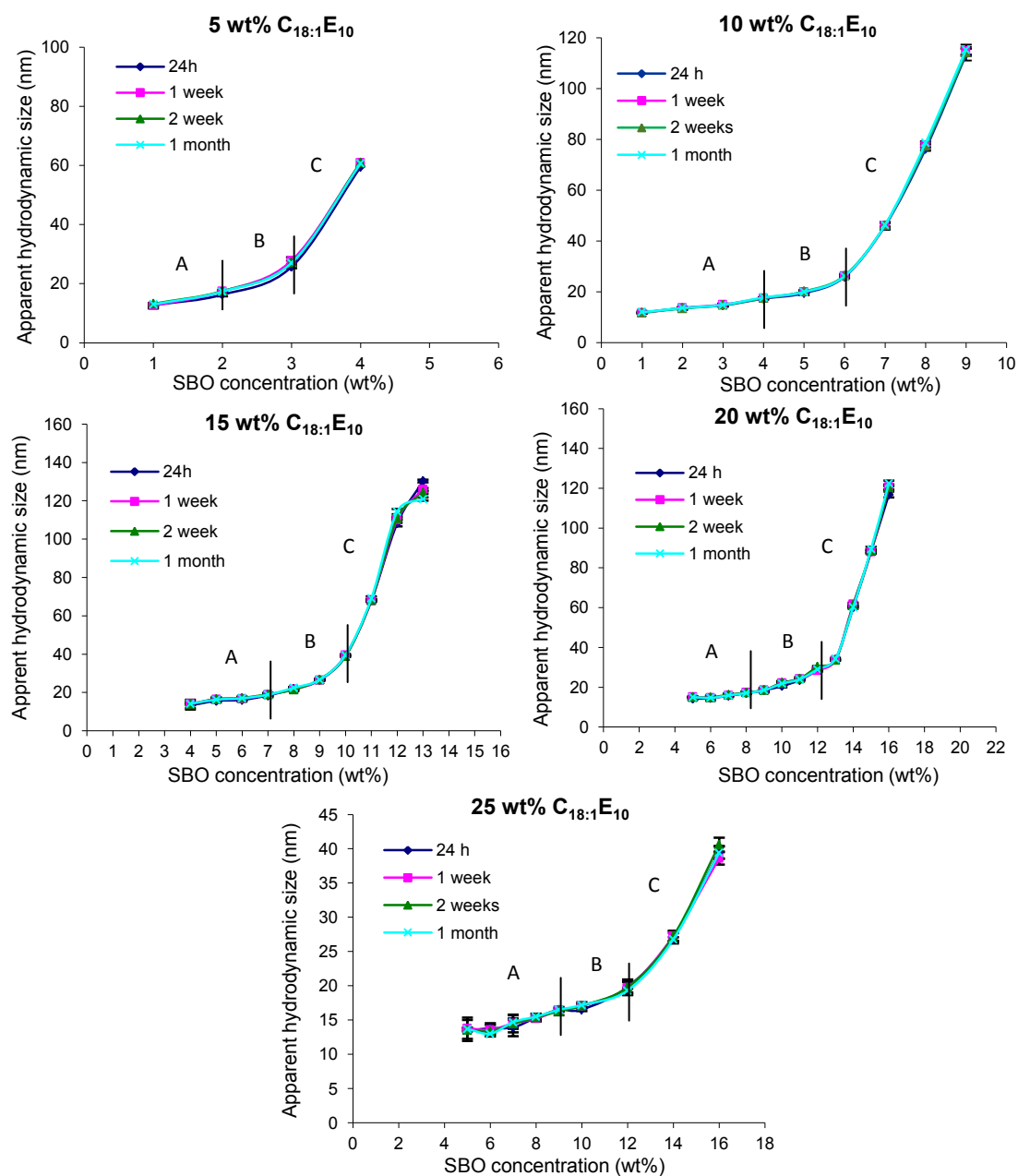


Figure 19 Variation in the mean hydrodynamic droplet sizes of the nanoemulsions containing soybean oil over a period of a month stabilized by $C_{18:1}E_{10}$ at different concentrations (mean \pm S.D., $n=3$).

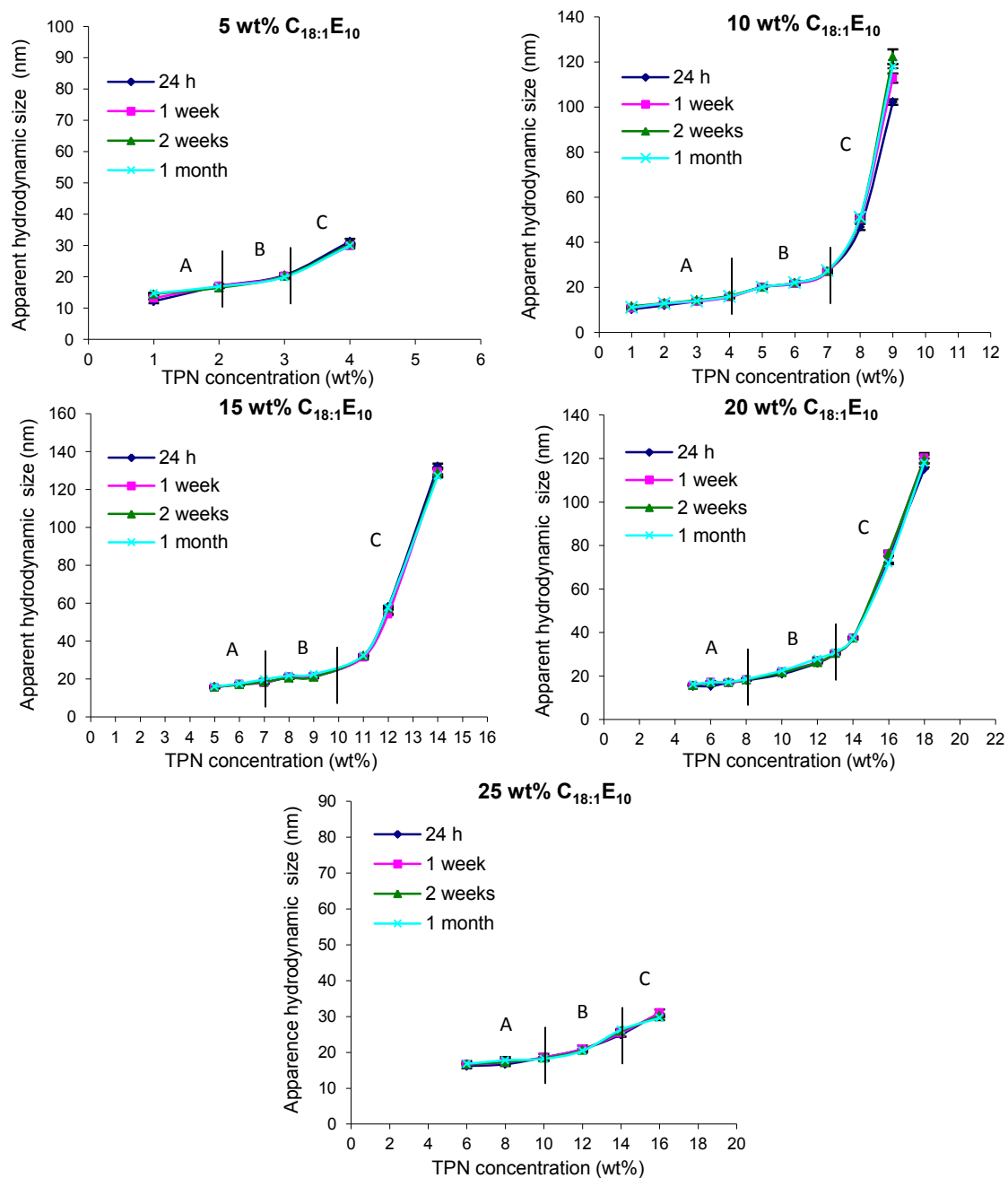


Figure 20 Variation in the mean hydrodynamic droplet sizes of the nanoemulsions containing tripalmitin over a period of a month stabilized by C_{18:1}E₁₀ at different concentrations (mean ± S.D., n=3).

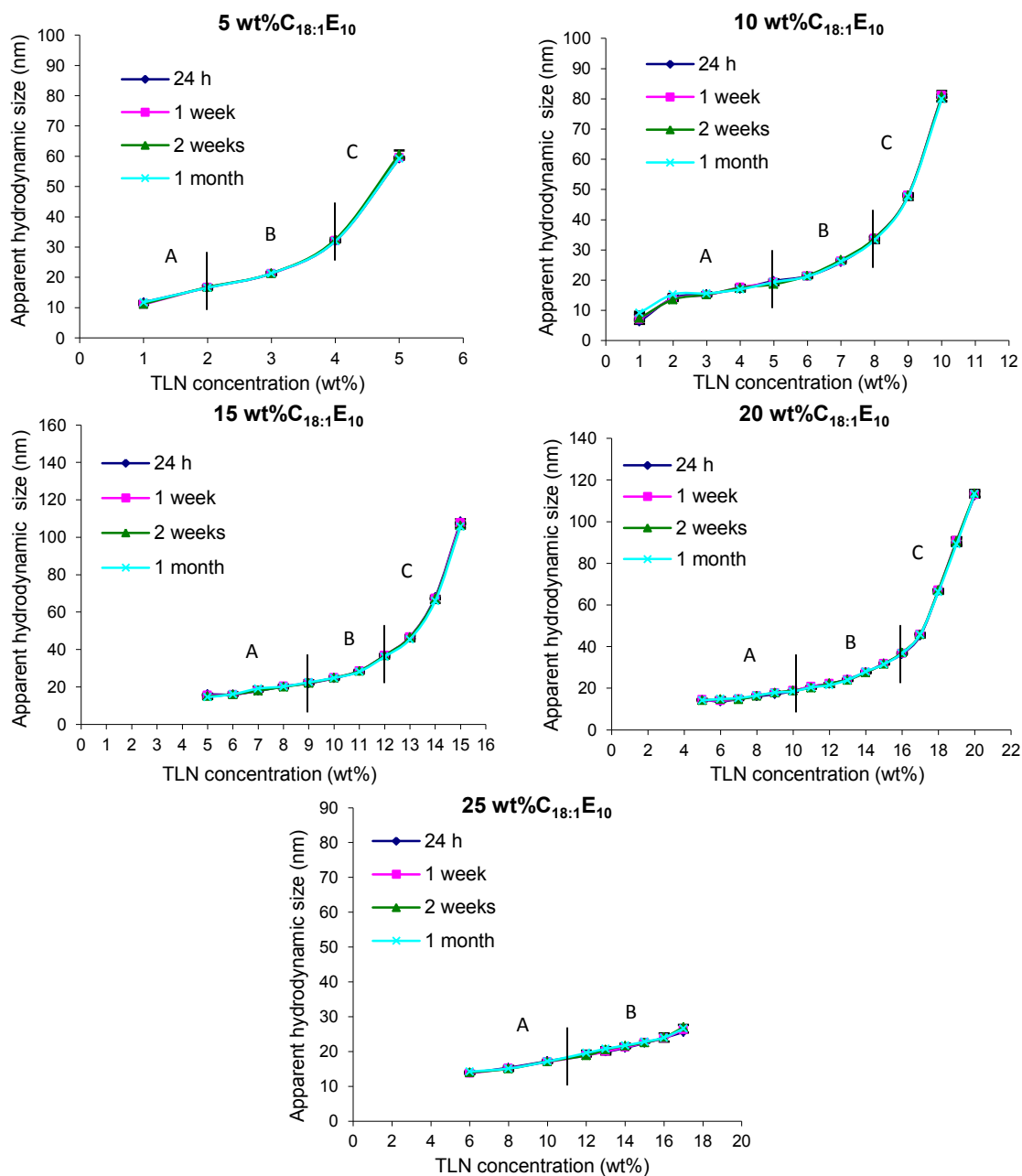


Figure 21 Variation in the mean hydrodynamic droplet sizes of the nanoemulsions containing trilaurin over a period of a month stabilized at by C_{18:1}E₁₀ at different concentrations (mean ± S.D., n=3).

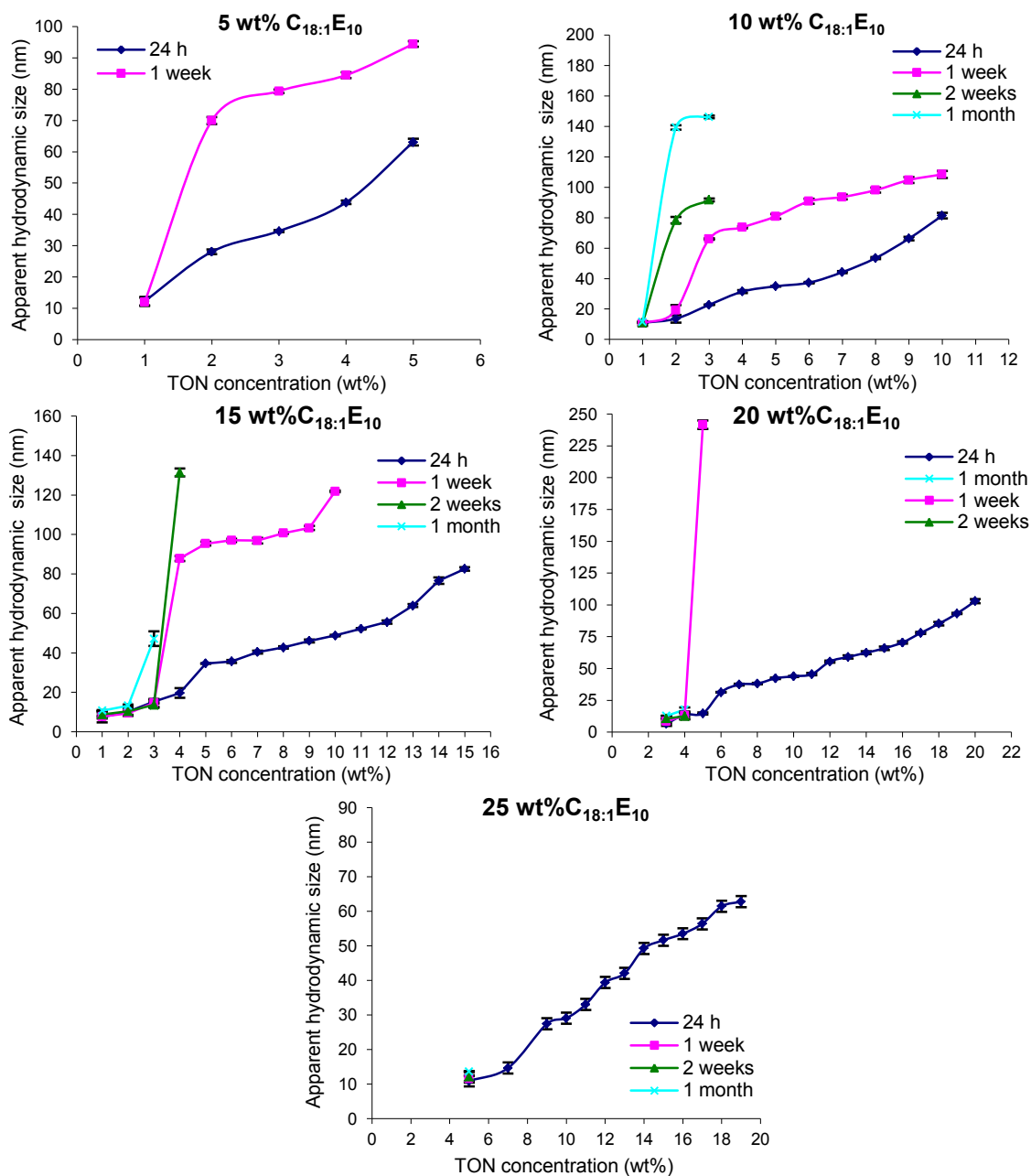


Figure 22 Variation in the mean hydrodynamic droplet sizes of the nanoemulsions containing trioctanoin over a period of a month stabilized by $C_{18:1}E_{10}$ at different concentrations (mean \pm S.D., $n=3$).

Regardless of the nature and amount of triglycerides in the preparation, the D_h of the NE droplets fell well within the size range quoted for NE (200 nm) with sizes of up to ~130 nm being recorded for NE with a triglyceride content just within the upper boundary of Region C. (Solan et al., 2005; Gutierrez et al., 2008). It is of note that the NE droplets in Region A tended to be less than 20 nm in size while those that were in the approximate range of 20 – 40 nm were either bluish or translucent (i.e. in Region B). For example, the D_h of 1- month-old samples prepared using 10 wt% $C_{18:1}E_{10}$ and containing the greatest amount of triglyceride in Region A were 17.5 ± 0.3 nm (4 wt% SBO), 16.0 ± 0.3 nm (4 wt% TPN), 19.2 ± 0.5 nm (5 wt% TLN) and 10.9 ± 0.4 nm (1 wt% TON), respectively. While samples prepared using the same concentration of $C_{18:1}E_{10}$ and containing the highest amount of oil in Region B were 26.2 ± 0.3 nm (6 wt% SBO), 27.2 ± 0.4 nm (7 wt% TPN) and 33.3 ± 0.6 nm (8 wt% TLN), respectively. Correspondingly, samples containing the highest amount of oil in Region C were 112.9 ± 1.1 nm (9 wt% SBO), 122.4 ± 3.3 nm (9 wt% TPN) and 80.9 ± 1.0 nm (10 wt% TLN), respectively. Results exhibiting a similar trend were seen for D_h of NE in Regions A and B prepared using the others tested $C_{18:1}E_{10}$ concentrations, although the D_h was varied upon different $C_{18:1}E_{10}$ concentrations for Region C. Furthermore, the D_h of the dilute NE droplets containing the various triglycerides were of comparable size for the same concentration of triglyceride in Regions A and B range. For example, the droplet sizes of samples prepared using 10 wt% $C_{18:1}E_{10}$ and containing the 5 wt% triglyceride were 20.0 ± 0.2 nm (SBO), 20.1 ± 0.2 nm (TPN) and 19.3 ± 1.3 nm (TLN). It was noted that no TON-NE

were formed at this composition. This suggests that the structures of the droplet are not much altered when either triglycerides SBO/TPN/TLN is incorporated in NE.

In addition, the D_h of the NE differing in starting compositions within Regions A and B at the same triglyceride to surfactant weight ratios were generally very similar in size as shown in **Figure 23**. The graph shows a fairly straight line for the composition at different triglyceride: surfactant weight ratios in Regions A and B; ratios of 0.2-0.6 for SBO-NE and TPN-NE, ratios of 0.2-0.8 for TLN-NE and ratio of 0.1 for TON-NE. For examples, D_h of samples with ratio 0.6 initially prepared using 5 wt% $C_{18:1}E_{10}$ and 3 wt% SBO, 10 wt% $C_{18:1}E_{10}$ and 6 wt% SBO, 15 wt% $C_{18:1}E_{10}$ and 9 wt% SBO, 20 wt% $C_{18:1}E_{10}$ and 12 wt% SBO and 25 wt% $C_{18:1}E_{10}$ and 14 wt% SBO were 27.1 ± 0.95 nm, 26.4 ± 0.71 nm, 26.8 ± 0.3 nm, 28.4 ± 0.4 nm and 27.3 ± 0.72 nm, respectively. In comparison, however, the D_h of samples in Region C containing the same weight ratio of triglyceride to $C_{18:1}E_{10}$ were differed; the D_h were either sharply increased or decreased. For example, D_h of samples at a ratio of 0.8, NE contained (1) 10 wt% $C_{18:1}E_{10}$ and 8 wt% SBO, (2) 15 wt% $C_{18:1}E_{10}$ and 12 wt% SBO and (3) 20 wt% $C_{18:1}E_{10}$ and 16 wt% SBO (all within Region C), were 75.3 ± 1.0 nm, 114.4 ± 1.4 nm and 122.5 ± 1.4 nm, respectively. The results showed that twice the initial amount of the $C_{18:1}E_{10}$ and triglyceride within the composition range in Regions A and B did not double the size but gave the similar in droplet sizes. These imply that the amounts of droplet were possibly two-fold in solution instead of increasing the size of droplet. At region C, there was no correlation found between the droplet size of the initial amount of the $C_{18:1}E_{10}$ and triglyceride and the doubled amount of these composition suggesting that the way the

droplets pack or arrange themselves in region C is not in the same manner as those in Regions A and B.

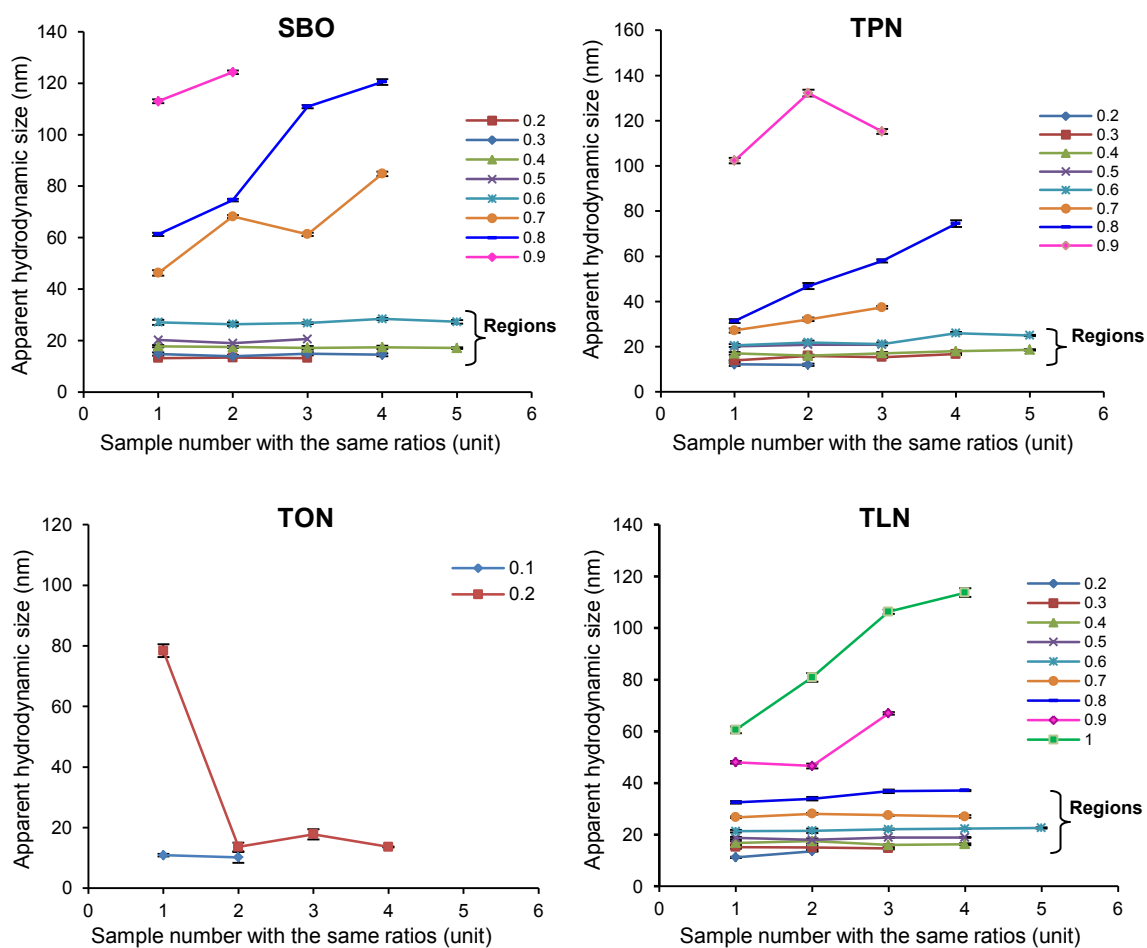


Figure 23 Variation in the mean hydrodynamic droplet sizes of the nanoemulsions containing SBO, TPN, TLN or TON at different weight ratios (0.2-1, shown as legend) of $C_{18:1}E_{10}$ to triglycerides (mean \pm S.D., $n=3$).

3. Cloud point and phase inversion temperature

The presence of a cloud point (CP) and phase inversion temperature (PIT) may limit the potential physical properties and performance of micelle ($C_{18:1}E_{10}$ /water system) and NE as a drug delivery vehicle especially if the CP and PIT are within or close to the temperature range in which the micelle and NE will be used. It is therefore essential to study the existence of a CP and PIT occurred in this $C_{18:1}E_{10}$ system. Moreover, the changes in CP and PIT could lead to indication of the physicochemical of the NE structure. The CP of a nonionic surfactant system is the temperature at which the total effective force between micelles changes from being repulsive to attractive (Sadaghiania and Khan, 1991; Mukherjee *et al.*, 2011). This change is generally considered to be due either to an increase in the attractive forces due to van der Waals forces and hydrophobic interactions between hydrophobic surfaces or to a decrease in repulsive forces owing to hydration forces at higher temperature, or combination of the two effects in addition to interrelated changes in micelle size and shape (Aveyard *et al.*, 1990). With ethylene oxide surfactants in particular, an increase in temperature results in dehydration of the ethylene oxide chains causing a reduction of surfactant head group area (a_0) hence an increase in the critical packing parameters (CPP), and the formation of more elongated aggregates of reduced curvature and a higher aggregation number (Kjellander, 1982; Aveyard and Lawress, 1986). This phase change is reversible. When the system is cooled to a temperature below the cloud point, the two phases merge into a clear solution again.

The PIT of a surfactant solution may be raised or lowered by the presence of various additives including a number of oils (Shigeta *et al.*, 2001; Schott, 2001). Results of the CP found for C_{18:1}E₁₀/water system and the PIT of NE (triglyceride/ C_{18:1}E₁₀/water) in Region A as a function of the type and amount of triglyceride and concentration of C_{18:1}E₁₀ are shown in **Figure 24**. The CP of the 10, 15, 20 and 25 wt% micellar solutions were recorded as $57.4 \pm 0.4^\circ\text{C}$, $59.7 \pm 0.4^\circ\text{C}$, $60.0 \pm 1.0^\circ\text{C}$ and $59.7 \pm 1.2^\circ\text{C}$ respectively which were very close to the temperatures recorded for C_{18:1}E₁₀ by Warisnoicharoen *et al.* (2000a).

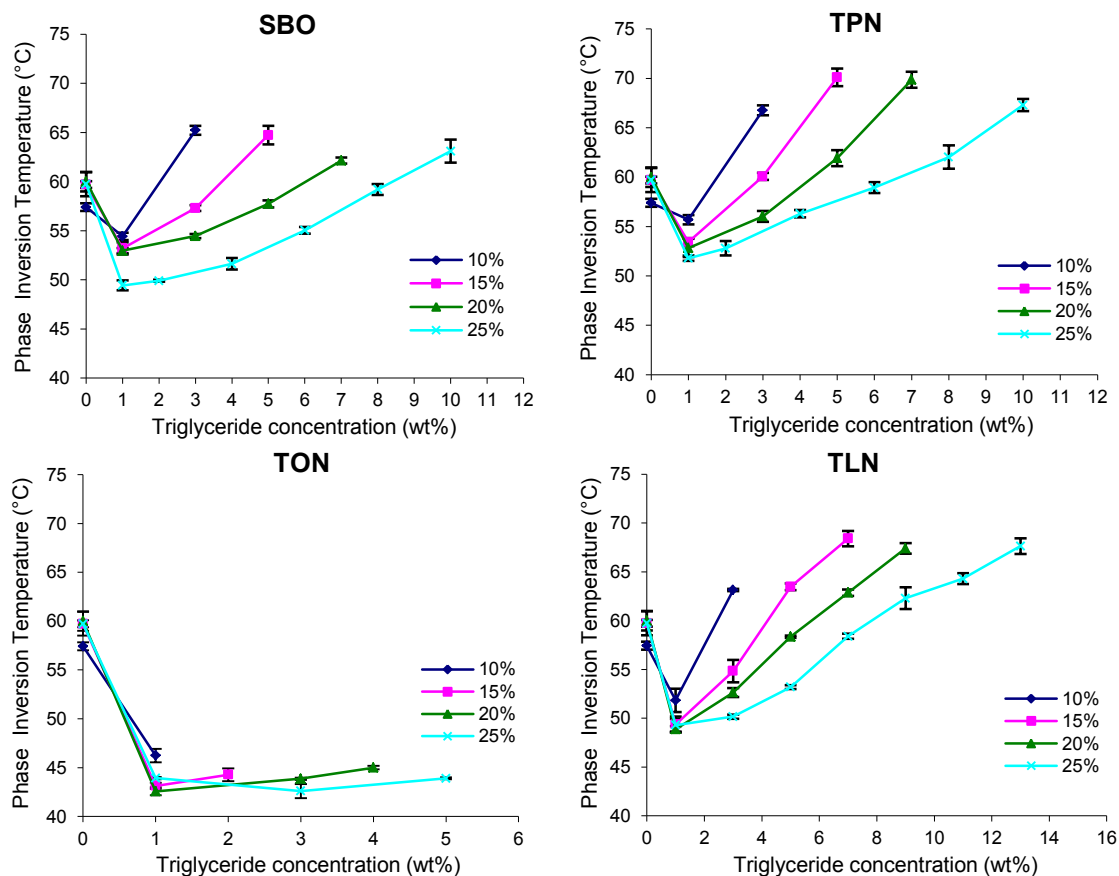


Figure 24 Variation in phase inversion temperature of nanoemulsions prepared using either 10, 15, 20 or 25 wt% $C_{18:1}E_{10}$ and containing either varying amounts of SBO, TPN, TLN or TON (mean \pm S.D., $n=3$).

The study on CP of micelle solution with increasing surfactant concentration in dilute regimes has been reported elsewhere for other nonionic surfactants. The previous report showed the dependence of CP of the mixtures of nonionic ethoxylated surfactants on their concentrations in water with increasing surfactant concentration. The CP decreased or, subsequently, increased after the decrease and eventually remained the

same (Li *et al.*, 2009). In contrast with the current result where the CP was independent of surfactant concentration, however, their tested concentrations (0.1 - 7 wt%) were really low compared to the concentrations used in this study (10 - 25 wt %).

The values of PIT found to illustrate the complex and concentration-dependent way in which the addition of triglyceride affects the CP. In all cases, the addition of 1 wt% of triglyceride to the $C_{18:1}E_{10}$ /water system resulted in a decrease in temperature from the CP of corresponding micelles, and this reduction was greatest when the largest amount of surfactant was used or, in other word, the weight ratio of oil to surfactant was lowest. At higher concentrations of SBO, TPN and TLN, an increase in the PIT of the NE was observed upon increasing triglyceride content whereas the addition of increasing amounts of TON did not result in any increase in the PIT. For NE containing the same triglyceride content, a decrease in the PIT was observed with increasing $C_{18:1}E_{10}$ concentration. For example, at lowest $C_{18:1}E_{10}$ concentration tested in this study, 10 wt% $C_{18:1}E_{10}$ for NE containing 3 wt% triglyceride, the PIT was higher than the CP of corresponding $C_{18:1}E_{10}$ /water system. On the other hand, at higher surfactant concentration, 15-25 wt% $C_{18:1}E_{10}$, the PIT of the NE containing 3 wt% triglyceride was lower than CP of corresponding $C_{18:1}E_{10}$ /water system and was lowest at 25 wt% $C_{18:1}E_{10}$.

A possible explanation for the effect of the triglyceride on CP is based on the shape of the aggregates formed; transformation of rodlike micelles into globular aggregates by solubilisation of hydrocarbon has been suggested for some ionic surfactants (Hoffmann and Ebert, 1988). For non-ionic surfactants it has been postulated

that if the hydrocarbon forms a core in the micelles interior, and if the micelles are originally asymmetrical thus the addition of the oil phase results in more spherical shape and the CP will be subsequently raised (Aveyard *et al.*, 1990). Moreover, the changes in PIT are typically explained in terms of the way in which oils of different volume/weight are solubilized into the droplets. For example, triglyceride with a large molecular volume is considered to form a core in the centre of the droplet and the smaller molecular volume triglyceride may act as a co-surfactant located in the surfactant hydrophobic tail and does not form a core. Obviously the definition of a „small“ and „large“ molecular volume oil is relative to the surfactant being studied, although it is generally considered that a small oil is one that has a chain length less than that of the hydrophobe of the surfactant, while oils with alkane chain lengths beyond that of the surfactant are considered to be large (Chen *et al.*, 1986; Evans *et al.*, 1986). It would not be unreasonable to consider the triglycerides used in the present study as “small” (TON), “medium” (TLN) and “large” (TPN and SBO).

The interpretation of PIT results depends upon the initial shape of the micelle; this can cause one of two effects. If the initial micelle droplet is spherical, the addition of a small amount of a large molecular volume oil does not significantly alter surfactant head group area and the hydrophobic volume of the surfactant, thereby allowing the droplet to maintain nearly the same degree of curvature and consequently exhibiting a PIT similar to the CP of the original micellar solution (Aveyard and Lawless, 1986). If, however, the micellar aggregate is initially slightly asymmetric, the addition of large molecular volume oil encourages a change in micelle shape from asymmetric to spherical, thereby

increasing the PIT of the system. In both instances the addition of higher amounts of the “large” molecular volume oils results in a further increase in PIT. In contrast, the addition of a low concentration of „small“ molecular volume oil acts in much the same way as a cosurfactant, increasing the effective hydrophobe volume (and decreasing the effective length of the hydrophilic head group) of the surfactant, thereby encouraging the formation of more asymmetric aggregates with lower spontaneous curvature and higher interparticulate interactions, and finally lowering the PIT (Monduzzi *et al.*, 1997). In some cases the addition of a higher concentration of “small” molecular volume oil may result in some of the oil going into the core of the droplet, transforming the asymmetric droplets to more symmetrical aggregates and thereby increasing the PIT.

In the current study, with the exception of TON, the PIT of the NE initially decreased and then increased as the concentration of oil was increased. This suggests that the micellar aggregates were originally asymmetric, a fact confirmed in a light scattering study (Warisnoicharoen *et al.*, 2000b; Malcolmson *et al.*, 2002) and most likely became spherical upon addition of a larger amount of oil due to the oil forming a core in the centre of the NE droplet. The fact that the addition of TON reduced the PIT of the NE compared to the CP recorded for the C_{18:1}E₁₀ micelles and the PIT did not increase to the CP temperature of the C_{18:1}E₁₀ micelles suggest that the oil chains might intimately mix with the surfactant hydrophobic tails. Furthermore, the PIT slightly increased as TON concentration increased suggesting that the aggregates probably encourage spherical aggregate otherwise the PIT would be lowered as the TON concentration increased. The

results here supported the hypothesis discussed earlier that the way TON incorporated in NE was different from the other three triglycerides.

On the basis of the change in PIT it would seem that TPN caused the largest increase in the PIT and therefore probably formed the largest triglyceride core in the center of the droplet, followed by SBO and then TLN. The largest core in the NE droplet is thought to provide more site of drug solubilisation. Comparison in PIT of systems prepared using either 10, 15, 20 or 25 wt% C_{18:1}E₁₀ is shown on **Figure 25**. On the basis of these results it might be reasonably expected that if the solubility of the drug, testosterone propionate, was similar in the various triglycerides then the TPN-contained NE would exhibit the greatest solubilisation of drug and TON-contained NE would exhibit the lowest solubilisation. While this explanation is plausible, it must be realized that it is based purely on phenomenological observation.

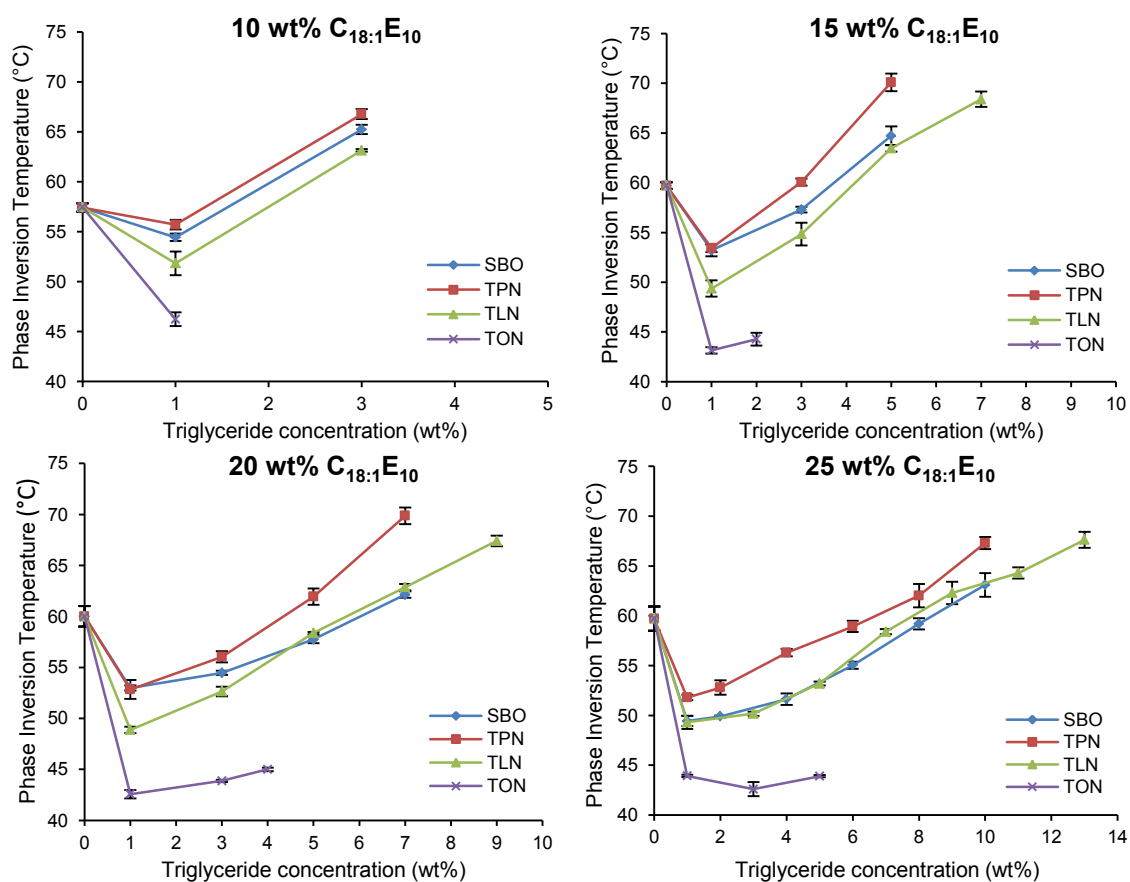


Figure 25 Comparison in phase inversion temperature of nanoemulsions prepared using either 10, 15, 20 or 25 wt% C_{18:1}E₁₀ and containing either varying amounts of SBO, TPN, TLN or TON (mean ± S.D., n=3).

4. Testosterone propionate solubility study

The level of solubilisation of the drug, testosterone propionate into triglyceride-in-water NE stabilized by $C_{18:1}E_{10}$ and containing both the liquid and solid triglycerides, has been determined at $22 \pm 2^\circ\text{C}$. From the information obtained from the phase diagram, compositions within Regions A to C were selected for solubility studies. The results of the solubilisation study of testosterone propionate (TP) in NE are given in **Figure 26**. As can be seen, all the NE, regardless of triglyceride, exhibited a significant increase in solubilisation of TP over the corresponding micellar solution suggesting that the presence of triglyceride has a positive effect on the level of incorporation of TP (**Figure 26**). The micellar solubility recorded in the present study for $C_{18:1}E_{10}$ is very similar to that reported by Malcolmson *et al.* (1998) as were the results obtained for the NE containing 2 wt% SBO and prepared using 10 wt% $C_{18:1}E_{10}$. Encouragingly, the results obtained in the present study were far more extensive than the limited solubilisation study performed by previous study. The drug solubility of NE produced by solid triglycerides has never been reported anywhere else, however, the solid lipid nanoparticles consisted of solid triglycerides has been reported as drug carrier (Wissing *et al.*, 2004; Dong *et al.*, 2009; Lopes *et al.*, 2012).

As can be seen, for systems prepared using 10 wt% $C_{18:1}E_{10}$, the solubility of TP increased in an approximately linear fashion with increasing triglyceride concentrations up to 5 wt% SBO, 2 wt% TPN and 7 wt% TLN followed by a level off prior the remarkably decreased at 6 wt% SBO, 7 wt% TPN and 8 wt% TLN. This levelling off of

drug solubility corresponded to added triglyceride concentrations just below the maximum level of incorporation of triglyceride in Region B (at the boundary between Regions B and C) and the decrease corresponded to the NE in Region C.

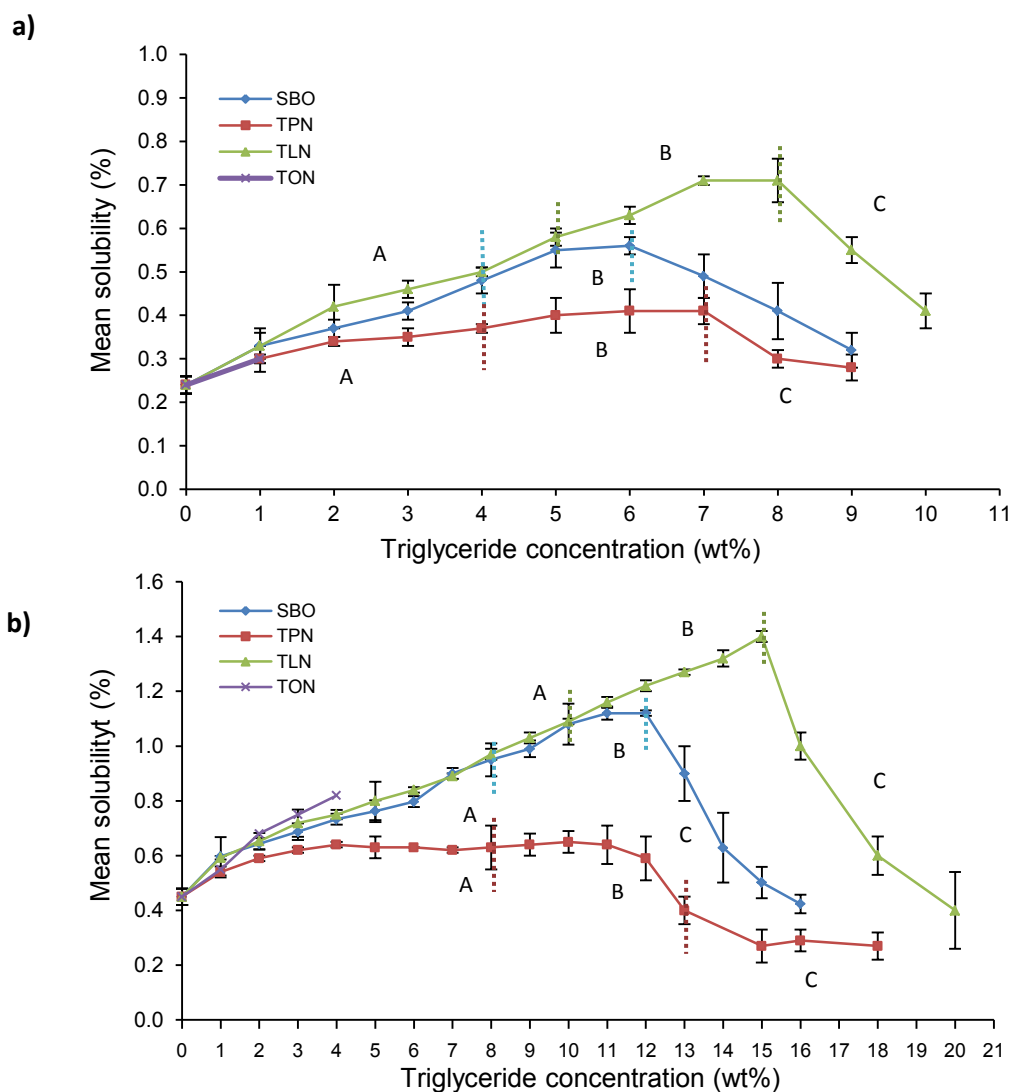


Figure 26 Solubilization of testosterone propionate in micelles and nanoemulsions stabilised using either a) 10 and b) 20 wt% C_{18:1}E₁₀ and containing either varying amounts of SBO, TPN, TLN or TON at 22 ± 2°C (mean ± S.D., n=4).

In the case of 20 wt% C_{18:1}E₁₀, the variation in the solubility of TP showed the same trend as was seen for the NE stabilized by 10 wt% C_{18:1}E₁₀ in that solubilisation significantly increased in an approximately linear fashion up to triglyceride concentrations of 11 wt% SBO, 4 wt% TPN, 15 wt% TLN and 4 wt% TON. After this point TP solubilisation of SBO-NE and TLN-NE rapidly decreased until the end of Region C. The levelling off of solubilisation was seen in the TPN-NE after 4 wt% TPN to the nearly maximum oil concentration (12 wt%) in Region B and greatly decreased at Region C. Interestingly, the concentrations of SBO, TPN and TLN where there was the linear increase in drug solubility of 20 wt% C_{18:1}E₁₀ approximately doubled the concentrations of SBO, TPN and TLN stabilized by 10 wt% C_{18:1}E₁₀ (compared at about the same triglyceride: C_{18:1}E₁₀ ratio). Also, these triglyceride concentrations were all within Regions A and B. These results were in line with the apparent hydrodynamic sizes which suggest the similar droplet size for the NE with the same triglyceride: surfactant ratio and that the NE stabilized by 20 wt% C_{18:1}E₁₀ contained double amount of droplet of NE stabilized by 10 wt% C_{18:1}E₁₀. The significant decrease in solubility from Regions B to C may suggest a change in structure of the NE droplets as this is the concentration which corresponds to the large increase in the apparent hydrodynamic size and suggests that these changes are not advantageous for drug solubilisation. Relationships between solubility and lipid microstructure have been reported (Sagar *et al.*, 2007) for instance, the solubility of lycopene changes dramatically with the different microstructures of the same mixture along the dilution line (Spernath *et al.*, 2002).

Previous work has shown that most drugs, even lipophilic drugs such as TP, are most likely to be solubilised in the interfacial region of a surfactant aggregate. Therefore, if the apparent aqueous solubility of a drug is to increase when an oil is present in the aggregate then the drug must have solubility in the oil and the oil must form a core in the aggregate (Malcolmson and Lawrence, 1993; Malcolmson *et al.*, 1998). If the oil behaves more like a cosurfactant and sits in the interfacial region of the surfactant aggregate then it will be expected to reduce solubilisation as it will disrupt the major site of solubilisation in the surfactant aggregate, offering no central core of oil in which the drug can dissolve. PIT studies clearly showed that the SBO, TPN and TLN did form a core in the centre of the NE droplet and it would be expected that the NE containing these triglycerides would exhibit an increase in testosterone solubility assuming that the triglyceride was present in a „liquid-like“ state. The NE containing TON might be expected to result in no increase in TP solubility according to the PIT result, however, solubilisation of TP did in fact increase in TON-NE. This result suggests that the TON could form partly an oil core and partially mixed with the surfactant tails interpreted from PIT result where the slight increase observed as TON concentration increased.

Particularly for the present study, the level of solubilisation obtained was comparable for SBO, TLN and TON at the same triglyceride concentration with slightly greater solubilisation being obtained for the TON-NE, TLN-NE and SBO-NE respectively. This results is encouraging as the TP solubility in bulk oil followed this order (the shortest chain triglyceride shows the greatest solubility) (Malcolmson *et al.*,

1998), though it is impossible to measure the TP solubility on bulk solid triglyceride. Significantly, opposite from the finding from PIT study, the increase in TP solubility in TPN-NE was lower than that obtained for SBO-NE, TLN-NE and TON-NE ($P < 0.01$), and obviously provided lowest solubility though the solubility was comparable at 1 wt% triglyceride prepared using 10 and 20 wt% $C_{18:1}E_{10}$. It is probable that the lower solubilisation recorded for the TPN-NE is a consequence of the triglyceride existing, at least partially, in the solid state in the NE droplets. The solubilisation capacity of TP in NE was also measured in 1-month-old NE where no significant change in solubilisation capacity was noted. This was despite the fact that TPN-NE appeared to show some instability in the form of a precipitate. The precipitation occurred at samples contained high TPN concentrations suggesting that TP affects the way TPN arrange in NE droplet.

5. Differential scanning calorimetry

Differential scanning calorimetry (DSC) was used to obtain an insight into the melting behaviour of triglyceride in the NE to aid in more understanding of the solubilisation experiments. DSC experiments on raw materials (water, $C_{18:1}E_{10}$ and triglycerides) were performed to observe their thermal behavior and employed as the control against the NE. **Figure 27** shows that the DSC experiments on water did not exhibit any thermal event as expected due to the freezing and melting point of water (0°C).

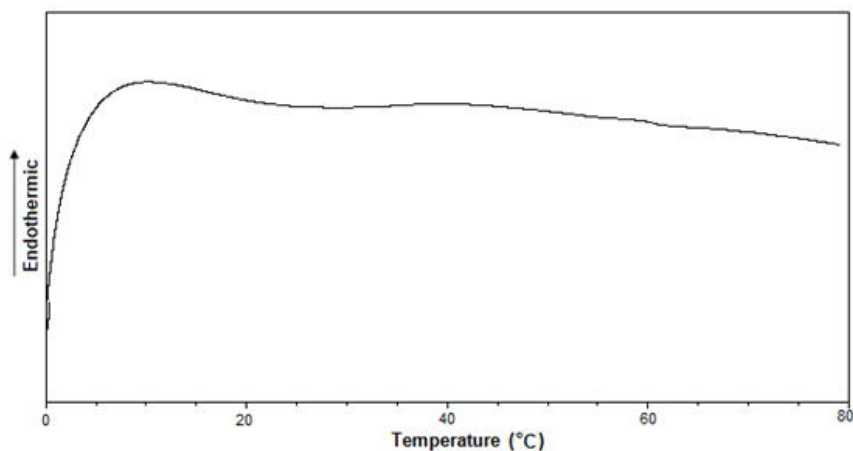


Figure 27 DSC thermogram of water heated at $1^{\circ}\text{C min}^{-1}$.

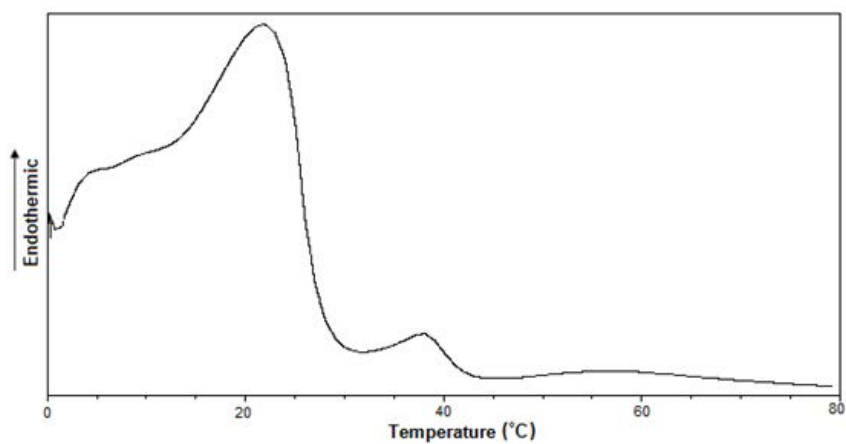


Figure 28 DSC thermogram of C_{18:1}E₁₀ heated at $1^{\circ}\text{C min}^{-1}$.

As illustrated in **Figure 28**, the melting endotherm of C_{18:1}E₁₀ was observed at 20°C and 37°C; the endothermic peak showed the melting point of the C_{18:1}E₁₀ due to their semisolid nature at room temperature ($22 \pm 2^{\circ}\text{C}$) and it is not surprising that C_{18:1}E₁₀ is required to heat to $50 \pm 5^{\circ}\text{C}$ prior the NE preparation.

DSC experiments on the bulk triglycerides showed that neither SBO nor TON exhibited a melting endotherm when the temperature of the sample increased from 0 to 80°C while TLN exhibited a single endotherm, corresponding to the melting of the β -form, at $\sim 50^\circ\text{C}$ and TPN at $\sim 65^\circ\text{C}$ (**Figure 29**). These measurements were in good agreement with previous DSC measurements made on bulk TLN and TPN (Hagemann, 1988; Heurtault *et al.*, 2003). The micellar solutions of 10 or 20 wt% $\text{C}_{18:1}\text{E}_{10}$ were also examined and showed none of melting endotherm within the 0-80°C temperature range (**Figure 30**). These results suggest that the melting endotherm may be expected for TLN-NE and TPN-NE but not TON-NE and SBO-NE and if there is any thermogram shown on TON-NE and SBO-NE it would be the influences of other phenomenon.

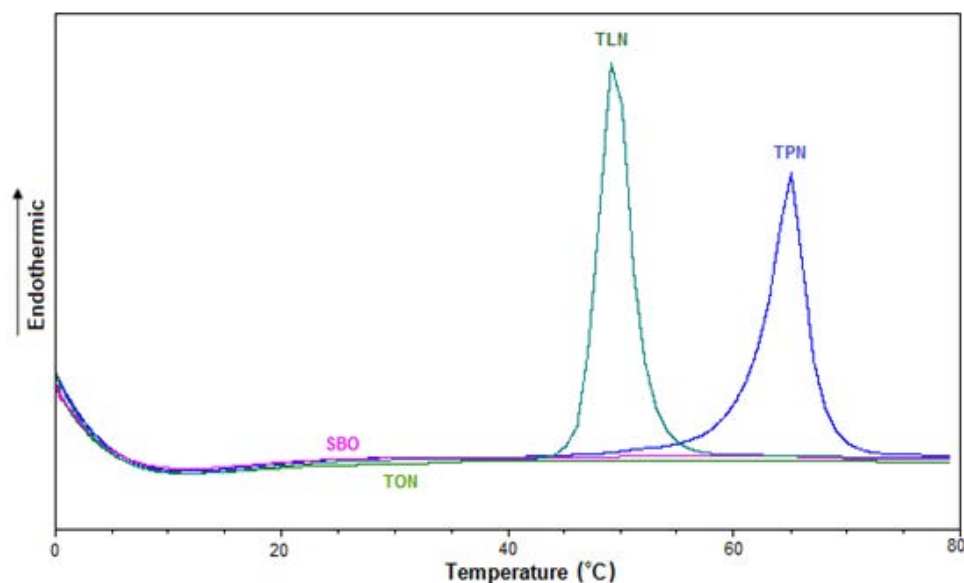


Figure 29 DSC thermograms of bulk triglycerides (SBO, TPN, TLN and TON) heated at 1°C min^{-1} .

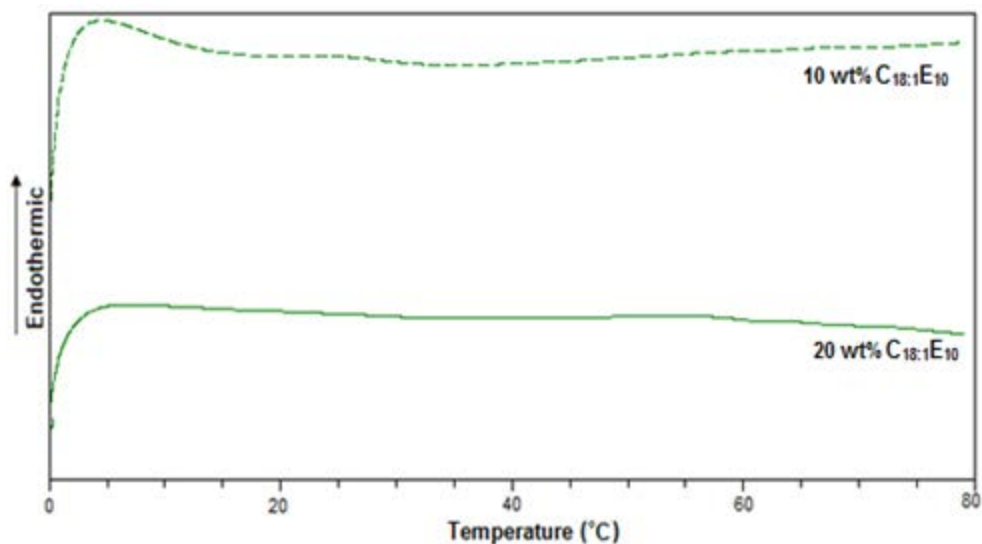


Figure 30 DSC thermograms of 10 or 20 wt% C_{18:1}E₁₀ micellar solutions heated at 1°C min⁻¹.

It has been widely reported that when solid triglycerides are incorporated into solid lipid nanoparticles it undergoes a series of endothermic and exothermic events upon heating which are typically assigned to particular lipid phase transitions (Himawan *et al.*, 2006). It is worth noting that the DSC experiments were performed by cooling the NE to 0°C and holding at this temperature for 30 minutes prior to heating the sample to 80°C. The DSC experiments were performed in this manner to see if any endothermic events were observable at temperatures below ambient. However, in order to ensure that cooling the NE to 0°C and holding at this temperature for 30 minutes did not induce any additional crystallization events, DSC experiments were also performed by starting the heating run at 20°C. Significantly, no differences were observed between the thermograms obtained using the two experimental conditions, most probably because the

re-crystallisation temperature of the NE did not happen at the temperature between 0-20°C. **Table 9** gives the melting temperature of the bulk (β -form) triglyceride and their recrystallisation temperature (α -form). It has also been reported that the re-crystallisation temperature decreases when a triglyceride is present in a SLN and that this decrease in the re-crystallisation temperature increases as the particle size of the SLN decreases (Unruh *et al.*, 1999; Bunjes and Unruh, 2007). Therefore, it is expected that the recrystallization temperature of NE containing triglycerides would be lower than the recrystallization temperature of bulk triglyceride shown on **Table 9**.

Table 9 The melting and recrystallisation temperature of the bulk triglyceride.

Triglyceride	Melting temperature (°C) (β -form)	Recrystallization temperature ¹ (°C) (α -form)
Soybean oil	< 0	< 0
Tripalmitin	~65	~42
Trilaurin	~50	~11
Trioctanoin	< 0	< 0

¹ Heurtault *et al.*, 2003

The DSC results of NE containing liquid triglycerides, TON-NE and SBO-NE prepared using either 10 or 20 wt% C_{18:1}E₁₀ are shown in **Figures 31-32**. DSC thermograms of TON-NE and SBO-NE showed that there were no any thermal events seen in any of the concentrations thus followed the physical behavior of their bulk triglycerides. On the other hand, the DSC results of NE containing solid triglyceride,

TLN-NE, did not exhibit the endothermic peak shown as bulk TLN. In fact, they did not exhibit any thermograms event; the flat lines occurred throughout the temperature range (**Figure 33**). Similar findings were reported by others researchers which indicated that TLN stabilized by phospholipid in combination with tyloxapol or bile salt was difficult to crystallize after processing into nanoparticles *via* a melt dispersion process. And the resulting dispersions could remain as supercooled melt (liquid-like) for several months if no special measures were taken to crystallize the nanoparticles (Westesen and Bunjes, 1995; Bunjes *et al.*; 1996, Heurtault *et al.*, 2003). Consequently, NE prepared from triglycerides which were solid at room temperature did not necessarily crystallize on common storage temperatures.

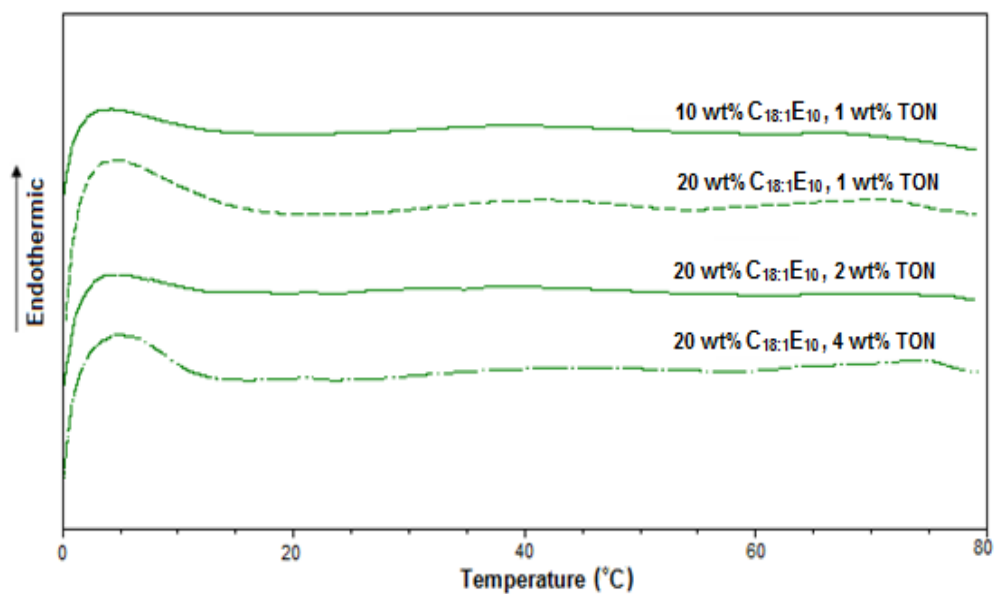
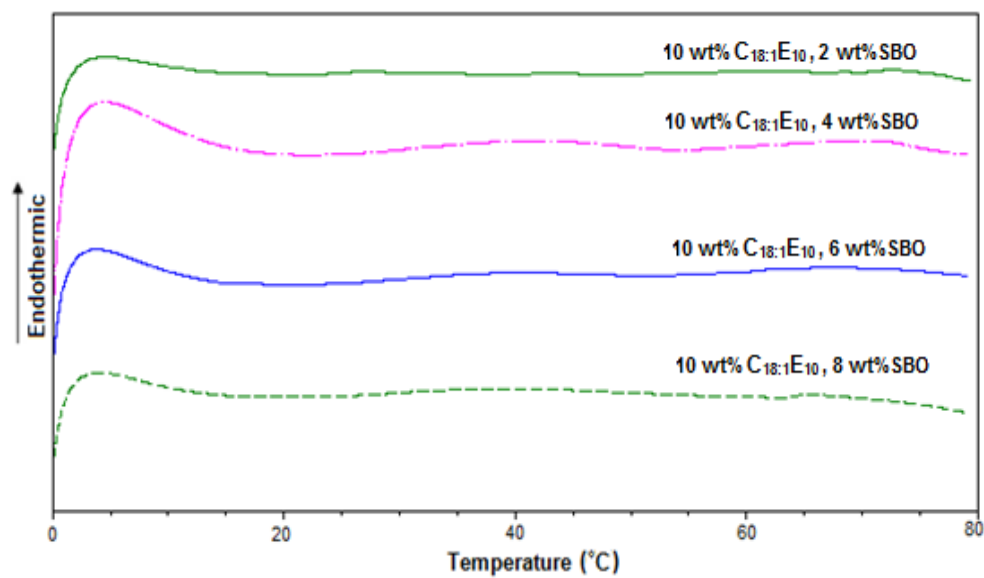


Figure 31 DSC thermograms of TON-NE stabilised by 10 wt% or 20 wt% C_{18:1}E₁₀ heated at 1°C min⁻¹.

a)



b)

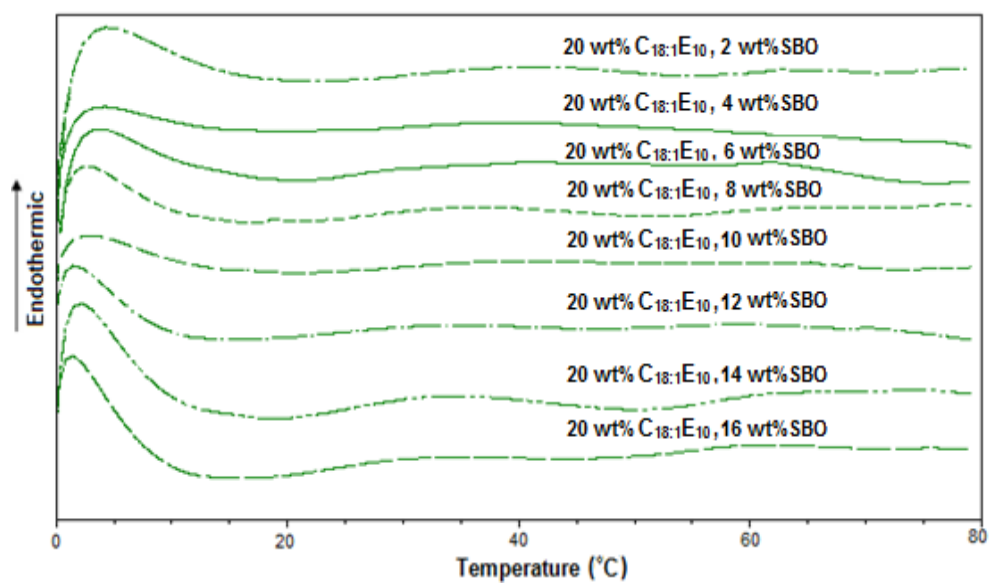


Figure 32 DSC thermograms of SBO-NE containing varying amounts of SBO stabilised by a) 10 and b) 20 wt% C_{18:1}E₁₀ and heated at 1 °C min⁻¹.

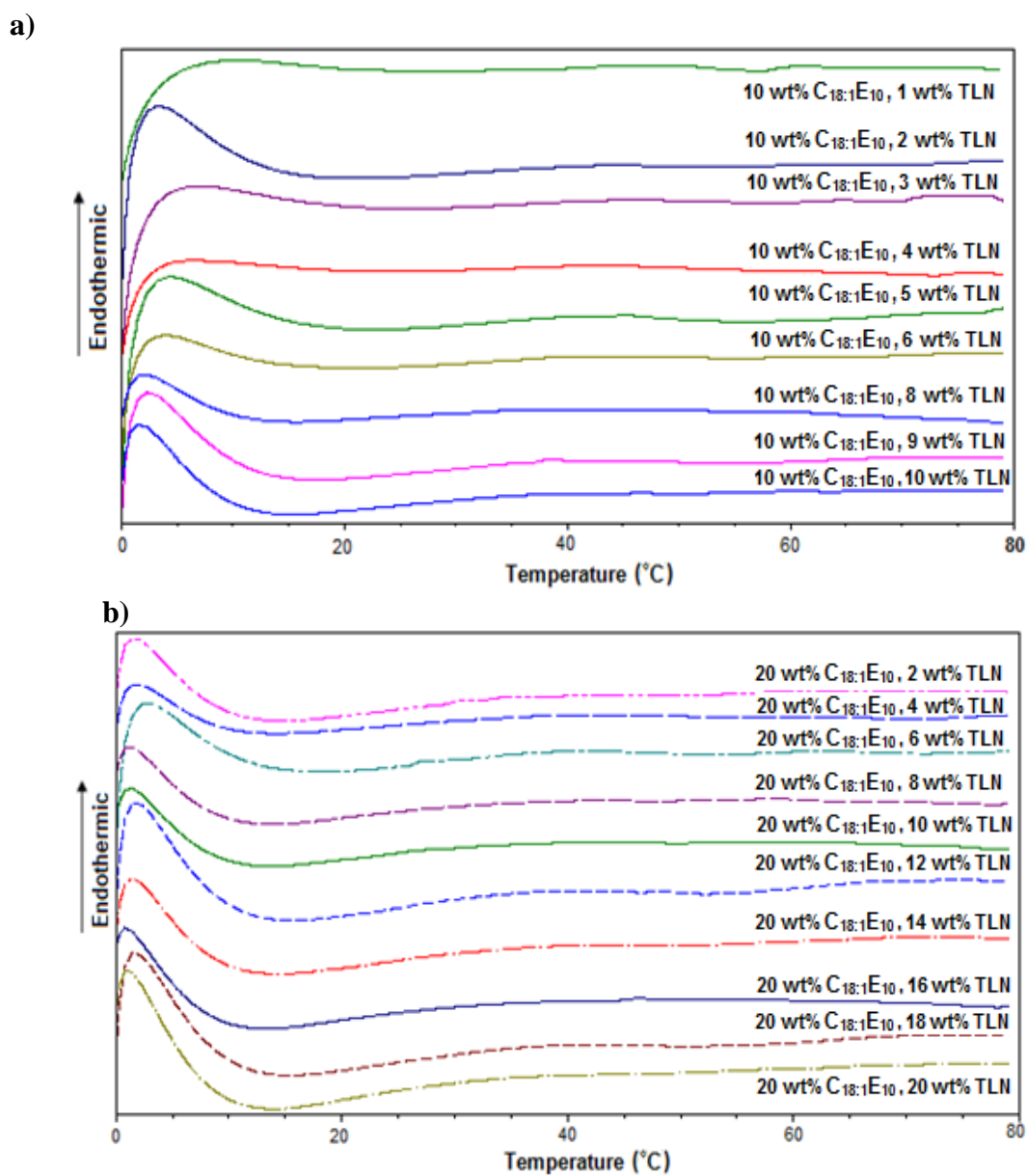
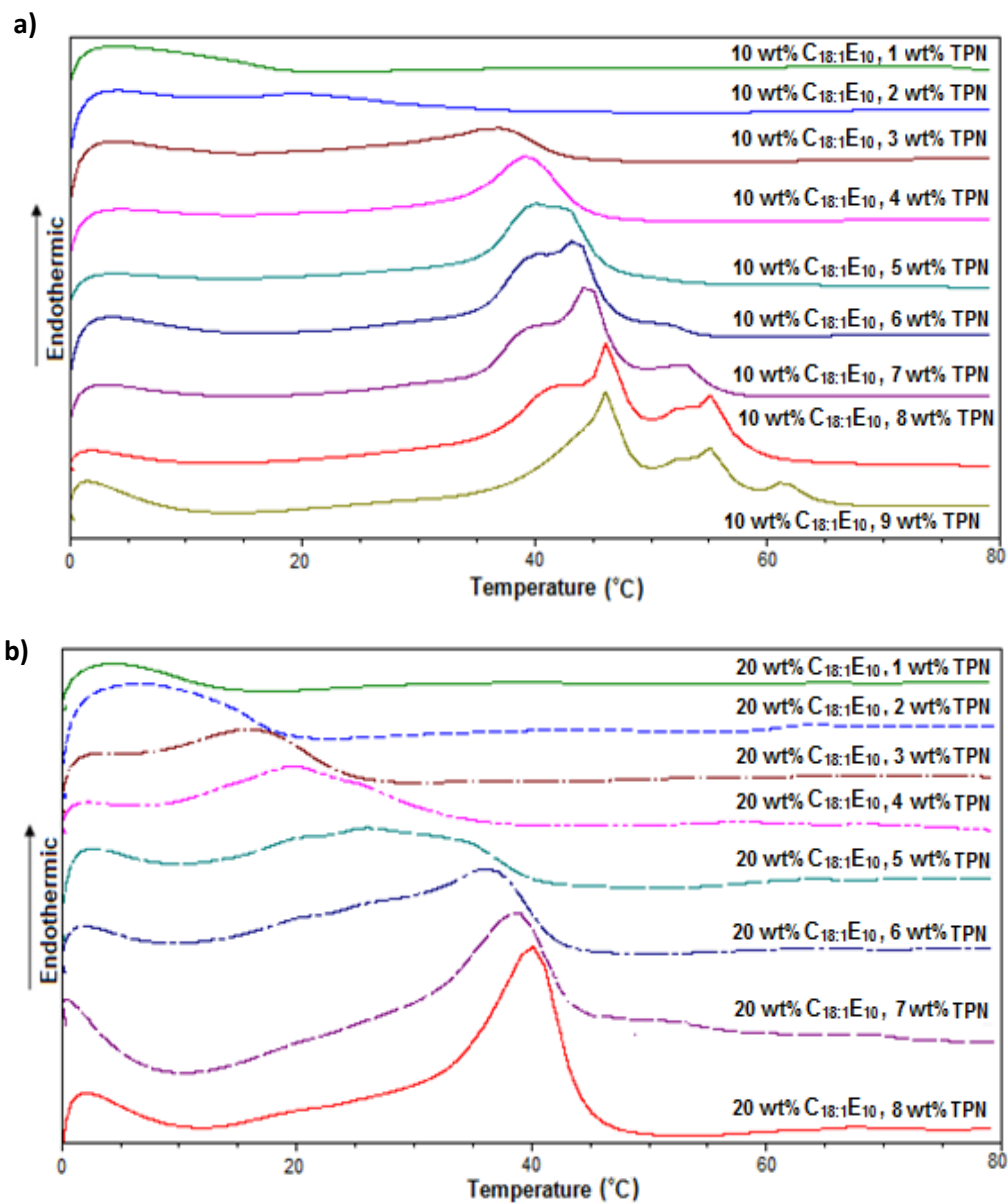


Figure 33 DSC thermograms of TLN-NE containing varying amounts of TLN stabilised by a) 10 and b) 20 wt% C_{18:1}E₁₀ and heated at 1°C min⁻¹.

The results above indicated that regardless of the triglycerides and surfactant concentrations, none of the NE containing SBO or TLN or TON exhibited any thermograms event over the temperature range studied suggesting that these triglycerides were incorporated into the NE in a „liquid-like“ state at experimental temperature ($22 \pm 2^\circ\text{C}$). This suggested that, at least under the conditions of the experiment, SBO, TLN and TON did not crystallize in the NE droplets. These support well with the solubility study as well as previous reports by others researchers for system containing TLN (Bunjjes *et al.*, 1996; Heurtault *et al.*, 2003). However, in recent publication, it was found that TLN nanoparticles transferred into the solid state by storing the TLN dispersion stabilized with egg yolk lecithin or fully saturated phospholipids for 24 hours at 0°C leading to virtually complete crystallization (Bunjjes and Koch, 2005). These results proposed that in order to maintain the dispersion containing solid triglyceride in liquid-like state, the storage temperature must be above the critical recrystallization temperature. The recrystallization for different dispersion depends on many factors such as the production method, type of surfactant, surfactant concentration and storage condition (Robb and Stevenson, 2000; Bunjjes and Koch, 2005).

In contrast to other NE, only in the TPN-NE was any thermal event recorded (**Figure 34**). It should be noted that regardless of concentrations of surfactant and triglycerides, the melting endotherms observed for the TPN-NE all occurred at temperatures lower than the PIT of the NE. This is a very important observation as it confirms that the observed thermal events are due to the NE and not a consequence of

any gross change in the nature (size and shape) of the NE droplet or any phase separation that may have occurred upon heating the NE above their PIT.



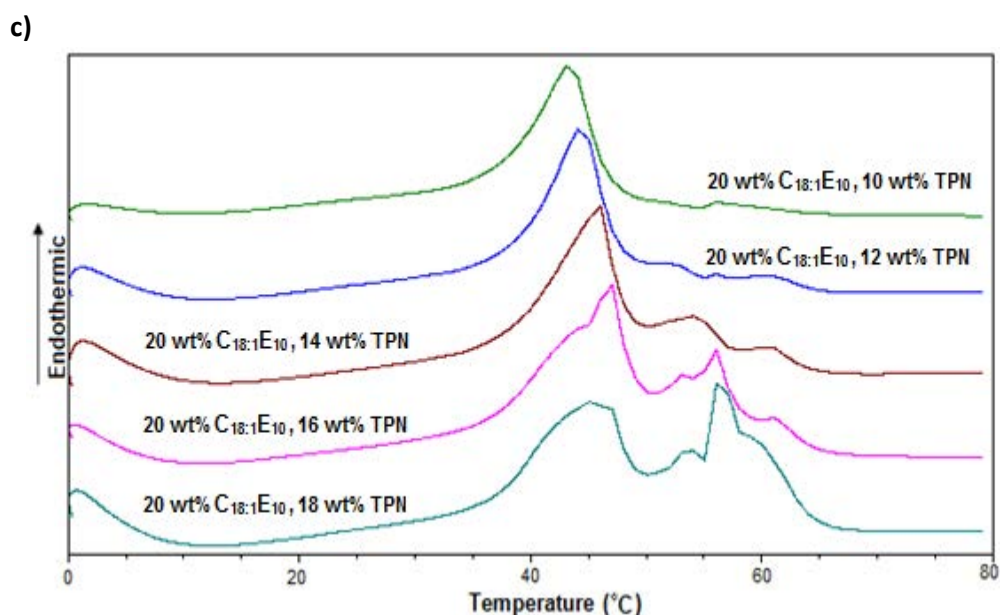


Figure 34 DSC thermograms of TPN-NE stabilised by a) 10 wt% C_{18:1}E₁₀ and b) 20 wt% C_{18:1}E₁₀ (1-8 wt% TPN) and c) 20 wt% C_{18:1}E₁₀ (10-18 wt% TPN). The samples were heated at 1°C min⁻¹.

In DSC, TPN-NE displayed differences in thermal transition depending on the TPN concentration used to prepare NE (**Figure 34a-c**). DSC thermograms of TPN-NE stabilized with 10 or 20 wt% C_{18:1}E₁₀ recorded 24 hours after preparation showed that the complexity of thermal transitions increased with increasing TPN concentrations. TPN-NE consisting 10 wt% C_{18:1}E₁₀ with 1 wt% TPN and 20 wt% C_{18:1}E₁₀ with up to 2 wt% TPN had no melting peak occurring at experimental temperature ($22 \pm 2^\circ\text{C}$), while 10 wt% C_{18:1}E₁₀ with 2 wt% TPN-NE and 20 wt% C_{18:1}E₁₀ with up to 4 wt% TPN-NE had the melting peak occurred at temperature around $22 \pm 2^\circ\text{C}$. The results suggested that NE prepared containing these amount of triglycerides were mostly if not all in liquid state at

$22 \pm 2^\circ\text{C}$ supporting the solubility results where there was the significantly increase in TP solubility up to these composition. With TPN concentrations up to 5 and 10 wt% stabilized by 10 and 20 wt% C_{18:1}E₁₀ respectively, the melting peak occurred at around 39-44°C (above experimental temperature, $22 \pm 2^\circ\text{C}$), which can be attributed to the melting of α -modification form (Siekmann and Westesen, 1994; Helgason *et al.*, 2009). At higher TPN concentration, DSC thermograms showed evidence of two polymorphic forms of TPN-NE upon heating with endothermic transition peaks at 44-46°C, 53-56°C and at highest TPN the extra endothermic peak at 61-62°C were displayed, which can be attributed to the melting of α , β^* and β crystal forms, respectively (Himawa *et al.*, 2006; Awad *et al.*, 2008; Wingbergs *et al.*, 2009). The lower melting point and the difference in transition kinetics are different from that described for bulk material due to the very small size of the particles and the high amount of surfactant molecules stabilized the NE (Unruh *et al.*, 1999; Mehnert and Mader, 2011; AL-Haj and Rasedee, 2009). Notably, the TPN-NE melted at about 3-4°C lower than the bulk TPN. These melting peaks agreed well with previously reported melting peaks observed in TPN nanoparticles (Bunjes and Koch, 2005; Helgason *et al.*, 2008), although for the thermogram obtained in the present study is far more complex than those reported. These results indicated that most of incorporated TPN exist in solid like state at 22°C in agreement with the solubility result where the TP solubility were not increased in NE consisting of these composition.

Bunjes *et al.* suggested that polymorphic transition in triglyceride nanocrystals was not only associated with molecular rearrangements but might also lead to alterations in general matrix structure and overall shape of the nanoparticles (Bunjes *et al.*, 2003;

Bunjes, 2011). Transition into a more stable triglyceride polymorph is accompanied by a rearrangement of the triglyceride molecules and an increase in lattice density (Sato and Ueno, 2011). Other authors suggested that the lipid matrix transforming from α to β polymorphic structures was driven the change of solid lipid nanoparticles from spherical to needle-shape (Jenning *et al.*, 2000; Bunjes *et al.*, 2007). Indeed, the size measurement study indicated that there was a sharp increase in size of NE in Region B where the thermal events of TPN-LN were complex and consisted of different polymorphic transitions indicating that the TPN might be incorporated into the NE in a variety of different ways. Despite of the confusion of the NE term where are universally known as the mixture of two immiscible liquids, the TPN stabilized by C_{18:1}E₁₀ that are in solid-like state are more appropriately classified as solid lipid nanoparticles.

DSC scans made on 1-month-old NE for all triglycerides showed no difference from those obtained from 24-hour-old samples, confirming that the NE were still stable at this stage after their preparation, A result was in agreement with the visual and dynamic light scattering experiments. Finally, repeated measurements on „fresh“ NE and month- old samples of identical composition yielded identical thermograms suggesting that the internal structure of the NE had not changed over this time period.

6. Effect of drug incorporation

NE cannot be considered to be inert carriers of drug because the presence of drug may alter their size, shape and stability of the NE, particularly if the drug exhibits some surface activity (as indeed many do) and sits in the interfacial surfactant region where it will disrupt the packing of the surfactant (Narang *et al.*, 2007). While testosterone propionate (TP) is not surface active, it is considered to be at least partially located at the boundary between the hydrophobic and hydrophilic portions of the surfactant and so its presence may affect NE stability. Although Malcolmson (1992) has reported that C_{18:1}E₁₀ microemulsions containing SBO were unaffected by the presence of an excess of TP drug (Malcolmson, 1992). Effect of drug loading on mean globule size has been reported and showed that drug incorporation can have significant influence on mean globule size and may precipitate upon dilution (Borhade *et al.*, 2008; Lijuan *et al.*, 2009). The effect of the addition of TP on the stability of the NE containing varying amounts of triglyceride was investigated in the present study by saturating NE prepared using 10 and 20 wt% C_{18:1}E₁₀. The excess drug was removed from the NE after 7 days by centrifugation. It is important to note that, from visual observation, there was no evidence of the centrifugation precipitating in any NE, either in the presence and absence of TP after centrifugation. The TP saturated NE prepared with SBO, TLN and TON were all stable for at least 2 months. The area of NE existence was the same; the clear, translucent and milky NE remained essentially the same. By way of contrast, however, samples containing TPN were unstable. For example, TP-loaded NE prepared with 10 wt% C_{18:1}E₁₀ and containing 7-9

wt% TPN were precipitated by third week, while those prepared with 4-6 wt% oil were unstable by fourth week and those with only 2-3 wt% oil by sixth week. Similar results were obtained for NE prepared using 20 wt% C_{18:1}E₁₀ and containing 14 – 18 wt% TPN were unstable by third week, while those prepared with 8 - 12 wt% lipid were unstable by fourth week and those with only 5 - 7 wt% lipid by sixth week. The drug-loaded TPN-NE generally manifested their instability more quickly than the corresponding TP-free NE. The only exceptions to this were the samples containing relatively small amounts of TPN, namely 1 wt% TPN and 10 wt% C_{18:1}E₁₀ and 2-3 wt% TPN and 20 wt% C_{18:1}E₁₀, which remained stable for at least 2 months, suggesting that the NE containing the lower concentrations of triglyceride were more stable. And that, at higher triglyceride concentrations, the NE could not re-arrange themselves to accommodate both the TP and the triglyceride within their structure. These results were supporting the DSC results in which 10 wt% and 20 wt% C_{18:1}E₁₀ containing 1 wt% and 2-3 wt% TPN were in liquid-like state under the experimental conditions.

An interesting observations made during the study was that the blank (i.e. drug-free) TPN-NE, which were treated in the same way as their TP-contained counterparts and as a consequence were centrifuged, were more unstable than those samples used for preparation of the phase diagrams which were not centrifuged (centrifugation being a common method of stressing emulsions to determine their stability). Centrifugation had no affect on the stability of the TP-contained and TP-free SBO, TLN and TON samples. These studies showed that the NE containing the fluid-like triglycerides (SBO, TON) and TLN exhibited more long term stability both in the absence and presence of the lipophilic

TP drug, whereas the stability of the NE containing the solid-like triglycerides, TPN, is less, particularly when high amount of TPN were used as the dispersed phase and loaded with TP. The high stability of the SBO-NE and TLN-NE, coupled with the relatively large NE region they exhibited suggested that the NE offer potential as drug delivery vehicles.

The effect of the addition of saturation amounts of TP on the apparent hydrodynamic size of TPN-NE and TLN-NE was measured 7 days after the addition of drug, with excess TP removed by centrifugation.

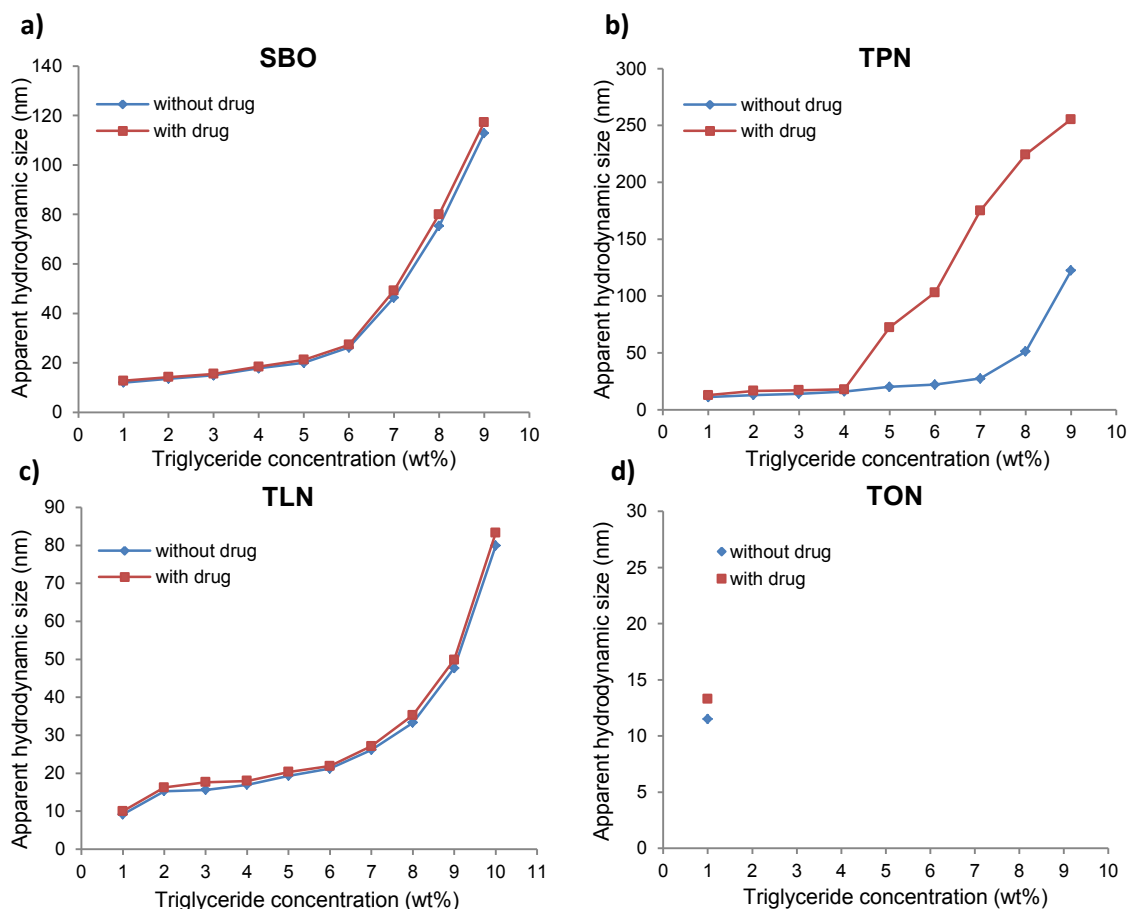


Figure 35 The comparison of the mean hydrodynamic sizes at $22 \pm 2^\circ\text{C}$ of the nanoemulsions with and without saturated amount of testosterone propionate prepared using a) SBO b) TPN c) TLN and d) TON and stabilised by 10 wt% $\text{C}_{18:1}\text{E}_{10}$ (mean \pm S.D., $n=3$).

In all cases the presence of the TP resulted in an increase in the apparent hydrodynamic size (D_h) of the droplets. This increase in D_h was small for all SBO-NE, TLN-NE and TON-NE (a maximum increase of about 2-5 nm was observed) but tended to be much larger for some TPN-NE (**Figures 35-36**).

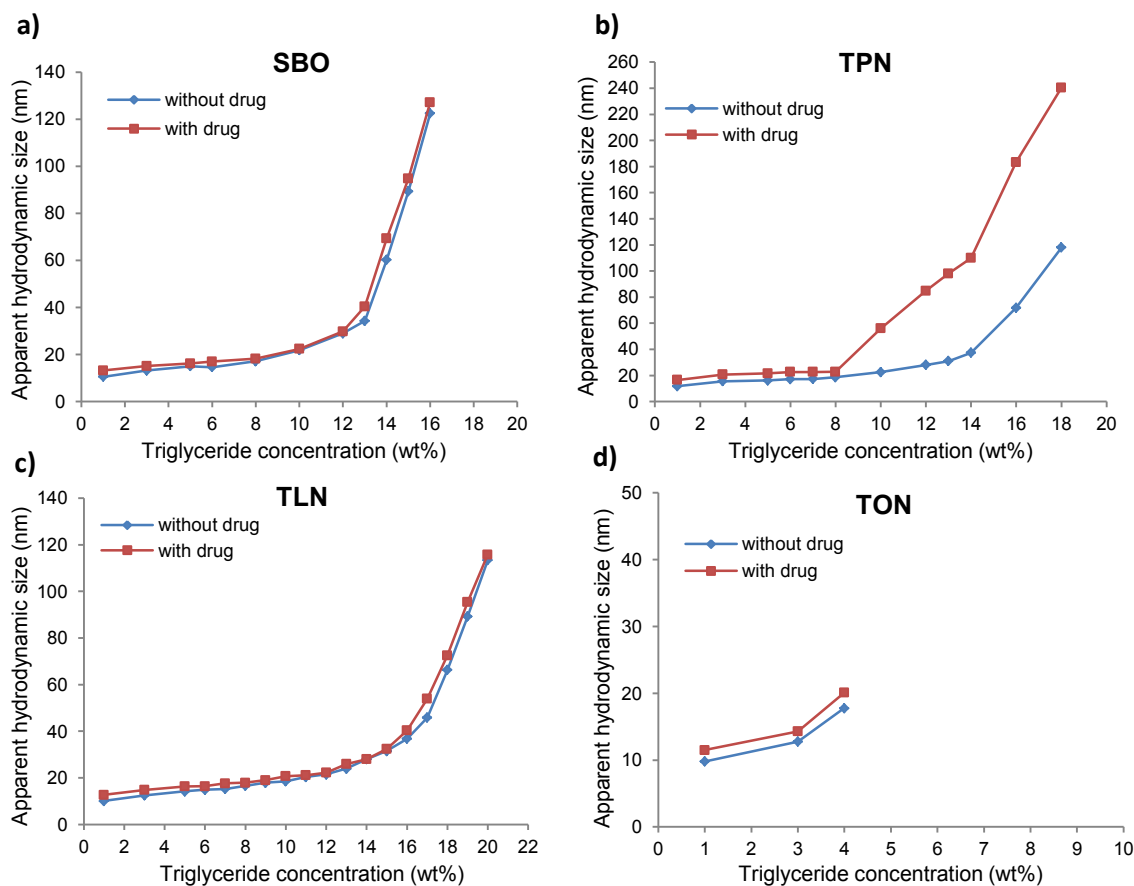


Figure 36 The comparison of the mean hydrodynamic sizes at $22 \pm 2^\circ\text{C}$ of nanoemulsions with and without saturated amount of testosterone propionate prepared using a) SBO b) TPN c) TLN and d) TON and stabilised by 20 wt% $\text{C}_{18:1}\text{E}_{10}$ (mean \pm S.D., $n=3$).

The droplet sizes were different only about 2-5 nm as observed by the D_h of TP-contained SBO-NE, TLN-NE and TON-NE suggesting that TP did not have any effect on these NE structure. **Figures 35b and 36b** show that droplet size of the drug-loaded TPN-NE prepared with 10 wt% $\text{C}_{18:1}\text{E}_{10}$ with up to 4 wt% TPN and 20 wt% $\text{C}_{18:1}\text{E}_{10}$ with up to 8 wt% TPN (Region A) were comparable to their corresponding TP-free NE. However,

the D_h of drug-loaded TPN-NE at high TPN concentrations (10 wt% $C_{18:1}E_{10}$ with 5-9 wt% TPN and 20 wt% $C_{18:1}E_{10}$ with 10-18 wt% TPN) were sharply increased from their corresponding TP-free samples; the D_h of TP-contained TPN-NE were at least 3 times higher than D_h of TP-free TPN-NE. This result agreed with the phase behavior study where the samples that sharply increased in D_h manifested their instability more quickly than the corresponding TP-free TPN-NE. According to the limitation of TP solubility in TPN-NE, beside this result, it is reasonable to consider that TP was unable to solubilize in TPN-NE that were considered to be mostly in solid state (high TPN concentration) and mainly in the core part of the structure. Subsequently, TP attempts to solubilize at the boundary between the hydrophobic and hydrophilic portions of the surfactant, affecting the arrangement in aggregate structure. NE cannot re-arrange themselves to accommodate both the TP and the TPN within their structure, affecting the way TPN arranges in NE droplet at these compositions.

The patterns of the CP and PIT of both drug-loaded micellar solution and NE were followed those of their corresponding TP-free samples, nevertheless, both CP and PIT reduced in comparison with the corresponding TP-free samples (**Figure 37**) suggesting that TP were partly located at the boundary between the hydrophobic and hydrophilic portions of the surfactant. The differences in PIT were least in TON-NE which were around 1-2°C followed by SBO-NE and TLN-NE in which the differences were around 3-5°C equivalent to the differences in CP of TP-free micellar solution and TP-loaded micellar solution. The finding indicated that TP was solubilised in the surfactant boundary of SBO-NE and TLN-NE similar to the micellar solution. For TON-

NE, TP might not solubilise at the surfactant boundary to the same extent as micellar solution since the TON might intimately mixed with the surfactant hydrophobic tails as mentioned in previous sessions and occupied the potential solubilising site of TP. In the case of TPN-NE, the PIT change seemed to be more in drug-loaded TPN-NE around 6-10°C implying that the TP was attempted to solubilise at the boundary between the hydrophobic and hydrophilic portions of the surfactant in TPN-NE. The decrease in PIT increased as the TPN concentrations increased hence the core of NE containing higher amount of TPN were more solid as supported by the DSC experiment, consequently, the ability of TP to solubilise in the core were decreased as TPN amount increased.

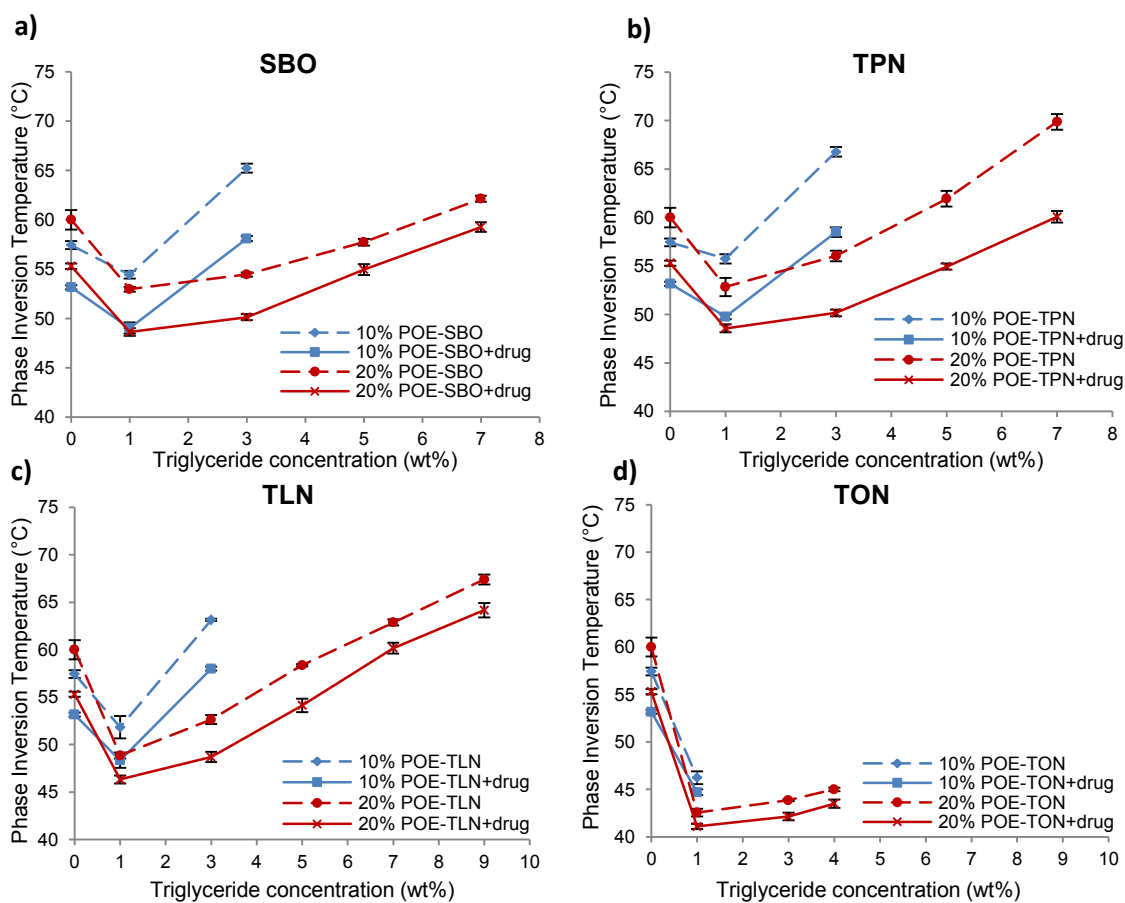
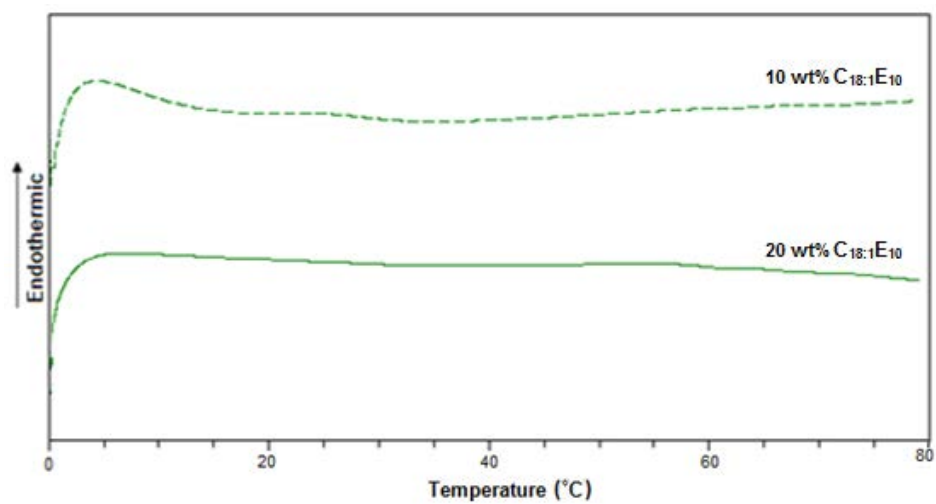


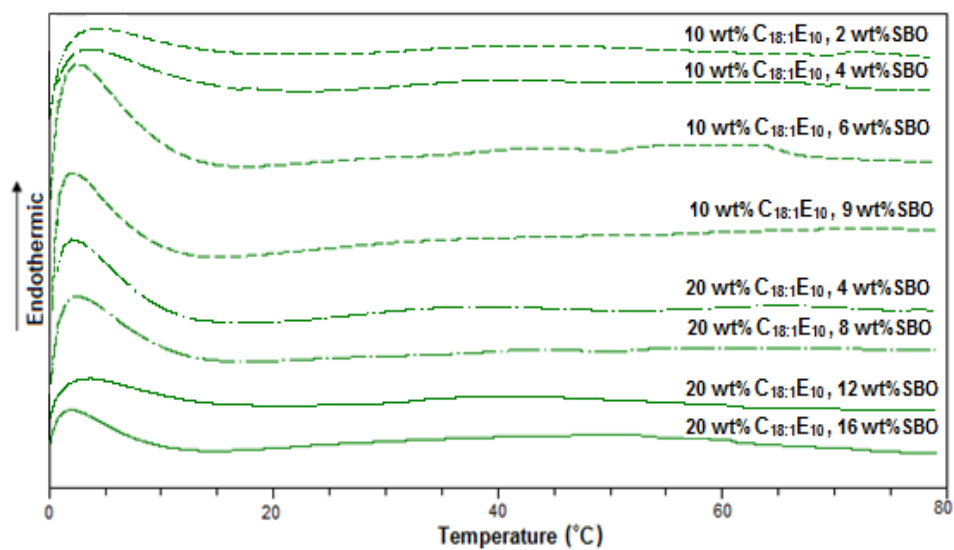
Figure 37 The comparison of the phase inversion temperatures of the nanoemulsions prepared using either 10 or 20 wt% $C_{18:1}E_{10}$ and containing either varying amounts of a) SBO, b) TPN, c) TLN or d) TON with and without the presence of a saturated amount of testosterone propionate at $22 \pm 2^\circ\text{C}$ (mean \pm S.D., $n=3$).

For DSC experiment, the effect of the presence of a saturation amount of TP on the thermal behaviour of the 10 and 20 wt% $C_{18:1}E_{10}$ micellar solutions showed that there were no differences in thermograms observed between the micellar solutions with and without the presence of TP (**Figure 38a**).

a)



b)



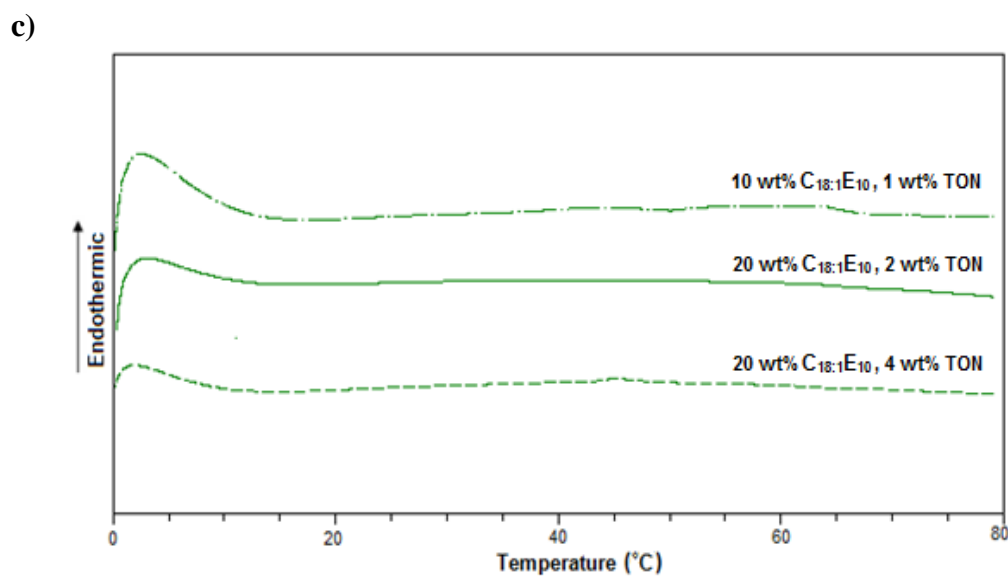
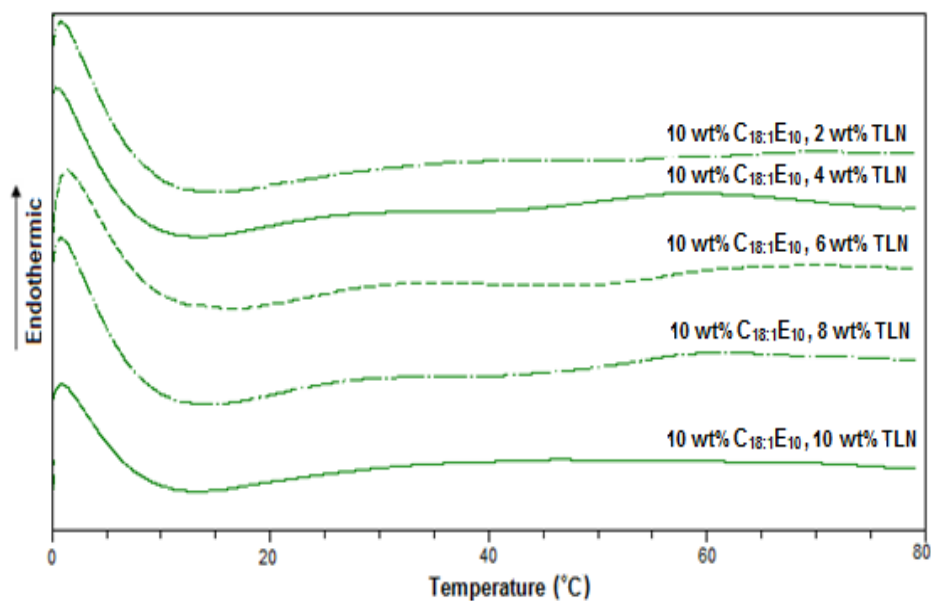


Figure 38 DSC heating curves ($1^{\circ}\text{C min}^{-1}$) of a) 10 or 20 wt% $\text{C}_{18:1}\text{E}_{10}$ micellar solutions containing drug, and drug-loaded nanoemulsions stabilized using either 10 or 20 wt% $\text{C}_{18:1}\text{E}_{10}$ and containing varying amounts of b) SBO and c) TON.

Also, the presence of saturation amount of TP had no discernable effect on the thermal behaviours of SBO-NE, TON-NE, TLN-NE and TPN-NE (**Figures 38-40**). Their DSC thermograms were the same as those of 24-hour-old samples (**Figures 31-34**) suggesting that TP was completely solubilized in these triglycerides. Even though TP notably affected the stability of NE stabilized by 10 wt% $\text{C}_{18:1}\text{E}_{10}$ and 20 wt% $\text{C}_{18:1}\text{E}_{10}$ containing 5-9 wt% TPN and 10-18 wt% TPN respectively as shown in droplet size measurement, the presence of TP clearly did not accelerate the solidification process on NE samples.

a)



b)

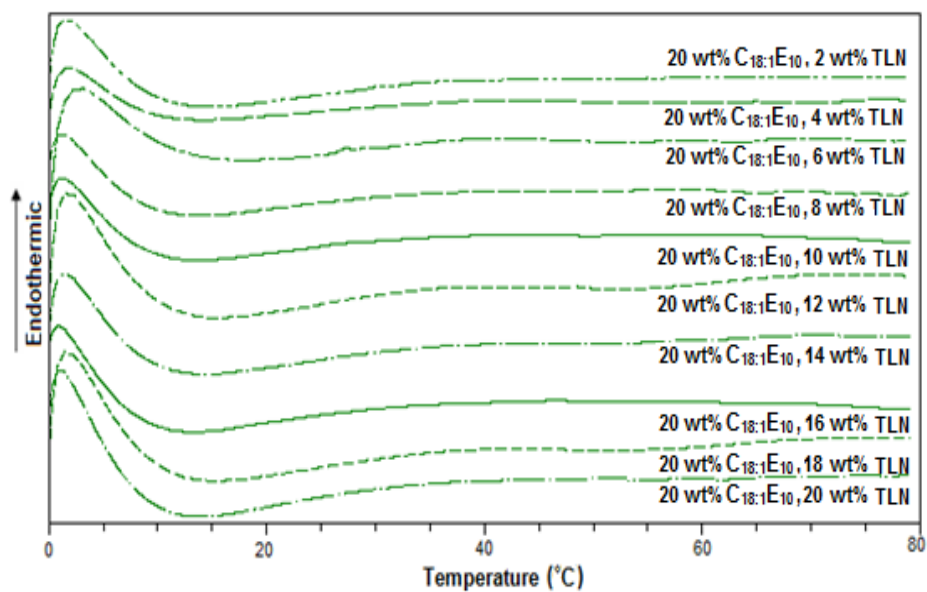
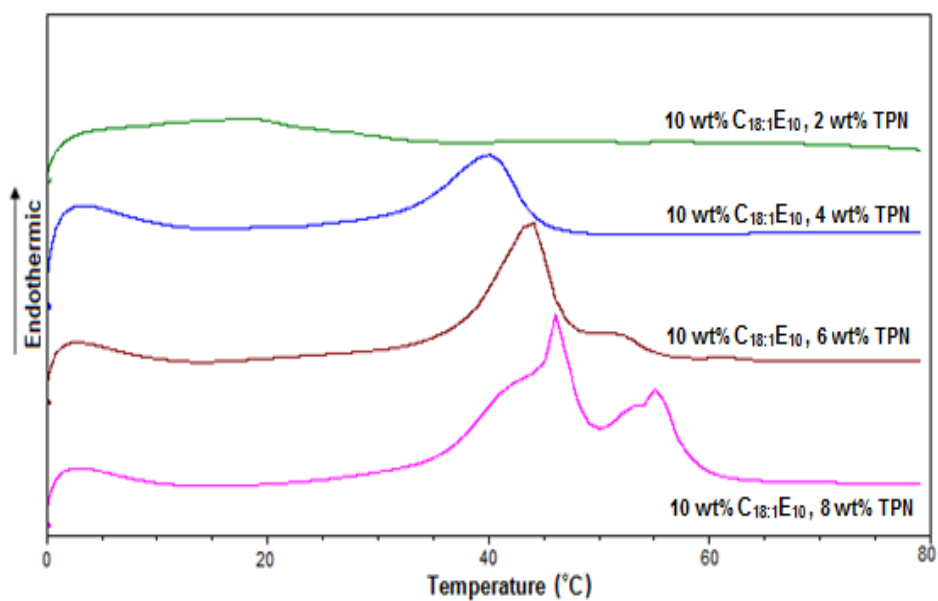


Figure 39 DSC heating curves ($1^{\circ}\text{C min}^{-1}$) of nanoemulsions containing a saturated amount of testosterone propionate and various amounts of TLN stabilized using either a) 10 or b) 20 wt% C_{18:1}E₁₀.

a)



b)

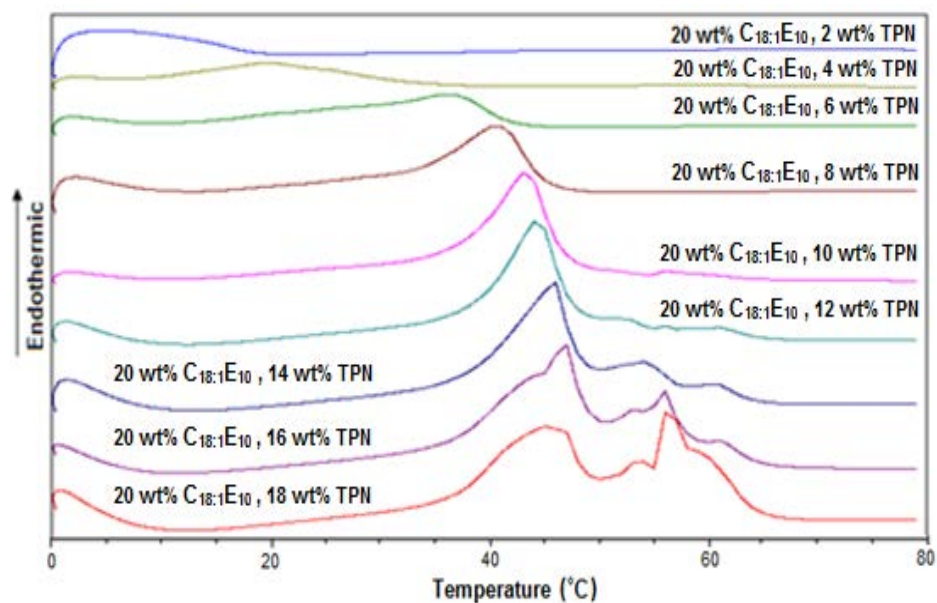


Figure 40 DSC heating curves ($1^{\circ}\text{C min}^{-1}$) of nanoemulsions containing a saturated amount of testosterone propionate and various amounts of TPN stabilized using either a) 10 or b) 20 wt% C_{18:1}E₁₀.

7. Small angle neutron scattering (SANS) study

7.1 SANS studies of C_{18:1}E₁₀/D₂O binary system

The micellar aggregate of C_{18:1}E₁₀ in D₂O were modeled using SANS data assuming monodispersed core-shell ellipsoidal shape. The model for the micelle adopted in the present study was assumed that a core was composed of the C₁₈ hydrocarbon chains of the surfactant and a shell was made up by the polar heads and some solvent molecules. The interparticle structure factor was modeled based on hard-sphere interactions solved by the Percus-Yevick approximation. A series of fits for the C_{18:1}E₁₀ micelles at various concentrations are shown in **Figures 41 and 42**. Dash lines were the structure factor $S(Q)$. Q and $I(Q)$ are scattering vector and scattering intensity respectively.

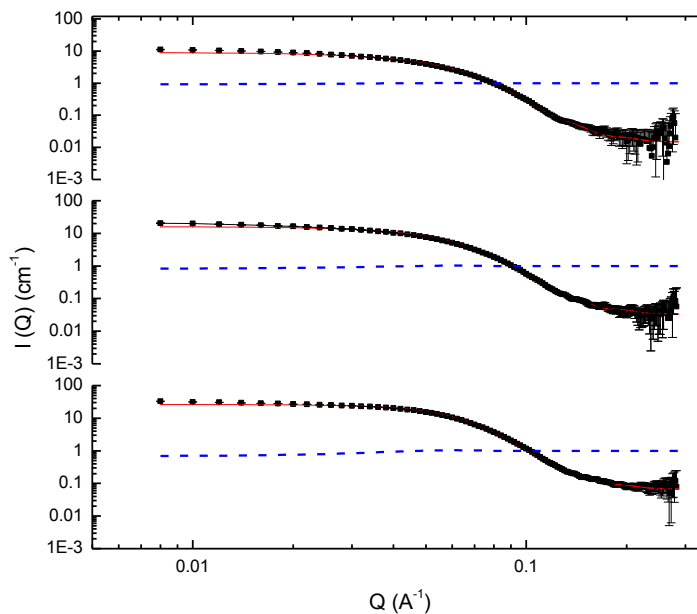


Figure 41 Three contrasts (core, drop and shell) of SANS data for 1.2% w/v, 2.4% w/v and 4.8% w/v $C_{18:1}E_{10}$ micelles (from top to bottom) at 25°C simultaneously fitted to the core-shell ellipsoid model with a hard sphere.

As can be seen in **Figure 41**, the curves of SANS data were similar for micelles containing surfactant concentrations 1.2- 4.8% w/v. At 12% w/v and 24% w/v surfactant concentrations, a peak appeared at a high Q value (0.06 \AA^{-1}) in the SANS profile (**Figure 42**), which indicated the presence of strong interparticle interactions as the best fit to the experimental scattering data and the hard sphere volume parameter increased as the $C_{18:1}E_{10}$ concentration increased (**Table 10**). The dimensions of micelles obtained from the fits, namely core radius (R_{core}), axial ratio (X), shell thickness, minor radius (b) and major radius (a) are listed in **Table 10**.

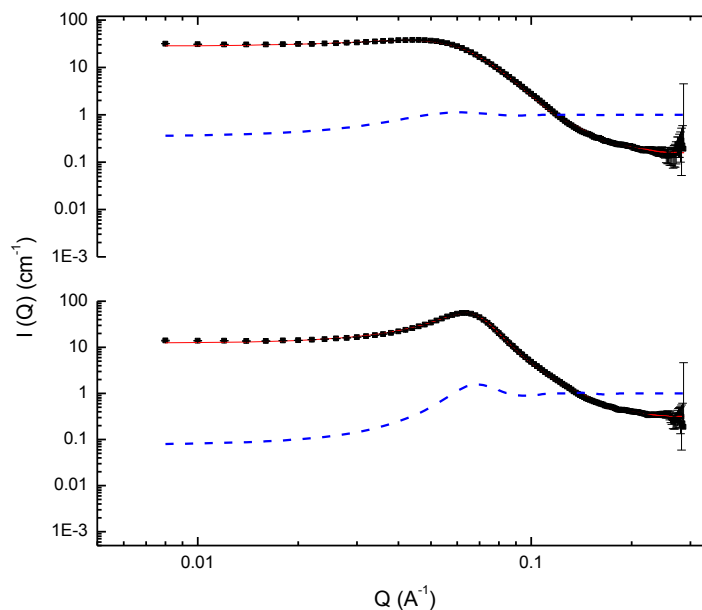


Figure 42 Three contrasts of SANS data for 12% w/v (top) and 24% w/v (bottom) of $C_{18:1}E_{10}$ micelles at 25°C simultaneously fitted to the core-shell ellipsoid model with a hard sphere.

From the SANS studies, no remarkably different results were observed among the different surfactant concentrations. The fitted parameters were as follows: the radius of the core (R_{core}) was 37.4-38.6 Å with axial ratio of core of 0.47-0.48, the head group thickness was 10.42-11.00 Å, a minor axis of the droplet was 28.37-29.42 Å, a major axis of the droplet was 47.82-49.60 Å. The results was similar to those reported for $C_{12}E_{10}$ micelles at 30°C in which the minor axis and major axis were 26.8 ± 1.3 Å and 41.5 ± 2.1 Å respectively (Sharma *et al.*, 2004). The SANS results were in line with the PCS results in which hydrodynamic droplet sizes of micelles at different $C_{18:1}E_{10}$ concentrations were similar.

Thus, the structure of the $C_{18:1}E_{10}$ micelle did not affect by the $C_{18:1}E_{10}$ concentrations. The schematic of $C_{18:1}E_{10}$ micelle is shown in **Figure 43**. The surfactant aggregation number was around 187.37-206.36 and 34-36% of the outer shell consisted of D_2O where the equivalent hard sphere (SPH) radius was 46.40-48.60 Å similar to the major semiaxis of the ellipsoid droplet. From the result, volume of one droplet of $C_{18:1}E_{10}$ in D_2O was around 271-302 nm³ comparable to the volume (324 nm²) at 20°C reported by Prak *et al.* (Prak *et al.*, 2011).

Due to the limited excess on the SANS experiment together with economically reason, a number of samples within Region A of TPN-NE and TON-NE were chosen to perform on this study. The results from previous experiments suggested that the structures of TPN-NE, SBO-NE and TLN-NE were in the same line while TON-NE structures were different.

Table 10 Summary of the individual fitting parameters for micellar solutions containing different $C_{18:1}E_{10}$ concentrations using a core-shell ellipsoid model and a hard sphere structure factor.

$C_{18:1}E_{10}$ (%w/v)	R_{core} (Å)	Axial ratio of core (X)	Headgroup thickness (Å)	Head group hydration (%)	Droplet major (b) (Å)	Droplet minor (a) (Å)	Axial ratio of droplet (X)	Hard sphere volume	Equivalent SPH radius (Å)	Surfactant aggregation number
1.2	38.00	0.48	10.87	36	48.87	29.11	0.59	0.01	46.40	196.01
2.4	38.40	0.48	10.99	36	49.39	29.42	0.59	0.03	47.96	206.36
4.8	38.60	0.47	11.00	36	49.60	29.14	0.59	0.05	47.53	203.98
12	37.40	0.48	10.42	34	47.82	28.37	0.59	0.14	48.60	187.44
24	37.40	0.48	10.60	35	48.00	28.55	0.59	0.32	46.41	187.37

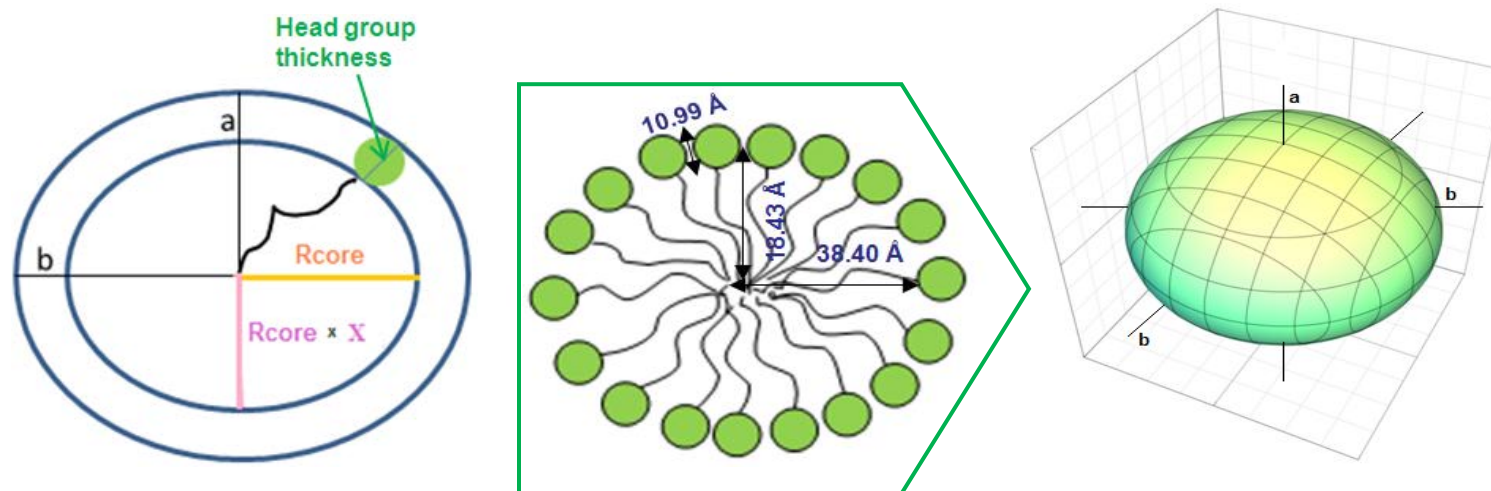


Figure 43 Schematic representation of the shape and molecular architecture of 2.4% w/v $C_{18:1}E_{10}$ micellar droplet.

7.2 SANS studies of TON-NE

After fitting all 3 contrasts (core, drop and shell) of TON-NE individually, it was clear that the model that consistently provided the best fit to the data was an oblate ellipsoid. The three contrasts measured for each composition were therefore fitted simultaneously using core-shell ellipsoid with assuming that the core only consisted of the oils and the shell consisted of the surfactant, water and probably some oil. In this simultaneous modeling, the scattering length density (SLD), volume fraction of each components and the thickness of the shell were constrained, while the core radius (R_{core}), the axial ratio of core (X), equivalent SPH radius and the volume fraction of the hard sphere droplets were all adjusted to obtain the best fit to the experimental scattering data. The fit of SANS data yielded two values for the radius, R_{core} and R_{shell} or shell thickness; the first corresponded to the size of the oil droplet and the second is the distance between the edge of the oil droplet and a position of the outer surfactant film. Since there is extensive hydration of the hydrophilic chains of the surfactant containing large hydrophilic head group (Borbely, 2000; Pederson and Gerstenberg, 2003), the parameter known as shell hydration was concerned. Base on the PIT study, short alkyl chain oil, TON, might penetrate into the hydrophobic layer of the interfacial film. Consequently, another parameter which called partition of oil in shell (the volume fraction of the oil penetrating into the surfactant shell) was also introduced to estimate the starting point of the TON in hydrophobic chains. **Figures 44 to 49** show the results obtained from simultaneous fit of the three contrasts measured for TON-1.0, TON-2.1, TON-2.4, TON-

3.0, TON-3.6 and TON-5.0 described by core-shell ellipsoid model. The dash line in Figures 44-49 represents the structure factor $S(Q)$.

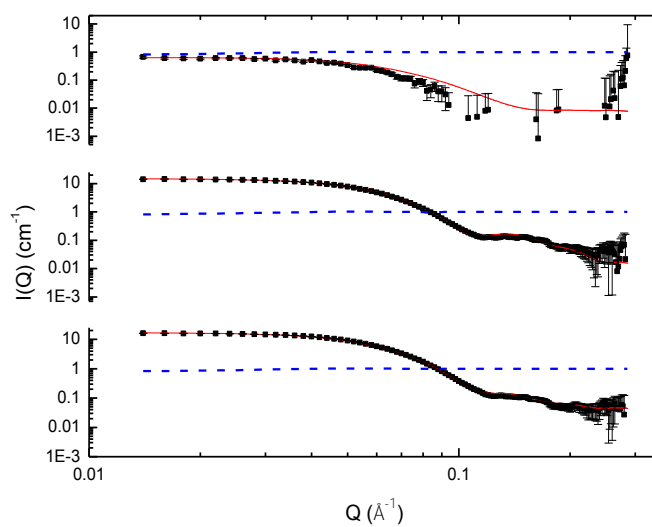


Figure 44 SANS data of TON-1.0 nanoemulsions with three contrasts (core, drop, shell) at 25°C, simultaneously fitted to the core-shell ellipsoid model with a hard sphere.

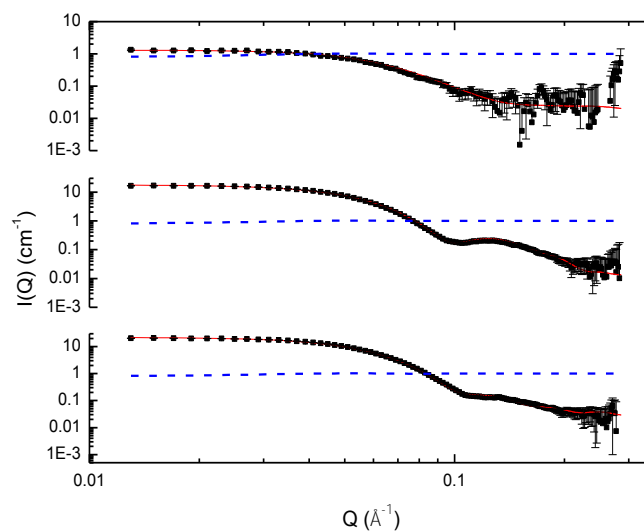


Figure 45 SANS data of TON-2.1 nanoemulsions with three contrasts (core, drop, shell) at 25°C, simultaneously fitted to the core-shell ellipsoid model with a hard sphere.

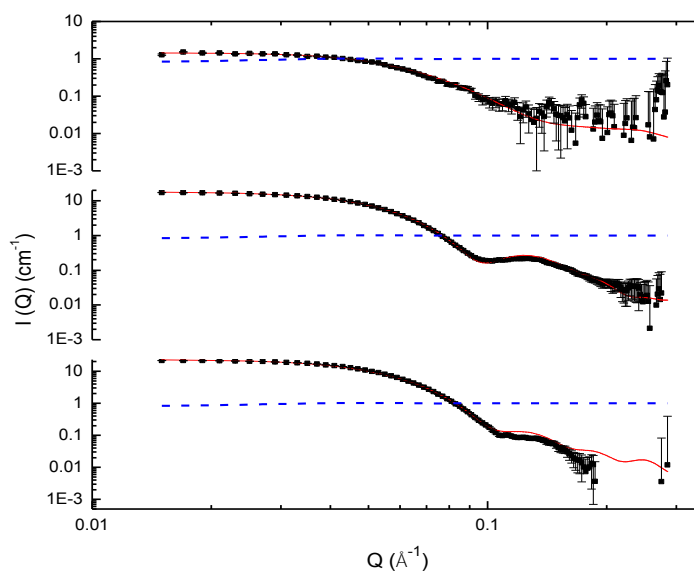


Figure 46 SANS data of TON-2.4 nanoemulsions with three contrasts (core, drop, shell) at 25°C, simultaneously fitted to the core-shell ellipsoid model with a hard sphere.

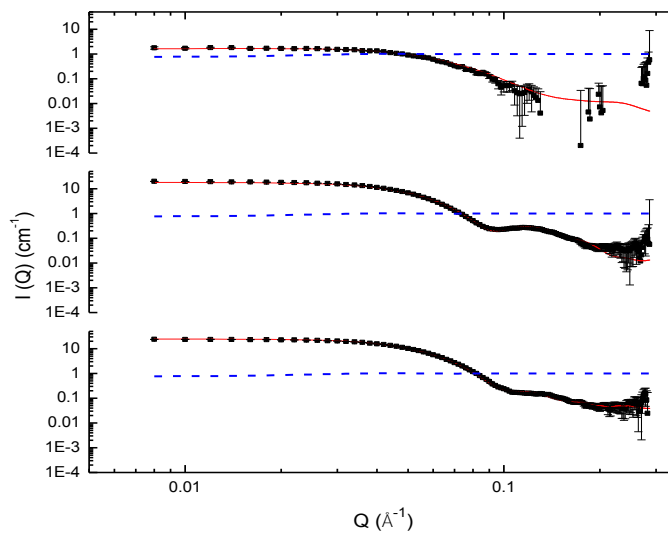


Figure 47 SANS data of TON-3.0 nanoemulsions with three contrasts (core, drop, shell) at 25°C, simultaneously fitted to the core-shell ellipsoid model with a hard sphere.

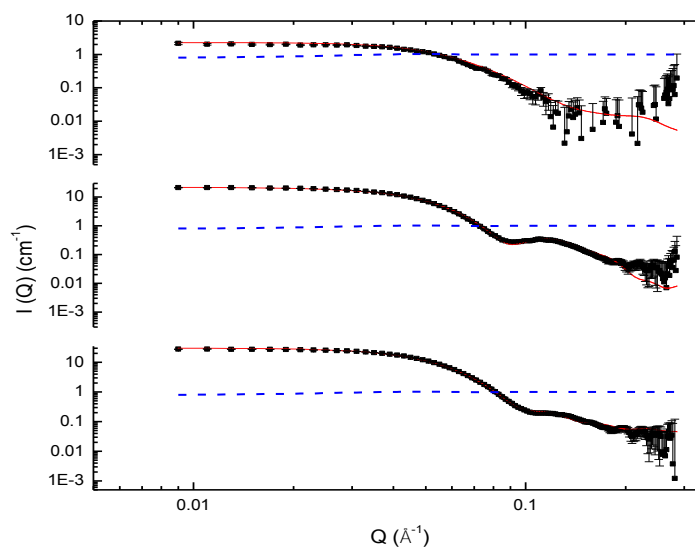


Figure 48 SANS data of TON-3.6 nanoemulsions with three contrasts (core, drop, shell) at 25°C, simultaneously fitted to the core-shell ellipsoid model with a hard sphere.

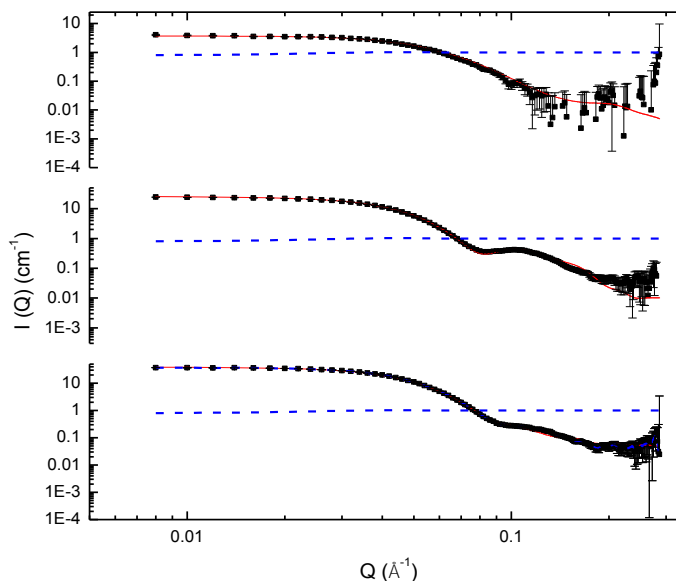


Figure 49 SANS data of TON-5.0 nanoemulsions with three contrasts (core, drop, shell) at 25°C, simultaneously fitted to the core-shell ellipsoid model with a hard sphere.

A summary of the parameters obtained by simultaneous fit of the SANS data is given in **Table 11**. The best fits of TON-NE at different oil concentrations gave a consistent surfactant shell thickness (with some oil and some water) at ~ 26 Å, despite an increase in the core radius from 19.90-33.94 Å with increasing TON concentrations. The partitioning of TON in surfactant shell for the TON-NE was consistent at approximately 0.3. The calculated number of TON molecules both in core and shell were increased from 7.14 to 68.41 (core) and 2.92 to 26.61 (shell) respectively upon increasing TON concentrations. The results reveal that as the TON concentrations increased not only the core part contained more TON molecules (forming a bigger core) but the TON molecules also penetrated more through the surfactant hydrophobic tail. This might be a reason why

the PIT results showed no significant increase as the TON amounts increased. The particle sizes of the TON-NE increased with increasing surfactant concentration as agreed with PCS experiments. The droplet major and minor radius increased from 46.28 to 59.47 Å and from 30.36 to 37.75 Å, respectively, with increasing TPN concentrations. Both the droplet major and droplet minor radius became more elongated resulting in the consistent axial ratio of droplet at 0.66 ± 0.02 . The shell hydration was highest at the lowest TON concentration. At TON-1.0 NE, the shell hydration occupied 30% of the shell and the hydration decreased to 21% afterward as the TON level increased to 0.21% w/v (TON-2.1) and remained constant at even highest TON concentration. The hard sphere volume of TON-NE was found to be 0.04 for all TON concentrations suggesting the fairly small interaction between droplets.

Table 11 Parameters obtained by simultaneously fitting the SANS data from the three contrasts examined for nanoemulsions prepared using 2.4% w/v C_{18:1}E₁₀ and containing varying amounts of TON at 25°C using the core-shell ellipsoidal model together with a hard-sphere structure factor.

TON (%w/v)	R _{core} (Å)	Axial ratio of core	Shell Thickness R _{shell} (Å)	Droplet major (b) (Å)	Droplet minor (a) (Å)	Axial ratio of droplet (X)	Shell hydration (%)	hard sphere volume	Equivalent SPH radius (Å)	Partition of oil in shell	Surfactant aggregation number
0.10	19.90	0.20	26.38	46.28	30.36	0.66	30	0.04	59.00	0.29	159.74
0.21	24.50	0.30	25.79	50.29	33.14	0.66	21	0.04	61.71	0.32	221.02
0.24	25.00	0.34	25.64	50.64	34.14	0.67	20	0.04	63.27	0.28	230.59
0.30	27.56	0.34	25.83	53.39	35.20	0.66	20	0.04	64.38	0.28	259.84
0.36	29.00	0.35	25.89	54.89	36.04	0.66	21	0.04	64.91	0.27	277.86
0.50	33.94	0.36	25.53	59.47	37.75	0.64	20	0.04	68.12	0.28	326.44

7.3 SANS studies of TPN-NE

The SANS data of TPN-NE were also fitted with core-shell ellipsoid model and the adjusted parameters used were identical to the parameter adjusted for TON-NE. **Figures 50-55** show the best fit of SANS data with dashed lines representing the structure factor $S(Q)$. The parameters obtained from the fit of SANS spectrum are summarized in **Table 12**. As expected, the R_{core} increased as the TPN concentrations increased in agreement with PCS and phase inversion temperatures experiments. The shell thicknesses obtained from the fits were about $24.00 \pm 1.50 \text{ \AA}$ which were slightly smaller than those of TON-NE ($26.00 \pm 0.50 \text{ \AA}$) probably due to the lower hydration of TPN-NE. Accordingly, the shell hydration of TPN-NE was found to be decreased from 20% (TPN-1.0) to 10 % (TPN-3.2) and remained at 10% at other higher TPN concentrations. The axial ratio of TPN-NE droplet was constant at 0.65 ± 0.01 which was comparable to that of TON-NE. The cores of the TPN-NE became more spherical as the TPN concentrations increased which shown by the increase in core axial ratio from 0.22 to 0.46 as TPN concentrations increased agreeing with the suggestion from PIT study. The droplet major and minor radius increased from 47.90 to 70.60 \AA and from 30.43 to 44.95 \AA , respectively, with increasing TPN concentrations. The surfactant aggregation number increased from 196.38 to 572.87 as TPN concentrations increased, hence TPN-NE required more surfactant molecules than TON-NE to stabilize the droplets. The hard sphere volume of 0.04 was found for TPN-NE at all TPN concentrations which were identical to TON-NE. The results suggested that no high interaction between droplets was

occurred as expected with the dilute NE system. Moreover, the data suggested that the TPN even at lowest concentration (TPN-1.0) did not penetrate into the hydrophobic surfactant shell once more supported the PIT results.

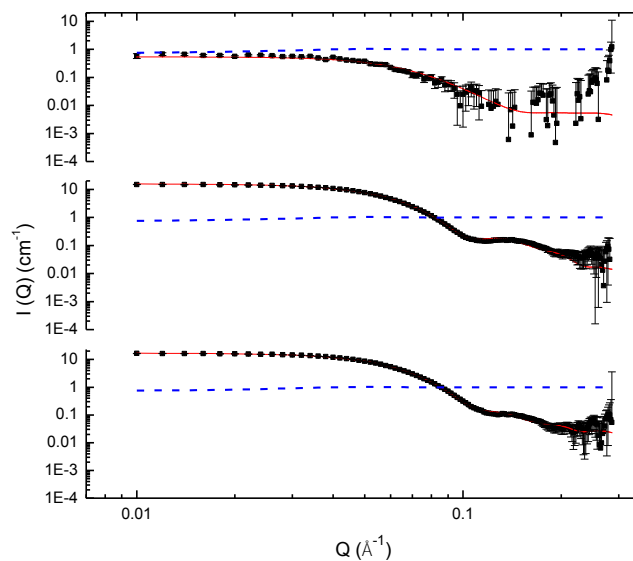


Figure 50 SANS data of TPN-1.0 nanoemulsions with three contrasts (core, drop, shell) at 25°C, simultaneously fitted to the core-shell ellipsoid model with a hard sphere.

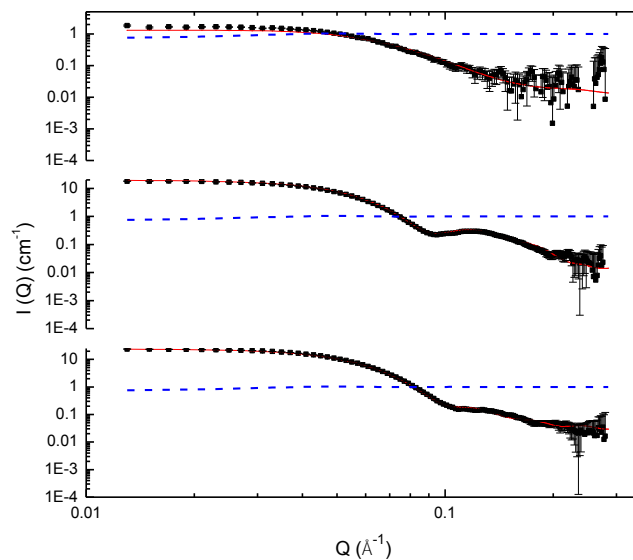


Figure 51 SANS data of TPN-2.4 nanoemulsions with three contrasts (core, drop, shell) at 25°C, simultaneously fitted to the core-shell ellipsoid model with a hard sphere.

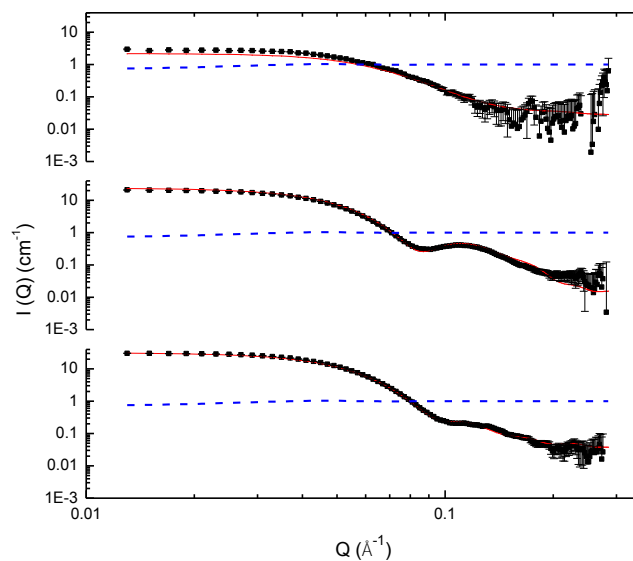


Figure 52 SANS data of TPN-3.2 nanoemulsions with three contrasts (core, drop, shell) at 25°C, simultaneously fitted to the core-shell ellipsoid model with a hard sphere.

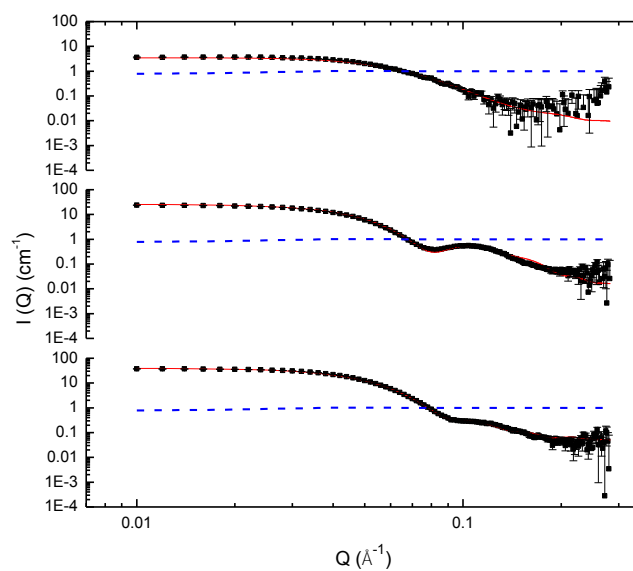


Figure 53 SANS data of TPN-4.0 nanoemulsions with three contrasts (core, drop, shell) at 25°C, simultaneously fitted to the core-shell ellipsoid model with a hard sphere.

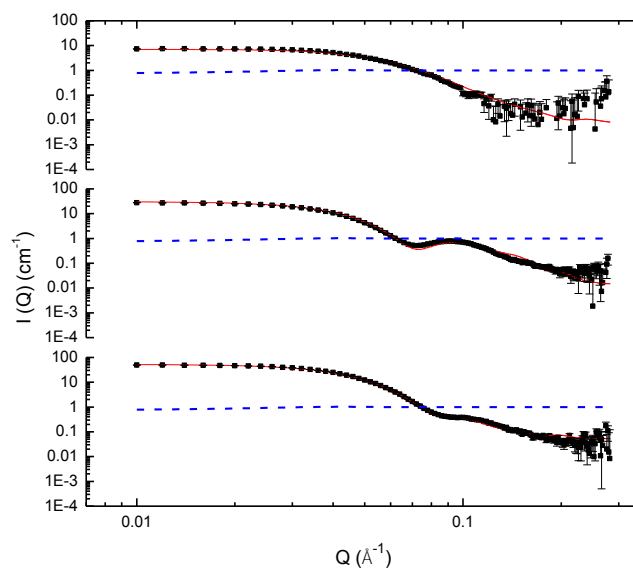


Figure 54 SANS data of TPN-5.5 nanoemulsions with three contrasts (core, drop, shell) at 25°C, simultaneously fitted to the core-shell ellipsoid model with a hard sphere.

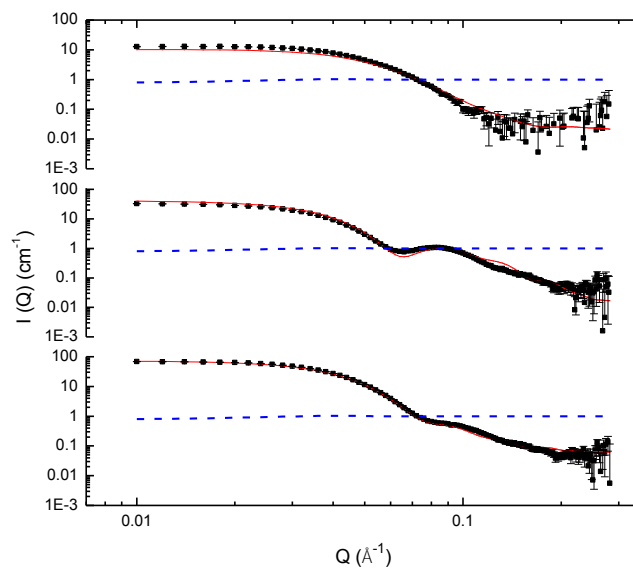


Figure 55 SANS data of TPN-7.0 nanoemulsions with three contrasts (core, drop, shell) at 25°C, simultaneously fitted to the core-shell ellipsoid model with a hard sphere.

Table 12 Parameters obtained by simultaneously fitting the SANS data from the three contrasts examined for nanoemulsions prepared using 2.4% w/v C_{18:1}E₁₀ and containing varying amounts of TPN at 25°C using the core-shell ellipsoidal model together with a hard-sphere structure factor.

TPN (%w/v)	R _{core} (Å)	Axial ratio of core	Shell thickness R _{shell} (Å)	Droplet major (b) (Å)	Droplet minor (a) (Å)	Axial ratio of droplet (X)	Shell hydration (%)	Hard sphere Volume	Equivalent SPH radius (Å)	Partition of oil in shell	Surfactant aggregation number
0.10	22.40	0.22	25.50	47.90	30.43	0.64	20	0.04	55.08	~ 0	196.38
0.24	29.20	0.34	24.20	53.40	34.13	0.64	15	0.04	58.25	~ 0	275.42
0.32	32.20	0.40	23.80	56.00	36.68	0.66	10	0.04	62.04	~ 0	332.54
0.40	35.10	0.42	23.50	58.60	38.24	0.65	10	0.04	65.46	~ 0	371.15
0.55	40.70	0.45	23.40	64.10	41.71	0.65	10	0.04	69.61	~ 0	461.29
0.70	47.50	0.46	23.10	70.60	44.95	0.64	10	0.04	70.28	~ 0	572.87

The simultaneous fit of the data allowed the information about the inner structure of the NE droplets. The parameters obtained from SANS experiment of both TON-NE and TPN-NE showed that the particle size increased with increasing triglyceride content while the triglyceride core became less ellipsoid as indicated by the increased in axial ratio of core. Overall, it can be concluded that the TON penetrated into surfactant chain region or shell of the NE droplet (oil partitioning in shell~0.3), resulting in the formation of smaller core droplet. In contrast, TPN formed a central core of oil in the NE droplets (oil partitioning in shell~0). A schematic representation of the molecular architecture of TON-2.4 or TPN-2.4 NE droplets is shown in **Figure 56a-b**. Even though there were some reports suggesting the effect of different molecular volume of oil on the NE formation, it should be noted these propositions were made based on indirect experimental data. In contrast to SANS experiments, as those reported here, provided detailed information of the inner structure by using contrast-matching technique. The results obtained in SANS study supported and clarified the results obtained earlier from phase behavior study, hydrodynamic droplet size measurements and the phase inversion temperature in that the internal structure of TPN-NE was different from TON-NE droplets. Moreover, the presence of TPN core with no penetration into the shell as opposed to TON-NE supported the hypothesis that the TPN were mostly in solid state and TP drug attempted to solubilize in the surfactant hydrophobic chain region, resulting in an increase in droplet size of NE especially at the higher TPN concentrations.

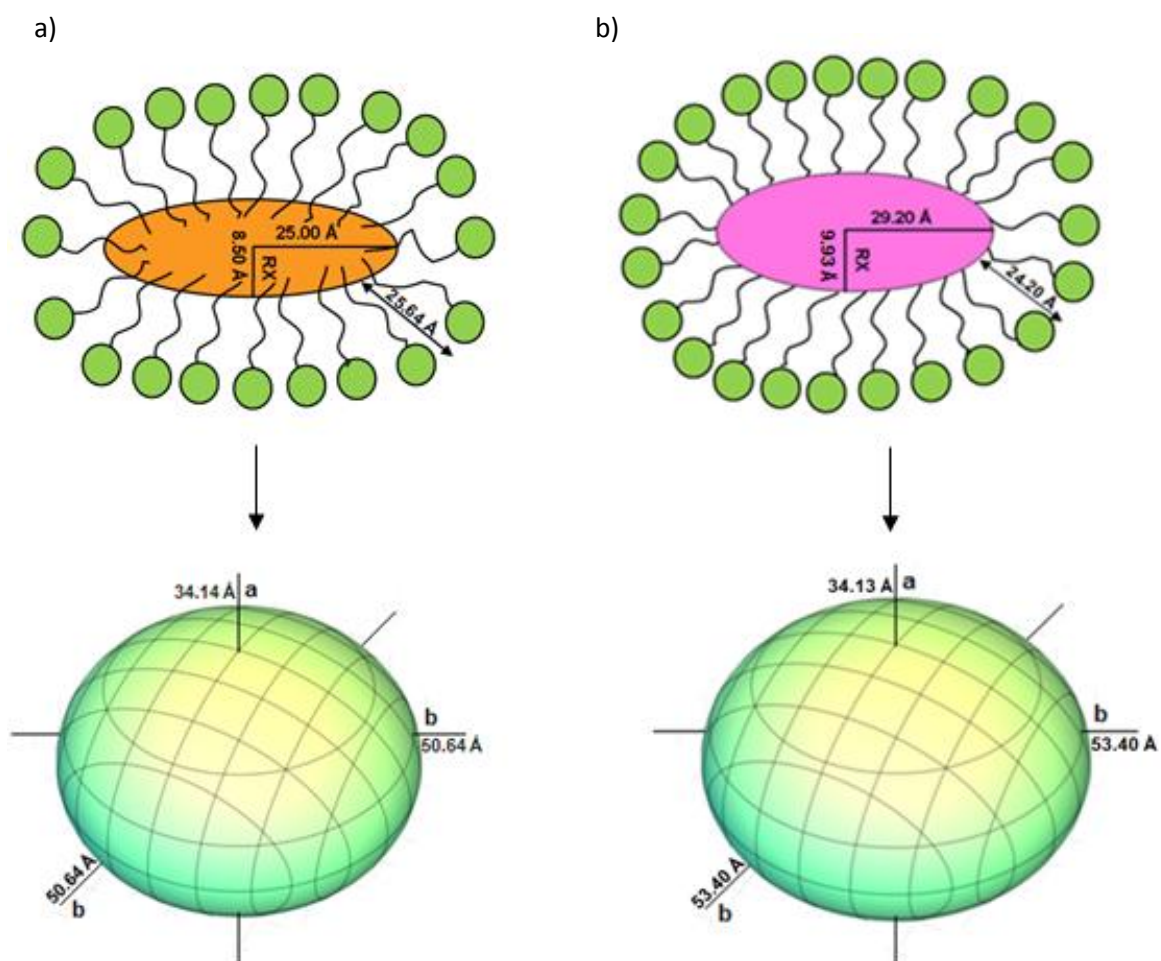


Figure 56 A schematic representation of the molecular architecture of a) TON-2.4 or b) TPN-2.4 nanoemulsion droplets.

CHAPTER V

CONCLUSION

The formation of nanoemulsions (NE) formation was influenced by triglyceride molecular weight in that the NE containing intermediate molecular weight triglyceride, TLN-NE, which has the molecular weight (of 639) similar to that of $C_{18:1}E_{10}$ surfactant (Mwt=709) exhibited largest total NE area followed by higher molecular weight SBO (Mwt=885.5), TPN (Mwt=807.3) and the smaller molecular weight TON (Mwt=471) which formed the smallest NE Region with $C_{18:1}E_{10}$. The findings in this study suggest the formation of NE containing solid triglycerides (TPN and TLN) are possible and are comparable to liquid triglycerides (SBO and TON). All NE samples were stable for at least 1 month with the exception of the data recorded for the TON-contained systems in which some samples were unstable after storage for 24 hours. For all four triglycerides, the apparent hydrodynamic droplet size (D_h) of the NE droplets increased as the amount of triglyceride increased; there were essentially linear increase in D_h with increasing triglycerides content in Regions A and B. In contrast, The D_h of droplet with triglycerides concentration was sharply increased in Region C suggesting that NE droplets in Region C possibly organized in different way from NE in Regions A and B. Both solid and liquid triglycerides could form an oil core required for solubilisation of the lipophilic drug as suggested by phase inversion temperature (PIT) in which the addition of a greater amount of triglycerides (SBO, TPN and TLN) for the same $C_{18:1}E_{10}$ concentration resulted in higher PITs. This observation may similarly be due to the formation of a larger oil core

which encourages more spherical shape in agreement with droplet size measurement which shows linear increase in D_h with increasing triglyceride content. The PITs of the lower molecular weight TON neither decreased nor increased when increased the amount of TON suggesting that the TON incorporated in NE in different way from other triglycerides. The formation of the core was influenced by the triglyceride molecular weight as demonstrated by the SANs results revealing that the TPN formed a distinct core in the centre of TPN-NE droplet and the radius of the core increased as the TPN amount increased. Conversely, the increase of TON concentrations not only resulted in a bigger oil core but the oil also penetrated more through the surfactant hydrophobic tail.

The solubility studies showed that all NE exhibited a significant increase in solubilisation of lipophilic steroidal drug, testosterone propionate (TP), over the corresponding $C_{18:1}E_{10}$ micellar solution. The solubility of TP increased in an approximately linear fashion with increasing triglyceride concentrations in NE (Regions A and B) containing SBO, TON and TLN which could be the oil core formation at increasing triglyceride concentrations. In addition, the PIT experiments suggested that TP was partly located at the boundary between the hydrophobic and hydrophilic portions of the surfactant. Though the NE containing TPN were expected to solubilise TP in the same manner as others triglyceride (i.e. due to the formation of oil core), the solubility of TP increased to some extent and were level off even with increasing the TPN amount further. The DSC experiments indicated that the solubility phenomenon was influenced by triglyceride melting point and concentration. The TPN (melting point of 65°C) was partially or mostly incorporated into the NE in a “solid-like” state at higher TPN

concentrations hence limited the TP solubilising capacity of the TPN-NE. In contrast, the lower melting point (50°C) solid triglyceride, TLN, did not solidify in the NE under the conditions of use. Accordingly, the solubility of TP in TLN-NE was not limited due to the “liquid-like” state of TLN. All NE in Region C showed no advantage on TP solubilisation, hence the way triglycerides incorporated in Region C were different from Regions A and B. The presence of TP caused no instability as observed in SBO-NE, TLN-NE and TON-NE; however, the drug affected the stability of NE prepared using high TPN concentrations as TP was unable to solubilize in the core of TPN-NE droplet that was in solid state. Consequently, TP attempted to solubilize more at the boundary between the hydrophobic and hydrophilic portions of the surfactant affecting the arrangement in TPN-NE structure, resulting in much reduction in PIT, an increase in D_h of droplet and finally destabilization of some TPN-NE.

Conclusively, NE prepared using a high melting point solid triglyceride such as TPN are less likely to be useful as drug delivery vehicles than NE containing liquid triglycerides and low melting point solid triglycerides.

REFERENCES

- Adams, M. L., Lavasanifar, A., and Kwon, G. S. 2003. Amphiphilic block copolymers for drug delivery. Journal of Pharmaceutical Sciences 92 (7): 1343–1355.
- Ahmed, M., Ramadan, W., Rambhu, D., and Shakeel, F. 2008. Potential of nanoemulsions for intravenous delivery of rifampicin. Pharmazie 63: 806-811.
- Al-Haj, N., and Rasedee, A. 2009. Solid lipid nanoparticles preparation and characterization. International Journal of Pharmacology 5(1): 90-93.
- Anton, N., and Vandamme, T. F. 2011. Nano-emulsions and micro-emulsions: clarifications of the critical differences. Pharmaceutical Research 28(5): 978-985.
- Anton, N., and Vandamme, T.F. 2009. The universality of low-energy nano-emulsification. International Journal of Pharmaceutics 377: 142-147.
- Anton, N., Gayet, P., Benoit, J.P., and Saulnier, P. 2007. Nano-emulsions and nanocapsules by the PIT method: An investigation on the role of the temperature cycling on the emulsion phase inversion. International Journal of Pharmaceutics 344: 44-52.
- Arima S., Ueji, T., Ueno, S., Ogawa, A., and Sato, K. 2007. Retardation of crystallization-induced destabilization of PMF-in-water emulsion with emulsifier additives. Colloids and Surfaces B: Biointerfaces 55: 98-106.

Attwood, D. 1994. Microemulsion. In: Kreuter, J. (ed.) Colloidal drug delivery systems. New York: Marcel Dekker.

Attwood, D., Currie, L. R. J., and Elworthy, P. H. 1974. Studies of solubilized micellar solutions. I. Phase studies and particle size analysis of solutions with nonionic surfactants. Journal of Colloid and Interface Science 46: 249-256.

Aveyard, R. and Lawless, T. A. 1986. Interfacial tension minima in oil–water surfactant systems. Journal of the Chemical Society, Faraday Transactions 182: 2951–2963.

Aveyard, R., Binks, B. P., Clark, S., and Fletcher, P. D. I. 1990. Cloud Points, solubilisation and interfacial tensions in systems containing nonionic surfactants. Journal of Chemical Technology and Biotechnology 48(2): 161-171.

Awad, T. S., Helgason, T., Kristbergsson, K., Decker, E. A., Weiss, J., and McClements, J. 2008. The effect of cooling and heating rates on polymorphic transformations and gelation of tripalmitin solid liquid nanoparticle (SLN) suspensions. Food Biophysics 3: 155-162.

Bellare, J. R., Haridas, M. M., and Li, X. J. 1999. Handbook of microemulsion science and technology. New York: Marcel Dekker.

Bergstrom, M., and Pedersen, J. S. 1999. Structure of pure SDS and DTAB micelles in brine determined by small-angle neutron scattering (SANS). Physical Chemistry Chemical Physics 1: 4437-4446.

- Bivas-Benita, M., Oudshoorn, M., Romeijn, S., Van Meijgaarden, K., Koerten, H., Van der Meulen, H., Lambert, G., Ottenhoff, T., Benita, S., Junginger, H., and Borchard, G. 2004. Cationic submicron emulsions for pulmonary DNA immunization. Journal of Controlled Release 100: 145-155.
- Borbely, S. 2000. Aggregate Structure in Aqueous Solutions of Brij-35 Nonionic Surfactant Studied by Small-Angle Neutron Scattering. Langmuir 16(13): 5540-5545.
- Borhade, V., Nair, H., and Hegde, D. 2008. Design and evaluation of self-microemulsifying drug delivery system (SMEDDS) of tacrolimus. American Association of Pharmaceutical Scientists Pharmaceutical Sciences and Technology 9 (1): 13-21.
- Brime, B., Moreno, M. A., Frutos, G., Ballesteros, M. P., and Frutos, P. 2002. Amphotericin B in oil-water lecithin-based microemulsions: formulation and toxicity evaluation. Journal of Pharmaceutical Sciences 91: 1178-1185.
- Brooks, B.W. , Richmond, H.N. , and Zerfa, M. 1998. In: Binks, B. P. (Ed.), Modern aspects of emulsion science, Cambridge: Royal Society of Chemistry Publication.
- Bunjes, H, and Unruh, T. 2007. Characterization of lipid nanoparticles by differential scanning calorimetry, X-ray and neutron scattering. Advanced Drug Delivery Reviews 59: 379-402.

- Bunjes, H. 2011. Structural properties of solid lipid based colloidal drug delivery systems. Current Opinion in Colloid & Interface Science 16(5): 405-411.
- Bunjes, H., and Koch, M. H. 2005. Saturated phospholipids promote crystallization but slow down polymorphic transitions in triglyceride nanoparticles. Journal of Controlled Release 107 (2): 229-243.
- Bunjes, H., and Westesen, K. 2001. Influences of colloidal state on physical properties of solid fats. In: Garti, N. and Sato, K. (eds.), Crystallization processes in fats and lipid systems, pp. 457–483. New York: Marcel Dekker.
- Bunjes, H., Koch, M. H. J., and Westesen, K. 2003. Influence of emulsifiers on the crystallization of solid lipid nanoparticles. Journal of Pharmaceutical Sciences 92 (7): 1509-1520.
- Bunjes, H., Steiniger, F., and Richter, W. 2007. Visualizing the structure of triglyceride nanoparticles in different crystal modifications. Langmuir 23 (7): 4005-4011.
- Bunjes, H., Westesen, K. and Koch, M. H. J. 1996. Crystallization tendency and polymorphic transitions in triglyceride nanoparticles. International Journal of Pharmaceutics 129 (1-2): 159-173.
- Chen, S.H. 1986. Small-angle neutron-scattering studies of the structure and interaction in micellar and microemulsion systems. Annual Review of Physical Chemistry 37: 351-399.

- Chevalier, Y., and Zemb, T. 1990. The structure of micelles and microemulsions. Reports on Progress in Physics 53, 270-371.
- Clause, D. 1998. Thermal behaviour of emulsions studied by differential scanning calorimetry. Journal of Thermal Analysis and Calorimetry 51: 191-201.
- Clause, D., Pezron, I., Gomez, F., Dalmazzone, C., Sacca, L. and Drelich, A. 2008. Differential scanning calorimetry as a tool for following emulsion evolution in microgravity conditions from the MAP-Project FASES. Journal of the Japan Society of Microgravity Application 25: 227-230.
- Clause, D. 2010. Differential thermal analysis, differential scanning calorimetry and emulsions. Journal of Thermal Analysis and Calorimetry 101:1071-1077.
- Corti, M., Minero, C., and Degiorgio, V. 2002. Cloud point transition in nonionic micellar solutions. The Journal of Physical Chemistry 88: 309-317.
- Coupland J. 2002. Crystallization in emulsions. Current Opinion in Colloid and Interface Science 7: 445-450.
- Croy, S. R., and Kwon, G. S. 2005. Polysorbate 80 and Cremophor EL micelles deaggregate and solubilize nystatin at the core-corona interface. Journal of Pharmaceutical Sciences 94: 2345-2354.
- Cucheval, A. and Chow, R. C. Y. (2008) A study on the emulsification of oil by power ultrasound. Ultrasonics Sonochemistry 15: 916-920.

- Dalmazzone, C., Noik, C., and Clause, D. 2009. Application of DSC for emulsified system characterization. Oil and Gas Science and Technology 64: 543-555.
- Das, S., and Chaudhury, A. 2011. Recent Advances in Lipid Nanoparticle Formulations with Solid Matrix for Oral Drug Delivery. American Association of Pharmaceutical Scientists Pharmaceutical Sciences and Technology 12 (1): 62-76.
- Date, A. A., and Nagarsenker, M. S. 2007. Design and evaluation of self-nanoemulsifying drug delivery systems (SNEDDS) for cefpodoxime proxetil. International Journal of Pharmaceutics 329(1-2): 166-172.
- Date, A.A., Desai, N., Dixit, R., and Nagarsenker, M. 2010. Self-nanoemulsifying drug delivery systems: Formulation insights, applications and advances. Nanomedicine 5:1595-1616.
- Dickinson, E., and Povey M. J. W. 1996. Crystallization kinetics in oil-in-water emulsions containing a mixture of solid and liquid droplets. Journal of the Chemical Society 92: 1213-1215.
- Dixit, N., Kohli, K., and Baboota, S. 2008. Nanoemulsion system for the transdermal delivery of a poorly soluble cardiovascular drug. Journal of Pharmaceutical Science and Technology 62: 46-55.

- Djekic, L., and Primorac, M. 2008. The influence of cosurfactants and oils on the formation of pharmaceutical microemulsions based on PEG-8 caprylic/capric glycerides. International Journal of Pharmaceutics 352: 231-239.
- Djekic, L., Primorac, M., and Jockovic, J. 2011. Phase behaviour, microstructure and ibuprofen solubilization capacity of pseudo-ternary nonionic microemulsions. Journal of Molecular Liquids 160 (2): 81-87.
- Djekic, L., Primorac, M., Filipic, S., and Agbaba, D. 2012. Investigation of surfactant/cosurfactant synergism impact on ibuprofen solubilization capacity and drug release characteristic of nonionic microemulsions. International Journal of Pharmaceutics 433: 25-33.
- Dong, X., Mattingly, C. A., Tseng, M. T., Cho, M. J., Liu, Y., and others 2009. Doxorubicin and paclitaxel-loaded lipid-based nanoparticles overcome multidrug resistance by inhibiting P-glycoprotein and depleting ATP. Cancer Research 69 (9): 3918-3926.
- Engelskirchen, S., Elsner, N., Sottmann, T., and Strey, R. 2007. Triacylglycerol microemulsions stabilized by alkyl ethoxylate surfactants-A basis study phase behavior, interfacial tension and microstructure. Journal of Colloid and Interface Science 312: 114-121.

- Evans, D. R., Mitchell, D. J., and Ninham, B. W. 1986. Oil, water and surfactant: properties and conjectured structure of simple microemulsions. Journal of Physical Chemistry. 90: 2817-2825.
- Farokhzad, O. C., and Langer, R. 2009. Impact of Nanotechnology on Drug Delivery ACS Nano 3 (1): 16-20.
- Feng, J. L., Wang, Z.W., Zhang, J., Wang, Z.N., and Liu, F. 2009. Study on food-grade vitamin E microemulsions based on nonionic emulsifiers. Colloid Surface A: Physicochemical and Engineering Aspects 339: 1-6.
- Flanagan, J. and Singh, H. (2006) Microemulsions: a potential delivery system for bioactives in food. Critical Reviews in Food Science and Nutrition 46: 221-237.
- Fryd, M. M., and Mason, T. G. 2012. Advanced nanoemulsions. Annual Review of Physical Chemistry 63: 493-518.
- Gabizon, A. 2003. Emerging role of liposomal drug carrier systems in cancer chemotherapy. Journal of Liposome Research 13: 17-20.
- Gaikwad, S. G., and Pandit, A. B. 2008. Ultrasound emulsification: effect of ultrasonic and physicochemical properties on dispersed phase volume and droplet size. Ultrasonics Sonochemistry 15: 554-563.

- Ghai, D., and Sinha, V. R. 2012. Nanoemulsions as self-emulsified drug delivery carriers for enhanced permeability of the poorly water-soluble selective β 1-adrenoreceptor blocker Talinolol. Nanomedicine-Nanotechnol 8: 618-626.
- Girard, N., Tadros, T. F., and Bailey, A. I. 1997. Styrene and methylmethacrylate oil-in-water microemulsions. Colloid and Polymer Science 275: 698-704.
- Gutiérrez, J. M., González, C., Maestro, A., Solè, I., Pey, C. M., and Nolla, J. 2008. Nano-emulsions: New applications and optimization of their preparation. Current Opinion in Colloid and Interface Science 13: 245-251.
- Hagemann, J. W. 1998. Thermal behaviour and polymorphism of acylglycerides, In: Garti, N., Sato, K. (Eds.), Crystallization and polymorphism of fats and fatty acids. Marcel Dekker, New York, pp. 9-95.
- Hauss, D. J. 2007. Oral lipid-based formulations, Advance Drug Delivery Review 59: 667-676.
- Hayter, J. B., and Penfold, J. 1983. Determination of micelle structure and charge by neutron small-angle scattering. Colloid and Polymer Science 261: 1022-1030.
- Heenan, R. K. 1989. Fish Data Analysis Program, Report RAL 89-129, Didcot: Rutherford Appleton Laboratory CCLRC.

- Helgason, T., Awad, T. S., Kristbergsson, K., McClements, D. J., and Weiss, J. 2009. Effect of surfactant surface coverage on formation of solid lipid nanoparticles (SLN). Journal of Colloid and Interface Science 334 (1): 75-81.
- Helgason, T., Awad, T. S., Kristbergsson, K., McClements, D. J., and Weiss, J. 2008. Influence of polymorphic transformations on Gelation of tripalmitin solid lipid nanoparticle suspensions. Journal of the American Oil Chemists' Society 85: 501-511.
- Heurtault, B., Saulnier, P., Pech, B., Proust, J. E., and Benoit, J. P. 2003. Physico-chemical stability of colloidal lipid particles. Biomaterials 24 (23): 4283-4300.
- Himawan, C., Starov, V. M., and Stapley, A. G. 2006. Thermodynamic and kinetic aspects of fat crystallization. Advances in Colloid and Interface Science 122 (1-3): 3-33.
- Hindle, S., Povey, M. J. W., and Smith, K. 2000. Kinetics of crystallization in n-hexadecane and cocoa butter oil-in-water emulsions accounting for droplet collision-mediated nucleation. Journal of Colloid and Interface Science 232: 370-380.
- Hoffmann, H., and Ebert, G. 1988. Surfactants, micelles and fascinating phenomena. Angewandte Chemie International 27 (7): 902-912.

- Hsieh, C. 2010. O/w microemulsions stabilized by the zwitterionic surfactant. PhD's Thesis, Department of Pharmacy, University of London PhD Thesis.
- Husseini, G. A., and Pitt, W. G. 2008. Micelles and nanoparticles for ultrasonic drug and gene delivery. Advanced Drug Delivery Reviews 60: 1137-1152.
- Inoue, T., and Yamakawa, H. 2011. Micelle formation of nonionic surfactants in a room temperature ionic liquid, 1-butyl-3-methylimidazolium tetrafluoroborate: Surfactant chain length dependence of the critical micelle concentration. Journal of Colloid and Interface Science 356: 798-802.
- Izquierdo, P., Feng, J., Esquena, J., Tadros, T. F., Dederen, J. C., Garcia, M. J., Azemar, N. and Solans, C. 2004. The influence of surfactant mixing ratio on nano-emulsion formation by the pit method. Journal of Colloid and Interface Science 285: 388-394.
- Jenning, V., Thünemann, A. F., and Gohla, S. H. 2000. Characterisation of a novel solid lipid nanoparticle carrier system based on binary mixtures of liquid and solid. International Journal of Pharmaceutics 199(2): 167-177.
- Jiao, J. 2008. Polyoxyethylated nonionic surfactants and their applications in topical ocular drug delivery. Advanced Drug Delivery Reviews 60: 1663-1673.

- Kentish, S., Wooster, T. J., Ashokkumar, M., Balachandran, S., Mawson, R., and Simons, L. 2008. The use of ultrasonics for nano-emulsion preparation. Innovative Food Science and Emerging Technologies 9: 170-175.
- Khoo, S. M., Shackleford, D. M., Porter, C. J. H., Edwards, G. A., and Charman, W. N. 2003. Intestinal lymphatic transport of halofantrine occurs after oral administration of a unit-dose lipid-based formulation to fasted dogs. Pharmaceutical Research 20(9):1460-1465.
- Kjellander, J. 1982. Phase separation of non-ionic surfactant solutions. A treatment of the micellar interaction and form. Journal of the Chemical Society, Faraday Transactions 2: Molecular and Chemical Physics 78(12): 2025-2042.
- Klumpp, C., Kostarelos, K., Prato, M., and Bianco, A. 2006. Functionalized carbon nanotubes as emerging nanovectors for the delivery of therapeutics. Biochimica et Biophysica Acta-Biomembranes 1758: 404-412.
- Ko, C. J., Ko, Y. J., Kim, D. M., and Park, H. J. 2003. Solution properties and PGSE-NMR self-diffusion study of C_{18:1}E₁₀/oil/water system. Colloids and Surfaces A: Physicochemical and Engineering Aspects 216: 55-63.
- Kumar, P., and Mittal, K.L. 1999. Handbook of microemulsion science and technology. New York: Marcel Dekker.

- Kunieda, H., and Friberg, S.E. 1981 Characterization of surfactants for enhanced oil recovery. Bulletin of The Chemical Society of Japan 54:1001-1010.
- Kunieda, H., Horii, M., Koyama, M., and Sakamoto, K. 2001. Solubilization of polar oils in surfactant self-organized structures. Journal of Colloid and Interface Science 236: 78-84.
- Kuntsche, J., Horst, J. C., and Bunjes, H. 2011. Cryogenic transmission electron microscopy (cryo-TEM) for studying the morphology of colloidal drug delivery systems. International Journal of Pharmaceutics 417 (1-2): 120-137.
- Lawrence, M. J., and Rees, G. J. 2012. Microemulsion-based media as novel drug delivery systems. Advanced Drug Delivery Reviews 64: 175-193.
- Li, J. L., Bai, D. S., and Chen, B. H. 2009. Effects of additives on the cloud points of selected nonionic linear ethoxylated alcohol surfactants. Colloids and Surfaces A: Physicochemical and Engineering Aspects 346: 237-243.
- Liggins, R. T., and Burt, H. M. 2002. Polyether-polyester diblock copolymers for the preparation of paclitaxel loaded polymeric micelle formulations. Advance Drug Delivery Reviews 54: 191-202.
- Lijuan, W., Jinfeng, D., Jing, C., Julian, E. and Xuefeng, L. 2009. Design and optimization of a new self-nanoemulsifying drug delivery system. Journal of Colloid and Interface Science. 330: 443-448.

- Lindner, P., and Zemb, T. H. 1991. Neutrons, X-rays and Light Scattering: Methods Applied to Soft Condensed Matter. In: Lindner, P., and Zemb, T. H. (ed.) Neutron, X-Ray and Light Scattering, pp. 199-221. North Holland-Elsevier, Amsterdam.
- Lindner, P., and Zemb, T. H. 1991. Neutrons, X-rays and Light Scattering: Investigative Tool for Colloidal and Polymeric Systems. In: Lindner, P., and Zemb, T. H. (ed.) Neutron, X-Ray and Light Scattering, pp. 127-144. North Holland-Elsevier, Amsterdam.
- Lopes, R., Eleuterio, C. V., Goncalves, L. M., Cruz, M. E. and Almeida, A. J. 2012. Lipid nanoparticles containing oryzalin for the treatment of leishmaniasis, European Journal of Pharmaceutical Sciences 45 (4) : 442-450.
- Lugo, D. M., Oberdisse, J., Lapp, A., and Findenegg, G. H. 2010. Effect of nanoparticle size on the morphology of adsorbed surfactant layers. The Journal of Physical Chemistry 114: 4183-4191.
- Maali, A., and Hamed, M. M. T. 2012. Preparation and application of nano-emulsion in the last decade (2000–2010). Journal of Dispersion Science and Technology 1: 1-24.
- Machado, A. H. E., Lundberg, D., Ribeiro, A. J., Veiga, F. J., Lindman, B., Miguel, M. G. and others. 2012. Preparation of calcium alginate nanoparticles using water-in-oil (W/O) nanoemulsions. Langmuir 28: 4131-4141.

- Maestro, A., Solè, I., González, C., Solans, C., and Gutiérrez, J. 2008. Influence of the phase behavior on the properties of ionic nanoemulsions prepared by the phase inversion composition method. Journal of Colloid and Interface Science 327: 433-439.
- Malcolmson, C. (1992) The physicochemical properties of nonionic oil-in-water microemulsions. PhD's Thesis, Department of Pharmacy, University of London
PhD Thesis.
- Malcolmson, C., and Lawrence, M. J. 1993. A comparison of the incorporation of model steroids into non-ionic micellar and microemulsion systems. Journal of Pharmacy and Pharmacology 45: 141-143.
- Malcolmson, C., and Lawrence, M. J. 1995. Three-component non-ionic oil-in-water microemulsions using polyoxyethylene ether surfactants. Colloids and Surfaces B: Biointerfaces 4:97-109.
- Malcolmson, C., Barlow, D. J., and Lawrence, M. J. 2002. Light scattering studies of testosterone enanthate containing soybean oil/C18:1E10/water oil-in-water microemulsions. Journal of Pharmaceutical Sciences 91: 2317-2331.
- Malcolmson, C., Satra, C., Kantaria, S., Sidhu, A., and Lawrence, M. J. 1998. Effect of the nature of the oil on the incorporation of testosterone propionate into nonionic oil-in-water microemulsions. Journal of Pharmaceutical Sciences 87: 109–116.

- Matsuyama, T., Morita, T., Horikiri, Y., Yamahara, H., and Yoshino, H. 2006. Enhancement of nasal absorption of large molecular weight compounds by combination of mucolytic agent and nonionic surfactant. Journal of Controlled Release 110: 347-352.
- McClements, D. J. 2012. Nanoemulsions versus microemulsions: terminology, differences, and similarities. Soft Matter 8: 1719-1729.
- Mehnert, W., and Mader, K. 2012. Solid lipid nanoparticles: production, characterization and applications. Advanced Drug Delivery Reviews 64: 83-101.
- Miller, C. C. 1924. The Stokes-Einstein law for diffusion in solution. Proceedings of the Royal Society of London. Series A, Containing Papers of a Mathematical and Physical Character 106: 724-749.
- Monduzzi, M., Caboi, F., Larch, F., and Olsson, U. 1997. DDAB microemulsions-dependence on the oil chain length. Langmuir 13: 2184–2190.
- Morales, D., Solans, C., Gutiérrez, J. M., Garcia, C. M. J., and Olsson, U. 2006. Oil/water droplet formation by temperature change in the water/C16E6/mineral oil system. Langmuir 22:3014-3020.
- Mukherjee, P., Padhan, S. K., Dash, S., Patel, S., and Mishra B. K. 2011. Clouding behaviour in surfactant systems. Advances in Colloid and Interface Science 162: 59-79.

- Nagao, M., Okabe, S., and Shibayama, M. 2005. Small-angle neutron-scattering study on a structure of microemulsion mixed with polymer networks. Journal of Chemical Physics 123 (14): 1620-1627.
- Narang, A. S., Delmarre, D., and Gao, D. 2007. Stable drug encapsulation in micelles and microemulsions. International Journal of Pharmaceutics 345(1-2): 9-25.
- Nobbmann, U., and Morfesis, A. 2009. Light scattering and nanoparticles. Materials Today 12: 52-54.
- Osawa, K., Solans, C., and Kunieda, H. 1997. Spontaneous formation of highly concentrated oil-in-water emulsions. Journal of Colloid and Interface Science 188: 275-281.
- Paciotti, G.F., Kingston, D.G.I. and Tamarkin, L. (2006) Colloidal gold nanoparticles: A novel nanoparticle platform for developing multifunctional tumor-targeted drug delivery vectors. Drug Development Research 67: 47-54
- Pasquali, M. 2010. Gelation: grow with the flow. Nature Materials 9 (5): 381-382.
- Pederson, J. S., and Gerstenberg, M. C. 2003. The structure of P85 Pluronic block copolymer micelles determined by small-angle neutron scattering. Colloids and Surfaces A: Physicochemical and Engineering Aspects 213 (2-3): 175-187.

- Percus, J. K., and Yevick, G. J. 1958. Analysis of classical statistical mechanics by means of collective coordinates. Physical Review 110: 1-13.
- Porkka-Heiskanen, T., Laakso, M. L., Stenberg, D., Alila, A., and Johansson, G. 1992. Increase in testosterone sensitivity induced by constant light in relation to melatonin injections in rats. Journal of Reproduction and Fertility 96: 331-336.
- Prak, D. J. L., Jahraus, W. I., Sims, J. M., MacArthur, A. H. R. 2011. An ¹H NMR investigation into the loci of solubilization of 4-nitrotoluene, 2, 6-dinitrotoluene, and 2, 4, 6-trinitrotoluene in nonionic surfactant micelles. Colloids and Surfaces A: Physicochemical and Engineering Aspects 375: 12-22.
- Prince, L. M. 1975. Microemulsions versus micelles. Journal of Colloid and Interface Science 52 (1): 182-188.
- Relkin, P. and Sourdet, S. 2005. Factors affecting fat droplet aggregation in whipped frozen protein-stabilized emulsions. Food Hydrocolloids 19: 506-511.
- Relkin, P., Jung, J. M., Kalnin, D., and Ollivon, M. 2008. Structural behaviour of lipid droplets in protein-stabilized nano-emulsions and stability of alpha-tocopherol. Food Biophysic 3: 163-168.
- Relkin, P., Jung, J. M., and Ollivon, M. 2009. Factors affecting vitamin degradation in oil-in-water nano-emulsions. Journal of Thermal Analysis and Calorimetry 98: 13-18.

- Robb, I. D., and Stevenson, P. S. 2000. Solubilization of trilaurin in surfactant solutions. Langmuir 16 (21): 7939-7945.
- Rübe, A., Hause, G., Mäder, K. and Kohlbrecher, J. 2005. Core-shell structure of Miglyol/poly(d,l-lactide)/Poloxamer nanocapsules studied by small angle neutron scattering. Journal of Controlled Release 107: 244-252.
- Ruckenstein, E., and Krishnan, R. 1980. Effect of electrolytes and mixtures of surfactants on the oil-water interfacial tension and their role in formation of microemulsions. Journal of Colloid and Interface Science 76: 201-211.
- Sadaghiana, A. S., and Khan, A. 1991. Clouding of a nonionic surfactant: The effect of added surfactants on the cloud point. Journal of Colloid and Interface Science 144 (1): 191-200.
- Sagar, G. H., Arunagirinathan, M. A., and Bellare, J. R. 2007. Self-assembled surfactant nano-structures important in drug delivery: a review. Indian Journal of Experimental Biology 45(2): 133–159.
- Saraceno, R., Chiricozzi, A., Gabellini, M., and Chimenti, S. 2013. Emerging applications of nanomedicine in dermatology. Skin Research and Technology 19(1): 13-19.

- Sato, K., and Ueno, S. 2011. Crystallization, transformation and microstructures of polymorphic fats in colloidal dispersion states. Current Opinion in Colloid and Interface Science 16: 384-390.
- Schott, H. 2001. Effect of inorganic additives on solutions of nonionic surfactants. Limiting cloud points of highly polyoxyethylated surfactants. Colloids and Surfaces A-Physicochemical and Engineering Aspects 186:129-136.
- Schubert, K.V., and Kaler, E.W. 1996. Nonionic microemulsions. Berichte Bunsenges Physical Chemistry 100: 190-205.
- Schultz, S., Wagner, G., Urban, K., and Ulrich, J. 2004. High-pressure homogenization as a process for emulsion formation. Chemical Engineering & Technology 27: 361-368.
- Shafiq, S., Shakeel, F., Talegaonkar, S., Ahmad, F. J., Khar, R. K., and Ali, M. 2007. Development and bioavailability assessment of ramipril nanoemulsion formulation. European Journal of Pharmaceutics and Biopharmaceutics 66: 227-243.
- Shah, P., Bhalodia, D., and Shelat, P. 2010. Nanoemulsion: a pharmaceutic review. Systematic Reviews in Pharmacy 1(1): 24-32.
- Sharma, K. S., Joshi, J. V., Aswal, V. K., Goyal, P. S., and Rakshit, A. K. 2004. Small-angle neutron scattering studies of nonionic surfactant: Effect of sugars. Indian Academy of Sciences 63(2): 297-302.

- Sharma, S. C., and Warr, G. G. 2012. Phase behavior, self-assembly, and emulsification of Tween 80/water mixtures with limonene and perfluoromethyldecalin. Langmuir 28(32): 11707-11713.
- Shigeta, K., Olsson, U., and Kunieda, H. 2001. Correlation between micellar structure and cloud point in long poly(oxyethylene)_n oleyl ether systems. Langmuir 17(16): 4717-4723.
- Siekman, B., and Westesen, K. 1994. Thermoanalysis of the recrystallization process of melt-homogenized glyceride nanoparticles. Colloids and Surfaces B: Biointerfaces 3: 159-175.
- Singh, K. K., and Vingkar, S. K. 2008. Formulation, antimalarial activity and biodistribution of oral lipid nanoemulsion of primaquine. International Journal of Pharmaceutics 347: 136-143.
- Solans, C., and Solé, I. 2012. Nano-emulsions: Formation by low-energy methods. Current Opinion in Colloid and Interface Science 17(5): 246-254.
- Solans, C., Esquena, J., Forgiarini, A., Morales, D., Usón, N., and Izquierdo, P. 2002. Nanoemulsion: formulation and properties. In: Shah, D., Moudgil, B. and Mittal, K.L. (eds.) Surfactants in solution: fundamentals and applications, Surfactant science series, pp. 525-554. New York: Marcel Dekker.

- Solans, C., Izquierdo, P., Nolla, J., Azemar, N. and Garcia-Celma, M.J. 2005. Nano-emulsions. Current Opinion in Colloid & Interface Science 10: 102-110.
- Spernath, A., and Aserin, A. 2006. Microemulsions as carriers for drugs and nutraceuticals. Advances in Colloid and Interface Science 130: 47-64.
- Spernath, A., Yaghmur, A., Aserin, A., Hoffman, R. E., and Garti, N. 2002. Food-grade microemulsions based on nonionic emulsifiers: mediato enhance lycopene solubilization. Journal of Agricultural and Food Chemistry 50(23): 6917-6922.
- Stuart, M. C. A., and Boekema, E. J. 2007. Two distinct mechanisms of vesicle-to-micelle and micelle-to-vesicle transition are mediated by the packing parameter of phospholipid–detergent systems. Biochimica et Biophysica Acta Biomembranes 1768(11): 2681-2689.
- Summers, M., Eastoe, J., Davis, S., and Du, Z. 2001. Polymerization of cationic surfactant phases. Langmuir 17: 5388-5397.
- Tadros, T.F. 1984. Microemulsions-An overview. In: Mittal, K.L. and Lindman, B. (eds) Surfactants in solution, Vol.3, pp.1501-1532. New York: Plenum Press.
- Tadros, T.F. 2005. Applied surfactants: principles and applications. New York: Wiley VCH.

- Tadros, T. F., Vandamme, A., Leveck, B., Booten, K., and Stevens, C. V. 2004. Stabilization of emulsions using polymeric surfactants based on inulin. Advances in Colloid and Interface Science 108-109: 207-226.
- Talegaonkar, S., Azeem, A., Ahmad, F. J., Khar, R. K., Pathan, S. A., and Khan, Z. I. 2008. Microemulsion: a novel approach to enhanced drug delivery. Recent Patents on Drug Delivery and Formulation 2: 238-257.
- Tan, C. H., Huang, Z. J., and Huang, X. G. 2010. Rapid determination of surfactant critical micelle concentration in aqueous solutions using fiber-optic refractive index sensing. Analytical Biochemistry 401: 144-147.
- Tchakalova, V., Testard, F., Wong, K., Parker, A., Benczedi, D., and Zemb, T. 2008. Solubilization and interfacial curvature in microemulsions I. Interfacial expansion and co-extraction of oil. Colloids and Surfaces A-Physicochemical and Engineering Aspects 331: 31-39.
- Teo, B. S. X., Basri, M., Zakaria, M. R. S., Salleh, A. B., Rahman, M. B. A. and other 2010. A potential tocopherol acetate loaded palm oil esters-in-water nanoemulsions for nanocosmeceuticals. Journal of Nanobiotechnology 8(4): 1-11.
- Tiwari, S. B., and Amiji, M. M. 2006. Nanoemulsion formulations for tumor-targeted. In: Amiji, M.M (eds.) Nanotechnology for cancer therapy, pp. 723-739. Boca Raton: CRC Press.

- Torchilin, V. P. 2001. Structure and design of polymeric surfactant-based drug delivery systems. Journal of Controlled Release 73: 137-172.
- Toth, G., and Madarasz, A. 2006. Structure of BRIJ-35 nonionic surfactant in water: a reverse Monte Carlo study. Langmuir 22: 590-597.
- Unruh, T., Bunjes, H., and Westesen, K. 1999. Observation of size-dependent melting in lipid nanoparticles. The Journal of Physical Chemistry B 103 (7): 10373-10377.
- Wang, L., Dong, J., Chen, J., Eastoe, J., and Li, X. 2009. Design and optimization of a new self-nanoemulsifying drug delivery system. Journal of Colloid and Interface Science 330: 443-448.
- Wang, L., Mutch, K. J., Eastoe, J., Heenan, R. K., and Dong, J. 2008. Nanoemulsions prepared by a two-step low-energy process. Langmuir 24: 6092-6099.
- Wang, L., Tabor, R., Eastoe, J., Li, X., Heenan, R. K., and Dong J. 2009. Formation and stability of nanoemulsions with mixed ionic-nonionic surfactants. Physical Chemistry Chemical Physics 11: 9772-9778.
- Wang, X., Jiang, Y., Wang, Y. W., Huang, M. T., Ho, C. T., and Huang, Q. 2008. Enhancing anti-inflammation activity of curcumin through O/W nanoemulsions. Food Chemistry 108 (2): 419-424.

- Warisnoicharoen, W., Lansely, A. B., and Lawrence, M. J. 2000a. Nonionic oil-in-water microemulsions: The effect of oil type on phase behaviour. International Journal of Pharmaceutics 198: 7-27.
- Warisnoicharoen, W., Lansely, A. B., and Lawrence, M. J. 2000b. Light scattering investigations on dilute nonionic oil-in-water microemulsions. American Association of Pharmaceutical Scientists Pharmaceutical Sciences and Technology 2: 16-26.
- Westesen, K., and Bunjes, H. 1995. Do nanoparticles prepared from lipids solid at room temperature always possess a solid lipid matrix?. International Journal of Pharmaceutics 115: 129-131.
- Windbergs, M., Strachan, C. J., and Kleinebudde, P. 2009. Influence of the composition of glycerides on the solid-state behaviour and the dissolution profiles of solid lipid extrudates. International Journal of Pharmaceutics 381: 184-191.
- Windbergs, M., Strachan, C. J., and Kleinebudde, P. 2009. Understanding the solid-state behaviour of triglyceride solid lipid extrudates and its influence on dissolution. European Journal of Pharmaceutics and Biopharmaceutics 71(1): 80-87.
- Wissing, S. A., Kayser, O., and Müller, R. H. 2004. Solid lipid nanoparticles for parenteral drug delivery. Advanced Drug Delivery Reviews 56(9): 1257-1272.

Yuan, Y., Gao, Y., Zhao, J., and Mao, L. 2008. Characterization and stability evaluation of β -carotene nanoemulsions prepared by high pressure homogenization under various emulsifying conditions. Food Research International 41: 61-68.

Zdziennicka, A., Szymczyk, K., Krawczyk, J., and Janczuk, B. 2012. Activity and thermodynamic parameters of some surfactants adsorption at the water-air interface. Fluid Phase Equilibria 318: 25-33.

APPENDIX

Table 13 The comparison of hydrodynamic droplet sizes of the NE containing SBO prepared by PIT method and sonication method.

C_{18:1}E₁₀ (% w/w)	SBO (% w/w)	Size (nm) from PIT method (mean±S.D.,n=3)	Size (nm) from sonication (mean±S.D.,n=3)
5	1	12.70±0.40	13.24±0.15
5	2	16.27±0.55	17.17±0.71
5	3	25.67±0.47	25.40±0.50
5	4	59.47±0.60	60.57±1.20
10	1	11.80±0.26	12.20±0.30
10	3	14.70±0.62	14.90±0.40
10	4	17.33±0.49	17.97±0.38
10	6	25.93±0.67	27.47±0.71
10	7	45.97±1.50	47.10±0.62
10	8	76.20±0.70	74.43±0.57
10	9	113.37±2.34	116.20±2.04
15	4	13.27±2.15	14.10±0.20
15	5	15.60±0.79	16.07±0.12
15	7	18.47±0.86	19.00±0.26
15	8	21.93±0.93	22.67±0.50
15	9	26.50±0.30	26.67±0.32
15	11	68.00±0.60	66.73±1.30
15	12	108.27±1.61	109.07±1.14
15	13	130.3±0.70	134.00±2.95
20	5	14.23±0.50	15.02±0.10
20	7	15.77±0.55	16.07±0.25
20	9	18.50±1.10	19.87±0.74
20	11	23.63±0.55	24.97±0.06
20	13	33.90±0.40	33.20±0.66
20	14	60.07±0.23	58.20±0.52
20	15	88.20±0.70	86.60±0.89
20	16	116.87±1.50	123.40±0.84
25	6	13.80±0.72	13.57±0.35
25	8	15.33±0.23	16.11±0.15
25	10	16.53±0.21	17.07±0.40
25	12	19.83±1.10	20.73±0.15
25	14	26.93±0.76	26.67±0.42
25	16	39.50±0.90	39.03±0.50
25	18	78.40±1.50	77.03±0.81

Table 14 The comparison of hydrodynamic droplet sizes of the NE containing TPN prepared by PIT method and sonication method.

C_{18:1}E₁₀ (% w/w)	TPN (% w/w)	Size (nm) from PIT method (mean±S.D.,n=3)	Size (nm) from sonication (mean±S.D.,n=3)
5	1	14.72±0.23	15.31±0.41
5	2	16.90±0.32	17.72±0.22
5	3	19.91±0.22	20.13±0.21
5	4	30.00±0.31	32.84±0.70
10	1	11.14±0.49	11.92±0.42
10	2	12.95±0.31	13.11±0.31
10	3	14.04±0.42	14.52±0.31
10	4	16.12±0.27	16.42±0.63
10	5	20.12±0.22	20.64±0.32
10	7	27.43±0.52	30.62±0.14
10	8	51.27±0.81	53.93±0.30
10	9	118.24±2.70	120.52±2.17
15	5	16.22±0.32	16.63±0.90
15	7	19.84±0.24	20.11±1.24
15	8	21.81±0.27	22.41±0.42
15	9	22.62±0.31	23.14±0.24
15	11	32.47±0.42	36.04±0.19
15	12	57.71±0.73	55.20±0.93
15	14	127.24±0.82	130.42±1.42
20	5	16.24±0.40	15.51±0.82
20	7	17.32±0.81	18.21±1.62
20	8	18.61±0.31	18.64±0.53
20	10	22.54±0.22	23.91±0.73
20	12	28.23±0.54	27.15±0.22
20	13	31.31±0.62	30.18±0.20
20	14	37.42±0.53	36.24±0.35
20	16	71.82±0.32	71.12±0.67
20	18	118.14±1.96	113.41±0.86
25	6	16.84±0.22	17.22±0.36
25	8	17.83±0.93	18.71±0.42
25	10	18.24±0.42	19.92±0.56
25	12	20.41±0.19	21.61±0.65
25	14	26.30±0.21	26.92±2.82
25	16	29.62±0.56	31.17±1.34

Table 15 The comparison of hydrodynamic droplet sizes of the NE containing TLN prepared by PIT method and sonication method.

C_{18:1}E₁₀ (% w/w)	TLN (% w/w)	Size (nm) from PIT method (mean±S.D.,n=3)	Size (nm) from sonication (mean±S.D.,n=3)
5	1	11.82±0.17	13.11±0.42
5	3	21.31±0.42	22.50±0.72
5	4	32.00±0.27	32.05±0.60
5	5	59.15±0.31	60.32±1.41
10	1	9.21±2.55	11.00±0.91
10	3	15.62±0.82	15.71±0.31
10	5	19.30±0.43	19.22±0.23
10	6	21.21±0.52	21.41±0.35
10	7	26.13±1.12	26.16±0.29
10	8	33.34±0.56	33.92±0.75
10	9	47.73±0.62	47.92±0.41
10	10	79.91±0.40	79.31±0.90
15	5	14.50±1.41	15.22±0.82
15	7	19.11±1.22	19.83±0.51
15	9	22.53±0.70	22.52±0.32
15	11	28.12±0.32	29.42±0.43
15	12	36.10±0.39	37.00±0.32
15	13	45.52±0.28	46.62±1.12
15	14	65.91±0.30	67.45±0.73
15	15	105.72±0.43	107.42±1.12
20	5	14.19±0.42	15.20±0.22
20	7	15.21±0.72	16.63±0.40
20	9	17.93±0.50	19.00±0.32
20	11	20.43±0.33	21.21±0.71
20	12	21.52±0.81	22.93±0.23
20	13	24.00±0.42	25.54±0.81
20	14	28.11±0.10	28.73±0.42
20	16	36.82±0.63	37.72±0.73
20	17	45.93±0.53	45.91±0.51
20	18	66.31±0.95	66.30±0.42
20	19	89.22±0.49	86.62±0.27
20	20	113.40±1.21	109.11±1.56

Table 16 The comparison of hydrodynamic droplet sizes of the NE containing TON prepared by PIT method and sonication method.

C_{18:1}E₁₀ (% w/w)	TON (% w/w)	Size (nm) from PIT method (mean±S.D.,n=3)	Size (nm) from sonication (mean±S.D.,n=3)
10	1	11.46±0.41	10.89±0.52
15	1	10.71±0.30	10.64±0.40
15	2	13.32±0.48	12.70±0.63
20	3	12.83±0.11	12.81±0.38
20	4	17.79±1.69	16.20±0.11
25	5	13.62±0.20	14.13±0.62

The mean average size obtained from Sonication method are not significant difference from the mean average size obtained from PIT method, $p > 0.05$ determined by One-way ANOVA.

Table 17 The variation in the mean hydrodynamic droplet size (mean±S.D., n=3) of the NE containing TON at different weight ratios of C_{18:1}E₁₀ to triglycerides

0.1	size (nm)	SD	0.2	size (nm)	SD
10%1%	10.9	0.4	10%2%	78.4*	2.1
15%2%	10.2	1.8	15%3%	13.6	1.4
			20%4%	17.8*	1.7
			25%5%	13.6	0.2

The mean average sizes of 0.1 weight ratios of C_{18:1}E₁₀ to triglycerides are not significant difference, $p > 0.05$ determined by One-way ANOVA. The mean average sizes of 0.2 weight ratios of C_{18:1}E₁₀ to triglycerides are significant difference, * $p < 0.05$ determined by One-way ANOVA.

Table 18 The variation in the mean hydrodynamic droplet sizes (mean±S.D., n=3) of the NE containing SBO at different weight ratios (R) of C_{18:1}E₁₀ to triglycerides.

R=0.2	size (nm)	SD	R=0.3	size (nm)	SD	R=0.4	size (nm)	SD
5%:1%	13.2	0.20	10%:3%	14.8	0.58	5%:2%	17.8	0.46
10%:2%	13.4	0.67	15%:4%	13.9	0.53	10%:4%	17.5	0.40
20%:4%	13.2	0.40	20%:6%	14.9	0.63	15%:6%	17.2	0.69
25%:5%	13.6	0.23	25%:7%	14.5	0.55	20%:8%	17.4	0.58
						25%:10%	17.1	0.35
R=0.5	size (nm)	SD	R=0.6	size (nm)	SD			
10%5%	20.2	0.60	5%3%	27.1	0.95			
15%7%	19.0	0.59	10%6%	26.4	0.71			
20%10%	20.6	0.61	15%9%	26.8	0.30			
			20%12%	28.4	0.40			
			25%14%	27.3	0.72			
R=0.7	size (nm)	SD	R=0.8	size (nm)	SD	R=0.9	size (nm)	SD
10%7%	46.3*	1.08	5%4%	61.3*	0.6	10%9%	113*	0.70
15%11%	68.2*	0.60	10%8%	74.6*	0.5	15%13%	124.3*	0.70
20%14%	61.3*	0.60	15%12%	110.9*	0.6	20%18%	P/S	-
25%18%	84.8*	0.90	20%16%	120.5*	1.1			
			25%20%	Gel	-			

The mean average sizes of 0.2-0.6 weight ratios of C_{18:1}E₁₀ to triglycerides are not significant difference, $p > 0.05$ determined by One-way ANOVA. The mean average sizes of 0.7-0.9 weight ratios of C_{18:1}E₁₀ to triglycerides are significant difference, * $p < 0.01$ determined by one-way ANOVA.

Table 19 The variation in the mean hydrodynamic droplet sizes (mean±S.D., n=3) of the NE containing TPN at different weight ratios (R) of C_{18:1}E₁₀ to triglycerides.

R=0.2	size (nm)	SD	R=0.3	size (nm)	SD	R=0.4	size (nm)	SD
5%:1%	12.2	0.64	10%:3%	13.9	0.31	5%:2%	17.0	0.59
10%:2%	12.0	0.56	15%:4%	15.9	0.42	10%:4%	16.0	0.44
			20%:6%	15.4	0.30	15%:6%	17.1	0.55
			25%:8%	16.7	0.40	20%:8%	18.0	0.30
						25%:10%	18.6	0.30
R=0.5	size (nm)	SD	R=0.6	size (nm)	SD			
10%:5%	20.1	0.52	5%:3%	20.5	0.69			
15%:8%	20.9	0.59	10%:6%	21.9	0.74			
20%:10%	20.9	0.10	15%:9%	21.2	0.67			
			20%:12%	26.0*	0.52			
			25%:14%	25.0*	0.31			
R=0.7	size (nm)	SD	R=0.8	size (nm)	SD	R=0.9	size (nm)	SD
10%:7%	27.2*	0.93	5%:4%	31.3*	0.85	10%:9%	102.3*	1.21
15%:11%	32.1*	0.75	10%:8%	46.8*	1.33	15%:14%	132.2*	1.52
20%:14%	37.4*	0.60	15%:12%	58.0*	0.70	20%:18%	115.2*	1.10
25%:18%	gel		20%:16%	74.4*	1.52			
			25%:20%	gel				

The mean average sizes of 0.2-0.5 weight ratios of C_{18:1}E₁₀ to triglycerides are not significant difference, $p > 0.05$ determined by one-way ANOVA. The mean average sizes of 0.6-0.9 weight ratios of C_{18:1}E₁₀ to triglycerides are significant difference, * $p < 0.01$ determined by one-way ANOVA.

Table 20 The variation in the mean hydrodynamic droplet sizes (mean±S.D., n=3) of the NE containing TLN at different weight ratios (R) of C_{18:1}E₁₀ to triglycerides.

R=0.2	size (nm)	SD	R=0.3	size (nm)	SD	R=0.4	size (nm)	SD	R=0.5	size (nm)	SD
5%1%	11.2	0.32	10%3%	15.2	0.61	5%2%	16.8	0.73	10%5%	18.7	0.41
10%2%	13.6	0.20	15%5%	15.0	0.56	10%4%	17.5	1.00	15%7%	18.0	0.41
			20%6%	14.7	0.40	15%6%	16.0	0.24	20%10%	18.9	0.13
						20%8%	16.3	0.40	25%12%	18.9	0.22
R=0.6	size (nm)	SD	R=0.7	size (nm)	SD	R=0.8	size (nm)	SD			
5%3%	21.3	0.52	10%7%	26.7	0.72	5%4%	32.5	0.45			
10%6%	21.5	0.90	15%11%	28.1	0.63	10%8%	33.9	0.70			
15%9%	22.1	0.31	20%14%	27.5	0.15	15%12%	36.8*	0.65			
20%12%	22.3	0.12	25%17%	27.0	0.47	20%16%	37.1*	0.21			
25%15%	22.6	0.30									
R=0.9	size (nm)	SD	R=1	size (nm)	SD						
10%9%	48.0	0.48	5%5%	60.6*	1.31						
15%14%	46.6	0.90	10%10%	80.9*	1.72						
20%18%	67.0*	0.52	15%15%	106.3*	0.80						
			20%20%	113.7*	1.69						

The mean average sizes of 0.2-0.7 weight ratios of C_{18:1}E₁₀ to triglycerides are not significant difference, $p > 0.05$ determined by one-way ANOVA. The mean average sizes of 0.8-1.0 weight ratios of C_{18:1}E₁₀ to triglycerides are significant difference,* at least $p < 0.05$ determined by one-way ANOVA.

Table 21 Variation in phase inversion temperature (mean±S.D., n=3) of systems prepared using either 10, 15, 20 or 25 wt% C_{18:1}E₁₀ and containing either varying amounts of SBO or TPN.

SAA (%)	SBO (%)	PIT (°C)	SD	SAA (%)	TPN (%)	PIT (°C)	SD
10	0	57.40	0.40	10	0	57.40	0.40
10	1	54.40	0.38	10	1	55.70	0.47
10	3	65.20	0.45	10	3	66.80	0.50
15	0	59.70	0.35	15	0	59.70	0.35
15	1	53.20	0.61	15	1	53.40	0.40
15	3	57.30	0.30	15	3	60.10	0.35
15	5	64.70	0.95	15	5	70.10	0.89
20	0	60.00	1.00	20	0	60.00	1.00
20	1	53.00	0.25	20	1	52.80	0.93
20	3	54.50	0.21	20	3	56.00	0.55
20	5	57.70	0.35	20	5	61.90	0.81
20	7	62.10	0.31	20	7	69.90	0.81
25	0	59.70	1.22	25	0	59.70	1.22
25	1	49.40	0.51	25	1	51.80	0.26
25	2	49.90	0.10	25	2	52.80	0.72
25	4	51.60	0.58	25	4	56.30	0.36
25	6	55.00	0.35	25	6	58.90	0.55
25	8	59.20	0.56	25	8	62.00	1.17
25	10	63.10	1.18	25	10	67.30	0.61

Table 22 Variation in phase inversion temperature (mean±S.D., n=3) of systems prepared using either 10, 15, 20 or 25 wt% C_{18:1}E₁₀ and containing either varying amounts of TLN or TON.

SAA (%)	TLR (%)	PIT (°C)	SD	SAA (%)	TON (%)	PIT (°C)	SD
10	0	57.43	0.40	10	0	57.43	0.40
10	1	51.83	1.18	10	1	46.23	0.68
10	3	63.13	0.12				
				15	0	59.73	0.35
15	0	59.73	0.35	15	1	43.13	0.32
15	1	49.37	0.81	15	2	44.27	0.65
15	3	54.83	1.14				
15	5	63.47	0.35	20	0	60.00	1.00
15	7	68.40	0.78	20	1	42.57	0.40
				20	3	43.87	0.12
				20	4	45.00	0.17
20	0	60.00	1.00				
20	1	48.87	0.32	25	0	59.73	1.22
20	3	52.63	0.47	25	1	43.93	0.12
20	5	58.37	0.12	25	3	42.60	0.72
20	7	62.87	0.32	25	5	43.90	0.10
20	9	67.40	0.53				
25	0	59.73	1.22				
25	1	49.30	0.66				
25	3	50.17	0.21				
25	5	53.20	0.20				
25	7	58.40	0.26				
25	9	62.30	1.13				
25	11	64.30	0.56				
25	13	67.63	0.81				

Table 23 Solubilization of testosterone propionate in micelles and NE stabilised using 10 wt% C_{18:1}E₁₀ and containing either varying amounts of SBO, TPN, TLN or TON at 22 ± 2°C (mean ± S.D., n=4).

Oil wt%	Drug solubilisation (%)							
	Soybean Oil	SD	Tripalmitin	SD	Trilaurin	SD	Trioctanoin	SD
0	0.24	0.02	0.24	0.02	0.24	0.02	0.24	0.02
1	0.33*	0.01	0.30*	0.01	0.33*	0.04	0.30*	0.03
2	0.37*	0.02	0.34*	0.01	0.42*	0.05	-	-
3	0.41*	0.02	0.35	0.02	0.46	0.02	-	-
4	0.48*	0.03	0.37	0.01	0.50*	0.01	-	-
5	0.55*	0.04	0.40	0.04	0.58*	0.02	-	-
6	0.56	0.02	0.41	0.05	0.63*	0.02	-	-
7	0.49	0.05	0.41	0.03	0.71*	0.01	-	-
8	0.41*	0.065	0.30*	0.02	0.71	0.05	-	-
9	0.32*	0.04	0.28*	0.03	0.55*	0.03	-	-
10					0.41*	0.04		

The mean TP solubility in all nanoemulsions are significantly increased from the mean TP solubility in micelle and are significantly increased as the triglycerides concentrations increased except for the tripalmitin,* $p < 0.05$ determined by one-way ANOVA. The mean TP solubility in nanoemulsions in Region C are significantly decreased from the mean TP solubility in Region B,* $p < 0.05$ determined by one-way ANOVA.

Table 24 Solubilization of testosterone propionate in micelles and NE stabilised using 20 wt% C_{18:1}E₁₀ and containing either varying amounts of SBO, TPN, TLN or TON at 20 ± 2°C (mean ± S.D., n=4).

Oil wt%	Drug solubilisation (%)							
	Soybean Oil	SD	Tripalmitin	SD	Trilaurin	SD	Trioctanoin	SD
0	0.45	0.03	0.45	0.03	0.45	0.03	0.45	0.03
1	0.60*	0.05	0.54*	0.02	0.59*	0.01	0.55*	0.02
2	0.64	0.02	0.59*	0.01	0.65*	0.03	0.68*	0.07
3	0.69*	0.03	0.62*	0.01	0.72*	0.05	0.75*	0.06
4	0.73*	0.02	0.64	0.01	0.75	0.02	0.82*	0.08
5	0.76	0.04	0.63	0.04	0.80*	0.07		
6	0.80*	0.02	0.63	0	0.84*	0.01		
7	0.90*	0.02	0.62	0.01	0.89*	0.01		
8	0.95*	0.06	0.63	0.08	0.97*	0.02		
9	0.99*	0.03	0.64	0.04	1.03*	0.02		
10	1.08	0.07	0.65	0.04	1.09*	0.01		
11	1.12*	0.02	0.64	0.07	1.16*	0.02		
12	1.12	0.01	0.59	0.08	1.22*	0.02		
13	0.90*	0.10	0.40*	0.05	1.27*	0.01		
14	0.63*	0.13	-	-	1.32*	0.03		
15	0.50*	0.06	0.27*	0.06	1.40*	0.02		
16	0.42*	0.03	0.29	0.04	1.00*	0.05		
18	-	-	0.27	0.05	0.60*	0.07		
20	-	-			0.40*	0.14		

The significant in the mean TP solubility are the same as stated for Table 23.

Table 25 The comparison of the mean hydrodynamic size (mean \pm S.D., n=3) at $22 \pm 2^\circ\text{C}$ of the NE with and without saturated amount of testosterone propionate prepared using SBO, TPN, TLN and TON and stabilised by 10 wt% C_{18:1}E₁₀.

TLR	Size (nm) without drug	SD	Size (nm) with drug	SD	TPN	Size (nm) without drug	SD	Size (nm) with drug	SD
1	9.17	2.57	10.00	0.74	1	11.10	0.50	12.80	0.20
2	15.27	0.64	16.27	0.64	2	12.90	0.30	16.60	0.20
3	15.63	0.76	17.63	0.76	3	14.00	0.30	17.20	0.30
4	16.97	1.26	17.97	0.58	4	16.00	0.30	17.90	0.20
5	19.33	1.27	20.33	0.66	5	20.10	0.20	72.50*	3.30
6	21.20	0.46	21.90	0.46	6	22.10	0.20	103.20*	4.20
7	26.13	0.35	27.13	0.83	7	27.40	0.50	175.00*	5.20
8	33.30	0.62	35.30*	0.44	8	51.20	0.80	224.40*	5.90
9	47.67	0.55	49.87*	0.53	9	122.40	3.20	255.40*	6.40
10	79.93	0.40	83.33*	0.50					
SBO	Size (nm) without drug	SD	Size (nm) with drug	SD	TON	Size (nm) without drug	SD	Size (nm) with drug	SD
1	12.00	0.56	12.70	0.42	1	11.50	0.40	13.30	0.40
2	13.60	0.25	14.20	0.31					
3	14.90	0.27	15.50	0.24					
4	17.80	0.17	18.40	0.41					
5	20.00	0.21	20.50	0.33					
6	26.20	0.25	27.30	0.71					
7	46.40	0.49	49.20*	0.50					
8	75.30	1.00	80.00*	0.55					
9	112.90	1.10	117.30*	0.40					

The mean average sizes of the NE with TP are significant different from the mean sizes of the NE without TP,* $p < 0.05$ determined by one-way ANOVA.

Table 26 The comparison of the mean hydrodynamic size (mean \pm S.D., n=3) at $22 \pm 2^\circ\text{C}$ of the NE with and without saturated amount of testosterone propionate prepared using SBO, TPN, TLN and TON and stabilised by 20 wt% $\text{C}_{18:1}\text{E}_{10}$.

TLR	Size (nm)		Size (nm)		TPN	Size (nm)		Size (nm)		SBO	Size (nm)		Size (nm)	
	without drug	SD	with drug	SD		without drug	SD	with drug	SD		without drug	SD	with drug	SD
1	10.10	0.40	12.70	0.20	1	11.70	0.40	16.53	0.57	1	10.50	0.30	13.20	0.12
3	12.50	0.30	14.80	0.25	3	15.50	0.30	20.70	0.30	3	13.20	0.40	15.10	0.24
5	14.17	0.35	16.30	0.25	5	16.20	0.40	21.60	0.40	5	15.00	0.15	16.20	0.27
6	14.87	0.76	16.40	0.29	6	17.10	0.50	22.60	0.50	6	14.60	0.32	17.00	0.19
7	15.23	0.65	17.60	0.46	7	17.30	0.80	22.60	0.40	8	17.10	0.10	18.20	0.3
8	16.57	0.35	17.90	0.26	8	18.60	0.30	22.80*	0.40	10	21.80	0.35	22.40	0.32
9	17.90	0.46	19.00	0.40	10	22.50	0.20	56.00*	3.00	12	29.00	0.50	29.80	0.44
10	18.50	0.10	20.70	0.30	12	28.00	0.50	84.80*	4.60	13	34.30	0.50	40.40*	0.53
11	20.40	0.26	21.10	0.40	13	31.00	0.60	98.00*	5.00	14	60.20	0.80	69.30*	0.48
12	21.47	0.80	22.20	0.25	14	37.40	0.50	109.90*	5.10	15	89.40	1.20	94.80*	1.17
13	23.97	0.40	25.90	0.38	16	71.80	0.30	183.33*	3.80	16	122.50	1.40	127.20*	1.43
14	27.97	0.12	28.00	0.29	18	118.00	1.96	240.40*	5.20					
15	31.50	0.10	32.40	0.82										
16	36.80	0.56	40.33*	0.42	TON	Size (nm)		Size (nm)						
17	45.87	0.50	53.97*	0.75		without drug	SD	with drug	SD					
18	66.27	0.95	72.57*	0.51	1	9.80	0.50	11.50	0.32					
19	89.20	0.46	95.40*	1.86	3	12.80	0.10	14.30*	0.21					
20	113.37	1.19	115.77*	1.66	4	17.80	1.70	20.10*	0.40					

The mean average sizes of the NE with TP are significant difference from the mean sizes of the NE without TP, * $p < 0.05$ determined by One-way ANOVA.

Table 27 The phase inversion temperatures (mean \pm S.D., n=3) of the NE prepared using either 10 or 20 wt% C_{18:1}E₁₀ and containing either varying amounts of SBO, TPN, TLN or TON with the presence of a saturated amount of testosterone propionate at 22 \pm 2°C.

SAA (%)	TPN (%)	PIT (°C)	SD	SAA (%)	SBO (%)	PIT (°C)	SD
10	0.00	53.17	0.21	10	0.00	53.17	0.21
10	1.00	49.77	0.25	10	1.00	49.03	0.57
10	3.00	58.50	0.50	10	3.00	58.10	0.26
20	0.00	55.30	0.26	20	0.00	55.30	0.26
20	1.00	48.57	0.40	20	1.00	48.63	0.40
20	3.00	50.17	0.35	20	3.00	50.13	0.31
20	5.00	54.93	0.31	20	5.00	54.97	0.55
20	7.00	60.07	0.60	20	7.00	59.27	0.49
SAA(%)	TLR (%)	PIT (°C)	SD	SAA (%)	TON (%)	PIT (°C)	SD
10	0.00	53.17	0.21	10	0.00	53.17	0.21
10	1.00	48.33	0.76	10	1.00	44.70	0.30
10	3.00	58.00	0.20				
20	0.00	55.30	0.26	20	0.00	55.30	0.26
20	1.00	46.33	0.42	20	1.00	41.10	0.26
20	3.00	48.70	0.53	20	3.00	42.13	0.40
20	5.00	54.13	0.71	20	4.00	43.50	0.44
20	7.00	60.17	0.58				
20	9.00	64.17	0.76				

VITA

Miss Prawarisa Wasutrasawat was born on February 18, 1986 in Bangkok. She did her undergraduate work at Broad Oak Toiletries in Tiverton, UK, in 2007 as assistant cosmetic chemist. She received her B.Sc. (Hons.) in Cosmetic Sciences from The University of the Arts London, UK, in 2008.